DISS. ETH No. 21993

STABILITY, MODIFICATION AND BIOMEDICAL DETECTION OF GRAPHITE-BASED NANOMATERIALS

A thesis submitted to attain the degree of

DOCTOR OF SCIENCES

(Dr. sc. ETH Zurich)

presented by

CHRISTOPH MARTIN SCHUMACHER

MSc Chemical and Bioengineering, ETH Zurich

born on 27.12.1985

citizen of Mels (SG)

Switzerland

accepted on the recommendation of

Prof. Dr. Wendelin J. Stark, examiner
Prof. Dr. Javier Pérez-Ramírez, co-examiner

2014

To my family
and in memory of
Fritz, my godfather, who had
to leave us all far too early.

La dernière démarche de la raison
est de reconnaître qu'il y a une infinité
de choses qui la surpassent.

Blaise Pascal, Pensées

Acknowledgments

Over the years during my PhD studies I had the opportunity to work with many great people. Hereby, I would like to highlight all their efforts for enriching my knowledge, my way of thinking and the contents of this work.

My sincere gratitude goes to my advisor, Prof. Dr. Wendelin J. Stark, for all his support throughout my thesis. With his broad knowledge and visionary mindset he demonstrates that thinking beyond classical paradigms is one of the most important things for bringing the world forward. Following his entrepreneurial spirit he taught me, that scientific and personal success is also a matter of communication and marketing. Doing things just in a good way is often not enough. Thank you so much for giving me this huge amount of advice, confidence and freedom throughout all my scientific and industrial projects!

Prof. Dr. Javier Pérez-Ramírez is kindly acknowledged for his interest in my work and spending his valuable time being my co-examiner. I would also like to thank Prof. Dr. Detlef Günther for being the chairman of my examination.

I would like to accent all the efforts of the mechanical workshop's team, particularly Urs Krebs. It is an absolutely unique feature at ETH that scientists can work closely together with so many talented craftsmen. Their skills and enthusiasm are indispensable key factors for many scientific achievements at this institution.

Furthermore, I want to take the opportunity to thank Prof. Dr. Beatrice Beck-Schimmer for her permanent commitment that enabled all the interdisciplinary work together with her team at the University Hospital of Zurich. Your cordiality and your encouraging way always made me feel welcome.

Then, I owe special gratitude to Dr. Inge Herrmann for all her help and support with nanomedical research when I started my PhD studies. I was very glad to have such a competent and patient advisor in this, by that time, entirely new field to me. A lot of the work in this thesis would never have been possible without you. Thank you very much for all the fruitful discussions and cheerful moments during the blood experiments at the University Hospital.

I want to thank Prof. Dr. Ann-Marie Hirt and Hanspeter Hächler for sharing their expertise by the magnetic characterization of the materials in this thesis. Many thanks also go to Max

Table of contents

Zusammenfassung

Die vorliegende Arbeit befasst sich mit graphitbasierenden Nanomaterialien. Beschichtungen welche aus wenigen Graphitlagen bestehen, werden dazu eingesetzt ansonsten sehr instabile magnetische Metallnanopartikel zu stabilisieren. Hier wurden Parameter welche die chemische Stabilität dieser Kompositmaterialien beeinflussen systematisch untersucht. Einzelne Lagen aus Graphit sind zudem ein vielversprechendes Ausgangsmaterial für neuartige hocheffiziente Halbleiter. Allerdings gestaltet sich das notwendige Zuschneiden und Verarbeiten dieser Strukturen auf der Nanoskala als schwierig. Aus diesem Grund wird hier ein neuer Ansatz präsentiert der es ermöglicht hochorientierten pyrolytischen Graphit, ein Basismaterial für einzelne Graphitschichten, mittels Nanopartikel-assistiertem Ätzen zu modifizieren. Nanomagnete und darunter speziell auch kohlenstoffbeschichtete Eisencarbidpartikel wurden vermehrt für eine magnetische Blutreinigung vorgeschlagen. Deshalb ist die Identifikation potentiell schädlicher Auswirkungen in Organismen von grosser Bedeutung. Ein nach wie vor schlecht gelöstes Problem ist die Detektion tiefkonzentrierter Nanomagnete in Blut und Gewebeproben nach langer Behandlungsdauer. Als speziell schwierig entpuppt sich sich die Detektion der bevorzugt eisenbasierenden Nanomaterialien. Aus diesem Grund wird hier ein neues Verfahren präsentiert das eine Langzeitdetektion mittels Edelmetalldotierung ermöglicht.

In **Kapitel 1** werden grundlegende Konzepte der Nanowissenschaften und spezielle Eigenschaften von Nanomaterialien im Zusammenhang mit den nachfolgend präsentierten Studien vorgestellt. Ein Hauptmerk liegt auf der Frage was Nanomaterialien so speziell macht. Einzigartige Besonderheiten und ihre Konsequenzen für die Materialeigenschaften werden vertieft behandelt und etablierte Verfahren für die Herstellung und chemische Modifikation anhand magnetischer Nanopartikel erläutert. Die erstmalige Entdeckung einzelner Graphitschichten im Jahr 2004 führte zu einer steigenden Nachfrage nach Verfahren zum Schneiden und Bohren auf sehr kleiner Skala. Die zurzeit am meisten verwendeten Prozessierungstechniken werden daher näher vorgestellt. Da magnetische Nanomaterialien vermehrt für medizinisch Anwendungen attaktiv werden, stellen sich auch Fragen bezüglich negativer Effekte. Ein Schlüsselelement für die Untersuchung solcher Effekte in Organismen stellt der Nachweis von tiefen Konzentrationen solcher Materialien dar. Die dafür am meisten verwendeten Methoden werden deshalb näher beleuchtet.

Kapitel 2 behandelt Grundlagen zur chemischen Stabilität von Graphitbeschichtungen auf Kobaltnanopartikeln. Dieses magnetische Material kann unter sehr harschen Bedingungen eingesetzt werden da die hochkristalline und daher sehr stabile Graphitbeschichtung die empfindlichen Metallkerne zuverlässig schützt. Die Möglichkeit zur kovalenten Anbindung aromatischer Spezies eröffnet ein ganzes Universum von Oberflächenfunktionalisierungen. Dennoch kann oft ein schleichender Zerfall dieser Nanokomposite beobachtet werden. Um die Materialeigenschaften zu verbessern, wurden die Einflüsse der Oberflächenfunktionalisierung, verschiedener harscher Medien und elektrochemischen Gradienten untersucht. Die daraus gewonnenen Erkenntnisse beinhalten einen detaillierten Abbaumechanismus in wässrigen Lösungen und Strategien um die chemische Stabilität dieser Materialien signifikant zu erhöhen.

Kapitel 3 setzt sich mit der Stukturierung von Graphitoberflächen auseinander. Nebst Modifikationen auf molekularer Ebene (Anbindung funktioneller Gruppen) kann Graphit auch nanoskalig zurechtgeschnitten werden. Dies ist speziell für die Halbleiterherstellung sehr interessant. Einzellagige Graphitschichten, auch Graphen genannt, weisen einzigartige elektronische Eigenschaften auf, welche gegenwärtig eingesetzte Materialien bei weitem übertreffen. Darüber hinaus könnten mit Graphen weitaus kleinere Bauweisen erreicht werden. Die Strukturierung von hochorientiertem Graphit, dem Basismaterial von Graphen, durch Zurechtschneiden auf winzigster Skala verlangt nach neuartigen Ansätzen wie dem Nanopartikel-assistiertem katalytischem Ätzen. Zu diesem Zweck wurden bislang Edelmetallnanopartikel eingesetzt, welche bei hohen Tempearaturen (> 800 °C) und unter Inertatmosphäre dünne Spuren in den Graphit schneiden können. Im Gegensatz dazu wird hier eine Technik vorgeschlagen welche sich katalytisch aktive Ceroxidnanopartikel zunutze macht, die bereits unter atmosphärischen Bedingungen bei tieferen Temperaturen (> 500 °C) funktioniert.

Gewebedurchdringende Magnetfelder können magnetische Nanopartikel einfach an gewünschte Orte in einem Organismus dirigieren. Allerdings werden potentiell schädliche Effekte kontrovers diskutiert. Die Langzeitdetektion von Nanomaterialien in verschiedenen Körperkompartimenten in diesem Zusammenhang ist sehr wichtig aber leider oft mit Hindernissen verbunden. **Kapitel 4** stellt ein neues Detektionsverfahren für eisenbasierende Nanomagneten vor. Blut und Gewebe enthalten beträchtliche Mengen an Eisen was kleine Mengen von Nanomagneten in unvorteilhafter Weise für die Detektion maskiert. Das sogenannte Flammensprayverfahren für die Herstellung der hier verwendeten Nanomagnete

erlaubt es aber die produzierten Materialien mit sehr kleinen und wohldefinierten Mengen an Nobelmetallen zu dotieren. Da diese in Organismen normalerweise nicht präsent sind, wird eine langzeitrobuste Analytik ermöglicht. Des Weiteren wird in diesem Kapitel die Wichtigkeit von guten magnetischen Charakteristiken für verlässliche Separationen beleuchtet.

Kapitel 5 schliesst die vorliegende Arbeit mit einem Ausblick und einigen Kommentaren zu den behandelten Themen ab.

Summary

This thesis is focused on graphite based nanomaterials. Few-layer graphite coatings can be used to chemically stabilize otherwise very labile magnetic metal nanoparticles. Parameters that influence the chemical stability of such nanocomposites were systematically investigated. Single-layer graphite is suggested as the base material for novel kinds of highly efficient semi-conductors. Nevertheless, the essential cutting and slicing at the nanoscale is cumbersome. Hence, a new approach based on nanoparticle-assisted catalytic etching of highly-oriented pyrolytic graphite, a base material of single-layer graphite is presented. Since nanomagnets, and amongst carbon-coated iron carbide nanoparticles, are increasingly suggested for use in magnetic blood purification, the identification of potential adverse effects in organisms is fundamental. A yet poorly resolved problem is the detection of low concentrated nanomagnets in blood and tissue samples after prolonged exposition. Especially the detection of iron-based nanomaterials turns out to be cumbersome due to the high background concentration of iron in the body. Therefore, a new long-term valid detection approach based on noble metal spiking is presented.

In **chapter 1**, general concepts of the nanoscience, special features of nanomaterials and further background regarding the studies in this thesis are explained. One of the main focuses remains on the question what renders nanomaterials special. In this context, some unique features and their consequences for the material properties are explained more in detail. Additionally, established concepts for nanomaterial fabrication and the opportunity for chemical modification are explained using the example of magnetic nanoparticles. The discovery of single layer graphite in 2004 has led to an increasing demand for cutting, slicing and drilling at a very small scale. The predominant processing techniques are therefore presented more in detail. Since more and more, especially magnetic, nanomaterials are suggested for medical use, questions regarding adverse effects arise. A key element for investigating the effects of these compounds in organisms is their traceability, even in very low doses. Hence, frequently applied methods are illustrated more in detail.

Chapter 2 deals with the fundamentals of the chemical stability of few-layer graphite coatings on cobalt nanoparticles. This material is often suggested for use under very harsh conditions since the graphite coating appears as a highly crystalline and thus very stable protection layer to the otherwise very sensitive metal cores. The opportunity for covalent attachment of aromatic moieties opens a whole universe of possible chemical surface

functionalization types. Despite of this, slight degradation of the nanocomposite can frequently be observed. In order to optimize the material properties, the influence of surface functionalization, different harsh media and electrochemical gradients on the particle degradation rate was fundamentally investigated. The findings of this study comprise a detailed degradation mechanism of this type of particles in aqueous media as well as options for enhancing the material's chemical stability significantly.

Chapter 3 focuses on a new approach for shaping graphite surfaces. Besides modifications on the molecular size level (*i.e.* attachment of functional groups), graphite can also be structured at the nanoscale. This is particularly interesting for future semi-conductor materials including graphene, a singular layer of graphite. Graphene exhibits superior electronic characteristics that outshine the currently used materials in the electronic industry. In addition, by far smaller semiconductor architecture would be enabled by the use of graphene-based semiconductors. Nevertheless, the structuring (by *i.e.* cutting, slicing) of highly oriented graphite, the base material for graphene, at very small scales calls for novel approaches including nanoparticle-assisted etching. So far, mostly noble metal particles were used to cut thin trenches into graphite at high temperatures (> 800 °C) under inert atmosphere. In contrast, a new technique using catalytically active cerium oxide particles under atmospheric conditions at lower temperatures (< 500 °C) is presented.

Due to the ease of controlling and direction by tissue pervading external magnetic fields, magnetic nanoparticles are increasingly suggested for use in nanomedicine. Potential adverse effects in organisms are a controversially discussed topic. In this context, long-term detection of nanomaterials in body compartments is often cumbersome but of major importance. In **Chapter 4**, a new detection approach for iron-based nanomagnets is presented. Blood and tissue contain considerable amounts of iron, which will mask the presence of iron-based nanoparticles in an unfavorable manner. By using flame-spray pyrolysis for the production of the presented nanomagnets, well-defined noble metal doping without changing the physical characteristics becomes possible. Hence, a long-term robust analytical method revealing the importance of good magnetic characteristics for reliable magnetic separation was established.

Finally, **chapter 5** closes this work with some future prospects and remarks regarding the examined topics.

1. Shaping Materials at the Nanoscale

1.1   Introduction

The creation, shaping and processing of materials represents one of the modern world's keystones. Controlling material aspects in a sophisticated and precise manner has led mankind to comfort, mobility and prosperity. The pace of progress over the last two centuries entirely outnumbers any anterior development. Emergence of the industrial mass production enabled manufacturing at the bulk scale and thus dropped costs of most goods dramatically. Subjects that previously were available for a minor circle of the population became virtually common.

The functions and characteristics of commodities are essentially linked to their morphology. Hence, addition of complexity and thus more value per mass or volume inherently implies controlling the small scale beyond registration by human eyes. Matter is assembled from smallest units which we call atoms. Their size is in the range of a few 10^{-10} meters and they represent a final lower limit of complexness that can be disclosed by the material science. With the uprising of analytical methods that visualize matter down to the atomic level,[1-5] progress reached the so-called nanoscale, which per definition comprises structures in the range of 10^{-9} – 10^{-7} meters. Such small objects frequently reveal properties that diverge from their corresponding analogs at the micro- to macroscale.[6, 7] It is therefore not further surprising that research on nanoscaled structures has attracted many scientists over the last decades.

This thesis focuses on the chemical stability of magnetic few layer graphite-coated metal nanoparticles[8] and, in dependence on, a method to create nano-sized cuts or holes in highly oriented pyrolytic graphite layers.[9] Magnetic nanoparticles are often suggested as tiny carriers for medical applications[10-14] since specifically acting drugs or toxin-binding species can be mounted to their surfaces.[15, 16] By injection into the body with later retention at desired locations using magnetic fields, they could *i.e.* counteract cancer.[17-19] Such new magnetic therapeutic agents however hold potential risks when brought into an organism.[20-23] In order to prove the reliability of suitable magnetic separation techniques, it is therefore crucial to be able to detect low amounts of these materials in analytically demanding matrices such as blood or tissue.[24, 25] Thus, a new long-term consistent analysis approach based on tracer elements is presented.[26] Prior to this, important fundamental characteristics of nanoparticulate matter, established manufacturing and modification techniques as well as analytical strategies are presented within this first chapter.

1.2   Special properties of nano-sized materials

The physical properties of a material are essentially defined by the character of its smallest constituents and thus the organization on the atomic level. Atoms can interact electronically amongst each other and form almost endless combinations, respectively arrangements. Nanomaterials lie within the scope of a handful to a few thousand of recurring structural entities when moving along a dimensional axis. This results in special physicochemical consequences. If one imagines nanoparticles as a result of cutting bulk matter more and more into smaller pieces, the amount of surface per mass, respectively the amount of atoms at a surface will rise in a non-linear manner.[7] This can further be clarified with a cube holding the edge length l. Since cubes present six equal planes, the total surface area per volume ratio, the so-called specific surface area calculates as follows:

$$\frac{A}{V} = \frac{6 \cdot l^2}{l^3} = \frac{6}{l}$$

This inverse dependence on the edge length leads to incessantly increasing specific surface areas when objects get smaller and smaller in size.

Figure 1.1: The overall surface area per material volume rises in non-linear manner when objects are sliced into smaller and smaller pieces.

This fact strongly influences the properties and prospects of nano-sized structures. Prime examples for this coherence are heterogeneous catalysts which can feature several hundred square meters of surface on a single gram of material.[27-29] Chemical species are usually transformed at even smaller structures, the so-called active-sites which are scattered all over the surface.[30] Therefore, large specific surface areas make these materials much more effective, since more activity and thus value can be charged per mass. Material property changes can also be a direct result of the dimensions. Liquid dispersions of gold nanoparticles for example show different colors depending on the particle size.[31] This phenomenon can be explained by the occurrence of surface plasmon resonance effects. Light in certain wavelength

ranges can collectively excite the electrons within the particles. This wavelength range depends on the particle size and their distances from each other. As a consequence, parts of the light passing through such dispersions are absorbed and the dispersions appear in different colors depending on the particle size.
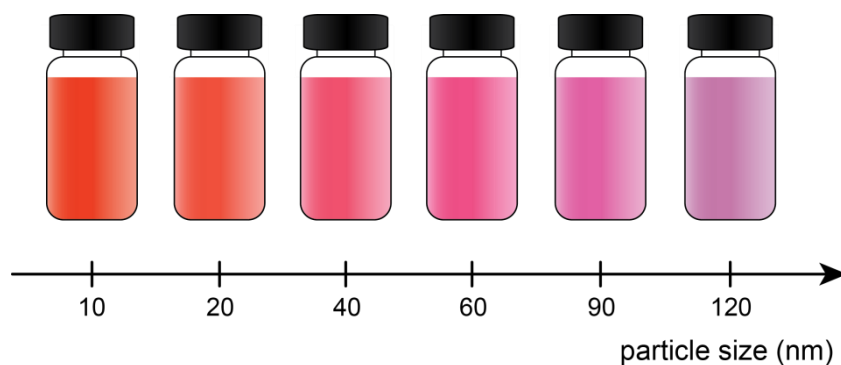
Figure 1.2: Aqueous gold nanoparticle dispersions. Surface plasmon resonance effects result in diverging light absorption depending on the particle size and thus varying colors.

Nanomaterials are widely used as functionality enhancing agents. Addition into established materials can augment or combine properties.[32] Thanks to the tiny dimensions, the macroscopic apparel remains homogeneous. Alternatively, the properties of different materials can be blended by combining two or several types of nanoparticles. An example is the combination of nano-sized cerium oxide and bismuth.[33] Cerium oxide is a very hard and electrically insulating material, whereas bismuth is a soft metallic element. United as a nanocomposite, the resulting material combines a high hardness and the electrically conducting properties of a metal. A very widely used concept is the surface chemical functionalization of nanoparticles.[34-36] Here, both the advantages of the high specific surface areas and the properties of the nanoparticle acting as a core, respectively as a carrier are used. The surface functionalization can be tailored to specifically interact with the environment. Magnetic nanoparticles represent a very prominent group in this research field and are highlighted more in detail within the next section.

1.3   Magnetic nanomaterials

Today, magnetic nanoparticles are used in various research fields including catalysis,[37-41] medicine,[42-44] as contrast[45, 46] or extraction agents.[47-49] When brought into liquid media, the particles can form pseudo homogeneous mixtures. Their magnetic features enable direction, control or recollection by application of external magnetic fields. For most purposes the surface of the nanomagnets is modified using different chemical species.[50] A main reason for this is the tendency of most nanomaterials to form agglomerates, which is problematic for many applications.[51] To overcome this issue, functional groups (often in the form of polymeric species) which sterically or electrostatically stabilize the particles within liquid media can be grafted to the particle surface. An accompanying positive effect of such coatings are the life-time enhancing features since the particles are often prone to dissolution, oxidation or other ways of chemical degradation.[34] Specific functionalities allow binding to desired structures or species and therefore allow *i.e.* magnetic extraction of low concentrated toxic species from water,[52] cancer-cell targeting[53] or magnetic labelling.[54]

1.3.1   Magnetic characteristics

The apparent magnetic character of bulk materials is based on many tiny internal magnetic domains. Such a domain is defined as a region in the material wherein the spins are equally aligned. The volumetric size of such a domain is material dependent and usually lies in the range of a few to a few tens of nanometers. When a particle's dimensions are below this critical domain size, it will consequently bear only a single magnetic domain. This results in high magnetic coercivity values (*i.e.* the magnetic field that is needed for complete demagnetization of the sample) for nanoparticles below the critical dimensional margins. Another phenomenon below these dimensions is called superparamagnetism. The spins of a magnetic domain can point in two energy-equivalent directions. Above the so-called blocking temperature, the energy barrier between them can thermally be overcome and thus makes rapid flipping between them possible. As a result, paramagnetic behavior occurs and no magnetic hysteresis and remaining magnetization without any external field can be observed any more.[34, 55]
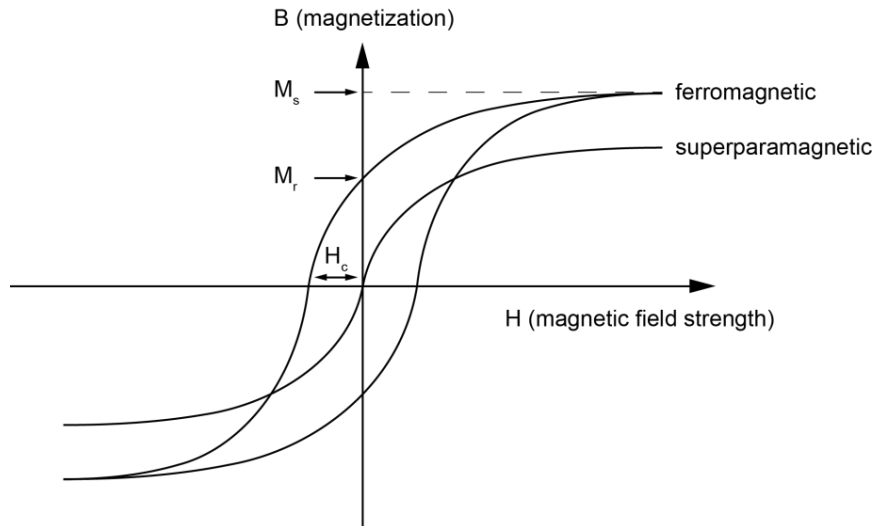
Figure 1.3: *Magnetization curves of a ferromagnetic and a superparamagnetic material. H_c represents the coercivity (i.e. the magnetic field that is needed to fully demagnetize the sample). M_r is the so-called remanence (i.e. the remaining magnetization of the sample without any external magnetic field present). M_s is the saturation magnetization. In the case of superparamagnetism, no hysteresis and magnetic remanence remain.*

1.3.2   Synthesis methods

There are various types of materials that are suitable for the creation of magnetic nanomaterials. Most prominent examples are iron oxides in the form of magnetite (Fe_3O_4)[56-58] and γ-hematite (γ-Fe_2O_3),[59, 60] spinel-type materials like for example $MnFe_2O_4$[61, 62] or $CoFe_2O_4$[63] and pure metals such as iron (Fe)[64, 65] and cobalt (Co).[66-68] Hereafter, some prevalent methods which are suitable for the large-scale production of magnetic nanomaterials are presented.

Wet-phase precipitation

Precipitative methods belong to the simplest methods to create magnetic nanomaterials. Typically, iron and cobalt salts (*e.g.* chlorides or nitrates) are dissolved in aqueous solutions.[69] Thereupon, a base is added which results in precipitation of nanoparticulate magnetic oxides. Depending on the frame conditions such as ionic strength, temperature and pH, the size, shape and composition of the particles can be controlled. However, this method is limited to oxidic particles with relatively low saturation magnetization, meaning that the materials exhibit a relatively poor response towards externally applied magnetic fields.

Thermal decomposition

Nanoparticles with good monodispersity can be obtained by decomposition of metalorganic complexes at temperatures of typically between 150°C and 300°C. Prevalently used precursor compounds include metal acetylacetonates, metal salts of fatty acids and metal carbonyls.[70, 71] High-boiling organic solvents such as long chained alkanes or ethers act as suitable liquid reaction media.[72] The particle morphology and size can be controlled by the temperature, addition of surfactants and the reaction time of typically several hours. Depending on the precursor type, also non-oxidic metallic nanomagnets can be produced (*e.g.* by the use of zero-valent cobalt in $Co_2(CO)_8$[73] or iron in $Fe(CO)_5$).[55]

Pyrolysis methods and flame spray pyrolysis

Pyrolysis techniques represent direct decomposition methods to produce nanoparticles. Metal organic complexes are degraded at very high temperatures whereby the organic part of the compounds passes off.[74] Pyrolysis methods, since the processes takes place in the gas phase, generate relatively polydisperse particles.[34] Under inert conditions, also metallic particles can be fabricated. An example for this is the decomposition of iron stearate at 900°C under argon atmosphere.[75] Liquid-feed flame spray pyrolysis[76] is based on an industrially well-known process for the manufacturing of pigments (*i.e.* TiO_2 or SiO_2) which however uses gaseous precursor compounds.[77] Metals, mostly in the form of carboxylates[78] and alcoholates,[79] are dissolved in cheap technical solvents such as xylenes, tetrahydrofurane or similar. These liquid precursors are pumped into a nozzle where oxygen is used for atomization. A surrounding support flame (CH_4/O_2) ensures ignition of the droplet/oxygen mixtures. Thereby, the organic fractions of the injected liquids are combusted and fusion processes of the remaining contents will form nanoparticles.[80] Since the particles form agglomerates after leaving the flame, they can thereafter be conveniently captured on glass-fiber filters. Precursor additives such as organophosphates or halogenated species furthermore enable generation of nano-sized salts.[81] A key advantage of the flame spray synthesis is the possibility to dope additional elements into the formed particles.[26, 82-84] Since the residence time of the particles within the flame accounts for milliseconds only, thermodynamically unstable phase configurations can be kinetically "frozen" in certain cases.[85] The above presented methods based on liquid reaction media and conventional pyrolysis work in time frames which are several orders of magnitude higher. Hence, they do not allow obtaining certain morphologies which are however accessible by flame spray synthesis.
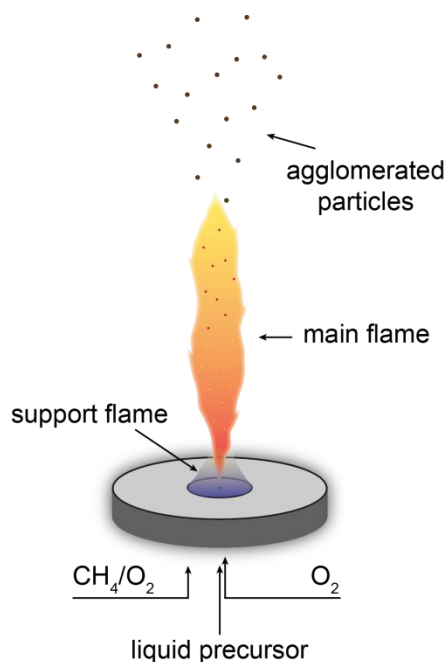
Figure 1.4: *Scheme of a flame spray pyrolysis burner in action. A support methane-oxygen driven flame ignites oxygen-atomized liquid precursor containing metal organic salts. All combustible organic parts are burnt like this and the remaining constituents form nanoparticles which leave the flame as agglomerates.*

Flame spray synthesis can also be realized under reducing conditions.[68, 86] In this case the flame is surrounded by an inert atmosphere such as nitrogen. By feeding lower amounts of oxygen into the flame which are not allowing complete combustion of the organic share, hydrogen and carbon monoxide are formed as combustion products. Both of them entail a reductive environment. Like this, initially oxidized constituents are immediately reduced to metal particles to from *e.g.* cobalt, iron or nickel. The nanomagnets which are presented in this thesis are produced by this method and under partially reducing atmosphere.

1.3.3   Oxidic and metallic nanomagnets

Magnetite (Fe_3O_4) is probably the most used base material for oxidic nanomagnets. Since magnetite provides a relatively large magnetic single domain size (estimated to account for 128 nm diameter for spherical particles),[34] the advantage of superparamagnetism is accessible by most manufacturing methods. After suitable chemical functionalization, these particles easily de-agglomerate when external magnetic fields are removed. Nevertheless, the saturation magnetization and thus the response to magnetic fields is lower than those of pure metallic nanoparticles. On the other hand, the single magnetic domain dimensions of metallic

iron and cobalt remain much lower (Fe: 15 nm and Co: 7 nm (fcc)) and they can therefore not be obtained as superparamagnetic nanopowders in most reported cases. Hence, due to their magnetic remanence, these particles tend to agglomerate strongly which is problematic for many applications. Formed agglomerates could for example block blood vessels in biomedical applications or the advantage of large accessible surface area can be depressed for extraction applications. Nevertheless, this issue can be overcome by suitable surface modification.[87] The main problem with metallic nanoparticles among the ferromagnetic elements however is their chemical instability. Due to the large specific surface area, oxidation processes occur very rapidly. In fact, even spontaneous ignition of such nanopowders may occur. Therefore, suitable protection strategies are needed.
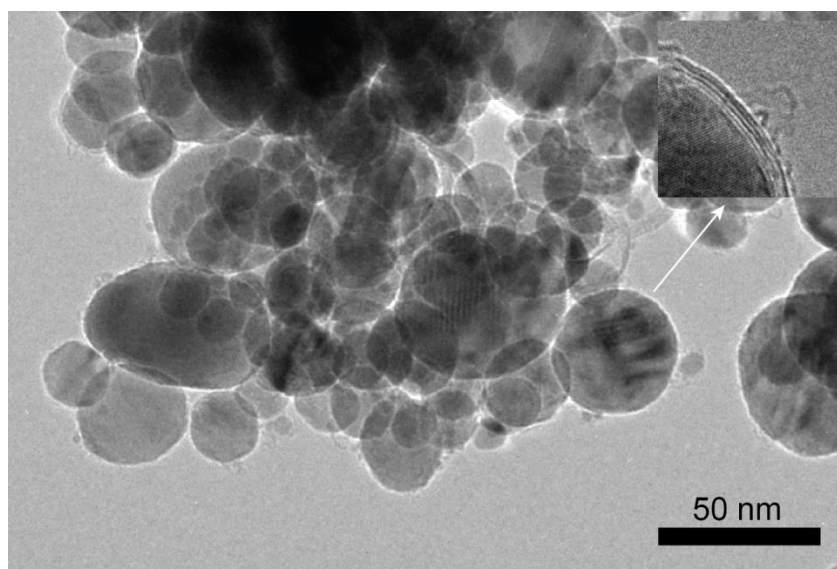
Figure 1.5: Transmission electron micrographs of carbon-coated cementite (Fe₃C) nanomagnets. The carbon-coating appears as a highly crystalline few-layer graphene structure and entails extraordinarily high chemical resistivity.

An early approach to stabilize for example cobalt nanoparticles rests upon partial oxidation of the metallic particle's outer shell under controlled conditions.[68] The resulting shell then protects the inner metal core from the environment. Under ambient conditions the stability of such particles is nevertheless temporally limited and when brought into aqueous solution they are prone to dissolution even under relatively mild conditions. Other protection methods by the use of polymeric surfactants[26] or silica-shells[88, 89] show better, but still relatively unsatisfying results. A very elegant way to protect the sensitive metal cores is to envelop them with a few layers of highly ordered graphite.[67] Despite such structures have been known for a considerable time,[66, 90-93] Stark et al. first presented a reducing flame spray pyrolysis approach

to fabricate this type of nanomagnets in expedient amounts.[67, 86] By additionally blowing acetylene into the reducing flame during particle production and taking advantage of the high temperatures to form well-ordered crystalline structures, they managed to obtain carbon-coated metallic nanocomposites with yet unachieved chemical resistivity.

1.4 Chemical modification of nanomagnets

Besides chemical stabilization, protecting surface layers create opportunities for specific functionalization.[94, 95] This entails specific binding to heavy-metal ions, toxins, cells or other surfaces.[15] The complexity of attached surface moieties can reach from basic groups (such as amines or sulfonic acids) to complex biological entities such as antibodies.[96] Since this thesis is widely focused on carbon-coated nanomagnets, the functionalization techniques for this type of surfaces are presented more in detail below.

An eligible way to covalently bind aromatic species to graphitic surfaces was initially suggested for stabilizing carbon-black in liquid solutions for ink-manufacturing. The simple method uses diazonium-salts which are known from the production of classic dyes.[97] Diazonium salts of aromatic species are usually unstable under room-temperature conditions and thus very reactive. With the exception of their corresponding tetrafluoroborate salts they can therefore only be created in-situ and in solutions. Nevertheless, this represents a convenient way to stably graft aromatic base species to carbon-coated nanomagnets by the formation of covalent carbon-carbon bonds.
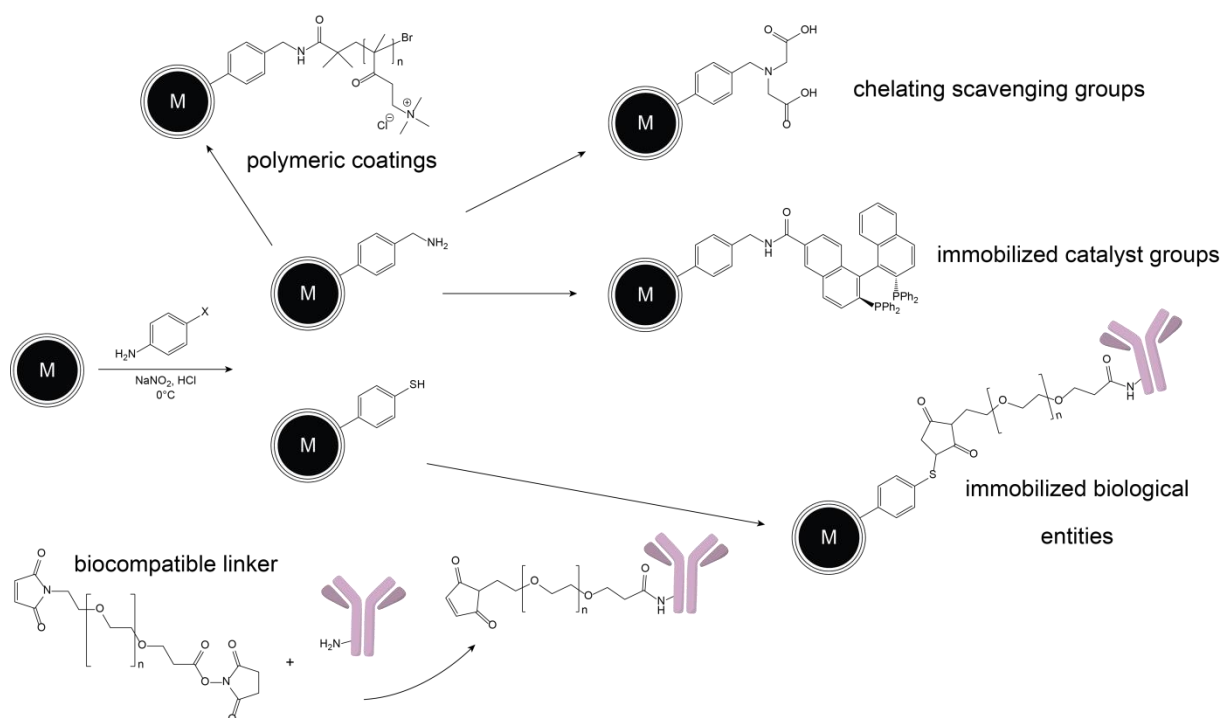
Figure 1.6: *Stable and covalent functionalization opportunities of carbon coated nanomagnets enabled by diazonium chemistry. Besides simple base and ion scavenging groups, complex structures as known from homogeneous catalysis, polymer science or biological entities can be conveniently engrafted.*

Typical functional loadings for simple aromatic species account for around 0.1 to 0.4 mmol per gram of particles (and thus a few weight percent of the magnetic nanomaterials). These functional groups form a powerful platform for more complex structures. Following a modular approach, homogeneous catalysts, polymers, chelating groups or biological entities can be stably attached.

1.5   Cutting, slicing and drilling on graphite surfaces

Besides functional modifications on the molecular sized level, more extensive structural changes at the nanoscale are of particular interest for semiconductor applications. Graphite is essentially assembled from numerous stacked carbon-layers in the form of polycondensated aromatic rings. A single isolated piece of these carbon layers is called graphene. Despite its simple structural character at first sight, graphene was never isolated for an experimental characterization before 2004.[98] Graphene combines superior electronic characteristics with ultimately small geometric extents.[99] Thus, it opens a whole universe for future applications.[100, 101] In 2010, the discoverers of graphene, Andre Geim and Konstantin Novoselov, were awarded the Nobel Prize in physics. The first isolated pieces of graphene were obtained by exfoliation of highly ordered natural or pyrolytic graphite. Despite the well-ordered character of the graphite, typical failure-free domains lie within several tens to hundreds of nanometers which is normally insufficient for semiconductor applications. Shortly after the discovery, new direct synthesis methods were demonstrated. The most prominent among them allows manufacturing of defect-free and micron-sized graphene sheets by the use of thermal carbon-deposition on copper foils.[102] Suitable transferring methods for conversion to semiconductor devices were presented along.[103] With respect to today's semi-conductor manufacturing, direct structuring of graphene or highly oriented graphite as a precursor material by means of controlled slicing and cutting into *i.e.* ribbons represents a key element towards technical employment.[104, 105] In addition, defined holes in graphene are potentially attractive for atmospheric nanoseparation[106-108] or the manufacturing of ion-selective membranes.[109]
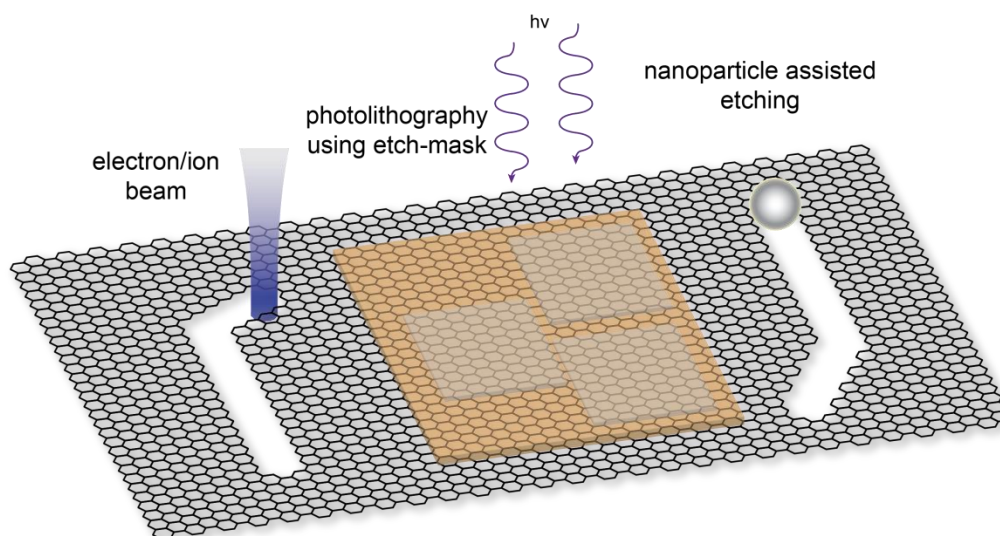
Figure 1.7: *Illustration of prominent graphene and graphite structuring techniques.*

Electron[110, 111] and ion-beam[112] as well as photolithography[113] represent well-established methods that are also suitable for specific tailoring of graphene sheets. Both electron and ion-beam techniques however suffer from low throughput paces and photolithography methods provide limited spatial resolution due to restrictions regarding optics for small wavelengths.

Nanoparticle and template assisted etching of graphitic surfaces represent attractive alternatives for graphene processing. Catalytically active noble metal nanoparticles have shown to be able to cut only one to few layer deep and usually crystallographically oriented traces into highly oriented pyrolytic graphite.[114, 115] Since the cuts appear within the size range of the particle size, this novel tool is most promising. Most of the presented studies use high temperatures above 700°C as well as inert or reducing conditions for etching. Alternatively, we described a method that allows cutting graphite at ambient atmosphere and comparable moderate temperatures (< 500°C) using cerium oxide nanoparticles.[9] This study is presented in detail in chapter 3.

1.6   Characterization of magnetic nanoparticles in biomedical samples

The field of nanomedicine allows fascinating perspectives towards new cancer-treatment strategies,[17, 48, 116-118] superior contrast agents,[119-121] and targeted drug-delivery by nanocarriers[18, 122, 123] or blood purification.[124, 125] Magnetic nanoparticles are prime candidates for this range of applications since direction and collection by external and tissue-pervading fields is facilitated. The required physicochemical characteristics for the nanomagnets are often comprehensive and specific. Various requirements such as good magnetic response quality, biocompatibility and chemical stability within the therapeutic timeframe have to be consolidated.[126] The main prerequisite of ferromagnetic characteristics limits the available material candidates to compounds involving the ferromagnetic elements iron, cobalt and nickel. However, since nickel and cobalt are known for miscellaneous adverse effects in biological systems, they are preferably avoided.[127] Iron, comparatively, is physiologically well accepted and thus the prime base material for medical nanomagnets. Besides general material based toxicity by means of *i.e.* leaching, risks can also arise from morphology, surface appearance and persistence. In the case of carbon-coated iron-carbide, which is featured in chapter 4, one of the potential hazards arises from its extraordinarily high chemical stability. Despite the fact that immunocompatible surface coatings facilitate much better acceptance by an organism, prolonged accumulation in certain body compartments can pose major risks.[128] Therefore, at the best, particles will not be given into the organism like for example in extracorporeal magnetic blood purification.[96] This technique suggests the use of specifically binding nanomagnets to remove especially larger drugs (at toxic concentrations) or inflammatory mediators from the blood circuit. This is particularly interesting for emergency medicine. Since the nanoparticles present readily available surfaces (no diffusion limitations), they enable rapid toxin removal within minutes (compared to hours for conventional blood dialysis). Nevertheless, magnetic separation could be insufficient or accidentally omitted. Hence, knowledge on the long term and the distribution behavior inside the body is a matter of consequences.

Tracing and quantifying low concentrated nanomagnets in body compartments represents a challenging task. Whereas non-quantitative characterization after reasonably short exposure times can be realized with passable effort, long-term characterization often turns out to be pretentious and strained with uncertainness. In view of the present limitations, the exploitation of novel analytical strategies is of particular importance. The attachment of fluorescent probes on the nanomagnet surfaces[129] for example is generally limited to shorter experimental times

since depletion of the latter may occur. Furthermore, this method is usually not quantitative. An advanced and elegant detection method rests on magnetic resonance imaging.[130] Magnetic materials strongly deviate from the behavior of the ambient organic matter and can therefore be well exposed by this technology. Magnetic resonance imaging has shown impressive spatial resolution of allocated nanomagnets within individual body compartments.[131] Unfortunately, reliable overall quantifications by this technique are prone to many error-sources. Besides magnetic measurement techniques such as vibrating sample magnetometry, more classical approaches such as elemental analysis offer major benefits. For iron-based nanomagnets this nevertheless turns out to be cumbersome since practically any body compartment presents relatively high concentrations of iron. Hence, the iron-background would considerably surmount the iron contribution of the nanomagnets and therefore compromise reliable quantification. A key advantage of the earlier presented flame spray pyrolysis for the manufacturing of magnetic nanoparticles is the opportunity to dope certain elements into the materials. Like this, an element which is normally not present in the body can incorporated into the nanomagnets at well-defined low proportions without changing their physicochemical behavior noticeable. This element can then be quantified after long time frames and uniquely be assigned to the nanomagnets. In chapter 4, the detailed development and validation of this new quantification approach based on platinum doping is presented.[26]
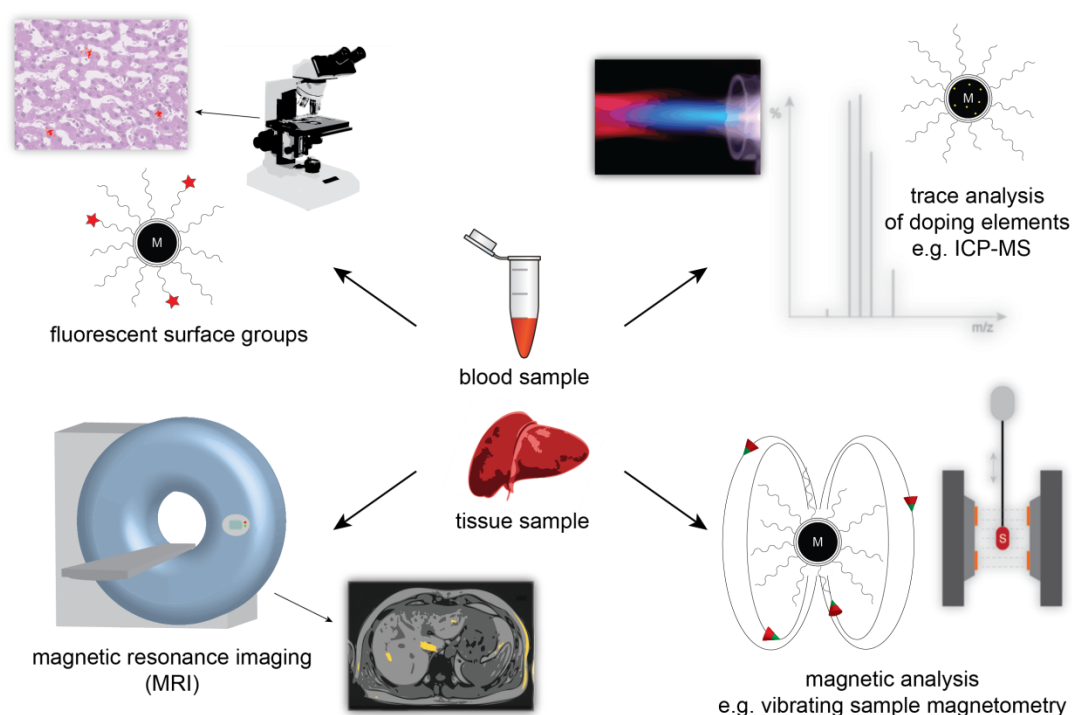
Figure 1.8: Illustration of widely used analytical approaches to quantify low concentrated nanomagnets in complex biological media such as blood or tissue.

2. Physical Defect Formation in Few Layer Graphene-like Carbon on Metals: Influence of Temperature, Acidity and Chemical Functionalization
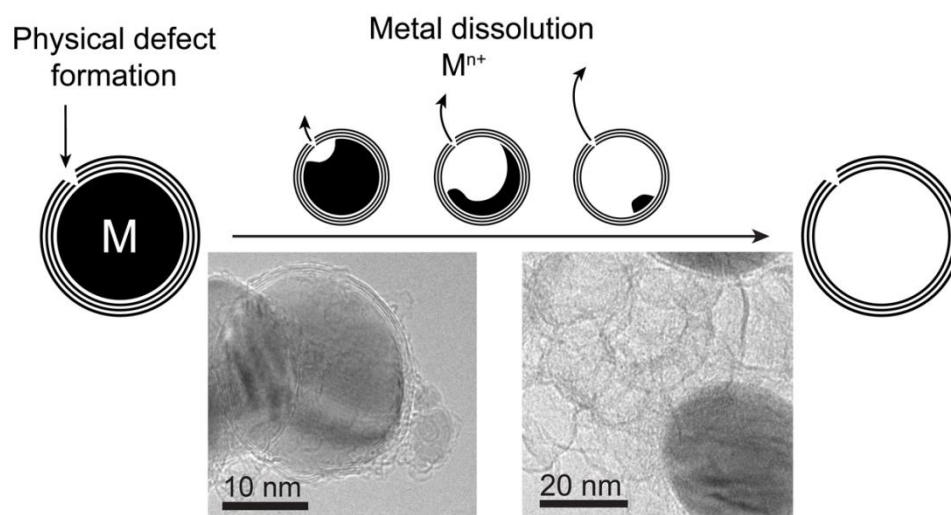
Published in parts as:

Christoph M. Schumacher, Robert N. Grass, Michael Rossier, Evagelos K. Athanassiou and Wendelin J. Stark

Abstract

A systematical examination of the chemical stability of cobalt metal nanomagnets with a graphene-like carbon coating is used to study the otherwise rather elusive formation of nanometer sized physical defects in few layer graphene as a result of acid treatments. We therefore first exposed the core-shell nanomaterial to well controlled solutions of altering acidity and temperature. The release of cobalt into the solutions over time offered a simple tool to monitor the progress of particle degradation. The results suggested that the oxidative damage of the graphene-like coatings was the rate-limiting step during particle degradation since only fully intact or entirely emptied carbon-shells were found after the experiments. If ionic noble metal species were additionally present in the acidic solutions the noble metal was found to reduce on the surface of specific, defective particles. The altered electrochemical gradients across the carbon-shells were however not found to lead to a faster release of cobalt from the particles. The suggested mechanistic insight was further confirmed by the covalent chemical functionalization of the particle surface with chemically inert aryl species, which leads to an additional thickening of the shells. This leads to reduced cobalt release rates as well as slower noble metal reduction rates depending on the augmentation of the shell thickness.

2.1   Introduction

The use of few layer graphene-like carbon (2-5 layers) as a coating on metal nanoparticles provides stability against air, water and common biological or reaction media.[34, 86, 132, 133] Today, such core/shell metal/carbon composite nanoparticles extend the applications of magnetic nanoparticles in catalysis,[38, 134, 135] water treatment[136-138] and enable the preparation of magnetic chemical reagents allowing rapid separation to facilitate everyday lab work.[139, 140] In medicine, they have been proposed for blood purification,[125, 141] drug delivery,[142-144] in cancer treatment[117, 145-147] or as contrast agents.[148, 149] Long-term reliability and design of novel magnetic reagents requires a detailed understanding of the stability of such carbon coatings. Unfortunately, associated physical defects, that are missing carbon atoms within the highly ordered layers, are most probably below 1 nm in size, and the nanoparticle's curvature makes them difficult to observe by classical methods such as atomic force microscopy (AFM). Moreover, statistically meaningful experimental observation of thousands of nanoparticles preferably *in situ* is most challenging.

Here, we therefore investigate the effects of temperature, acidity and redox-active metals on the degradation of few layer graphene-like carbon shells with a metallic cobalt core. This model compounds provide an elegant way to follow the degradation of the about 1 nm carbon coatings: If the carbon shell surrounding a single metal nanoparticle (5-50 nm diameter) is chemically degraded at one spot, the metal core oxidizes very fast, and is emptied into the surrounding solution, releasing metal ions. This strategy therefore allows a systematic study of nanometer sized physical defect formation rate in such few layer graphene-like carbon.

Physical defect formation and the metal core destruction process are formally oxidation reactions. Next to temperature and pH, we therefore systematically investigated the effects of additional metal ions with increasing electrochemical potential as potential reaction partners during this oxidative destruction process. If noble metal ions are used, the carbon and metal core oxidation will result in noble metal reduction and deposition (*e.g.* Pt, Pd or Au metal).[150]

The necessary electron transfer from the particles to the solution was further investigated with regards to possible explanations using Marcus theory. The distance of the solution to the carbon surface was systematically modified using redox-inert phenyl substituents as spacers by covalent chemical carbon shell functionalization.[67]

2.2   Experimental

2.2.1   Preparation of carbon coated cobalt metal nanoparticles

The starting carbon coated cobalt nanoparticles were either prepared according to[67] or purchased (Nanostructured & Amorphous Materials, Inc.). In order to remove oxide impurities, a starting sample of 25 g C/Co with an average size of 17 nm was kept in 400 mL partially diluted hydrochloric acid (24 wt% HCl) for two weeks whilst exchanging the acid every day.[150] The particles were carefully washed with deionized water (3 x) and acetone (3 x). This washing procedure was applied after all functionalization steps (see below) to remove remaining reagents. The black powder was dried under vacuum at 50 °C and is further denoted as C/Co.

Severe oxidation by HNO_3/HCl

In order to probe the maximum degree of defect formation by oxidation, a fraction of 2.00 g C/Co was further exposed to 60 mL of concentrated aqua regia (3 parts concentrated hydrochloric acid, 1 part concentrated nitric acid) in a 100 mL roundneck-flask at 100 °C under reflux conditions. The stirred dispersion was retained until no further nitrous gas formation took place and was then replaced by freshly prepared aqua regia after typically 2 hours. This procedure was repeated until there was no further colorization of the acid caused by cobalt dissolution. Only the most resistant fraction of the particles endures this treatment. After this, the material was washed and dried in the same manner as mentioned before. The resulting particles had a black color and are further denoted as C/Co-HNO_3/HCl.

2.2.2   Chemical functionalization

The carbon-shells were modified by the covalent attachment of aromatic functional groups using aqueous diazonium chemistry.[67]

Iodobenzene functionalization -($C_6H_4I)_n$. A sample of 0.88 g 4-iodoaniline (4 mmol, Aldrich) was added to 60 mL of water and 2 mL of fuming hydrochloric acid (Sigma-Aldrich). After adding 1.00 g C/Co, a total of 0.42 g sodium nitrite (6.1 mmol, Fluka) in 10mL of water was added. Nitrogen bubble formation confirmed the start of the reaction between the in situ formed iodo-phenyl-diazonium species and the particle carbon surface. The reaction mixture was kept well mixed overnight, then washed as described above.

Pentafluorobenzene functionalization -(C₆F₅)ₙ. A total of 0.37 g pentafluoroaniline (2 mmol, ABCR) was added to 60 mL of water and 1 mL fuming hydrochloric acid (Sigma-Aldrich). The mixture was sonicated for 5 min (Sonorex Digitec DT 103 H, 560 W, Bandelin) for full dissolution. After adding 1.00 g of C/Co, a solution containing 0.23 g sodium nitrite (3.3 mmol, Fluka) in 10 mL water was added resulting in a bright yellow coloration. The solution was mixed well and kept overnight, then washed as described above. This preparation was done a second time with doubled amounts of educts (aniline and nitrate) to prepare a second material with a different functional loading (moles functional group per mass of particles; typical units are in millimoles per gram material).

Nonafluorobiphenyl functionalization -(C₁₀F₉)ₙ. A sample of 0.66 g 4-aminononafluorobiphenyl (2 mmol, Matrix-Scientific) in 60 mL of water and 1 mL of fuming hydrochloric acid (Sigma-Aldrich) was brought in solution by strong sonication using a sonotrode (UP400S, 24 kHz, Hielscher GmbH). After adding 0.23 g of sodium nitrite (3 mmol) a light yellow coloration confirmed the formation of the corresponding diazonium salt. Subsequently 1.00 g C/Co was added, followed by repeated brief sonication (3 times 10 seconds). The reaction mixture was stirred overnight and the material was washed thrice, using the following series of solvents: Water, acetone, hexane, acetone, water and acetone before being dried. IR spectroscopy and element analysis were used to confirm the absence of adsorbed reaction remainders.

2.2.3   Material characterization

The specific surface area of the produced materials was determined according to the BET – method (Brunauer Emmett Teller) by adsorption of nitrogen at -196 °C. The surface functionalization was verified by diffuse reflectance infrared Fourier transform spectroscopy (DRIFTS) with KBr powder containing 5 wt% of particles (Tensor 27 Spectrometer, Bruker DiffusIR™, Pike technologies) as proposed by.[67] Untreated C/Co in KBr (5 wt%) was used as a background. For the quantification of the surface functionalization, quantitative element microanalysis was used (LECO CHN-900 for C, H, N and F, I by Schöniger oxidation) as previously described.[151] To image the particles, transmission electron microscopy (TEM) micrographs were recorded (Tecnai F30 ST, FEI, operated at 300 kV).

Physical defect formation rate. In typical experiments, a systematic series of particle samples (10 mg in a total reagent volume of 10 mL) were first dispersed (high-speed mixer; Ultra-Turrax, T10 basic, 125 W, IKA; external cooling) and removed after 30 s, 1, 2, 5 and 10 min. The particles were immediately separated magnetically from the solution (few seconds) and physically removed to avoid entrainment of later released metal. The metal concentration in the clear solutions was determined using flame atomic absorption spectroscopy (Spectra AA 220FS, Varian).

pH dependence. The defect formation rate was assessed at 6 different pH levels, namely from 1 - 5 and 7 by measuring the cobalt core metal release. The solutions with pH 1 and 2 were obtained by diluting hydrochloric acid with deionized water. All other solutions, except for the neutral run, were 0.1 M potassium biphthalate buffered. Previous control experiments had shown that the concentration of this buffer does not significantly influence the metal release rate. In contrast, acetate buffered solutions were found unsuitable. Buffered solutions ($\geq$ pH 3) are required in order not to fully consume the acid by core material dissolution and therefore causing large variations in the acidity of the solutions during an experiment. The pH was controlled after each experiment and confirmed to stay within $\pm$0.1 pH units.

Temperature dependence. To determine the temperature dependence of the leaching, the solutions were conditioned in a temperature regulated water bath or ice/water mixtures at a constant pH 2 using pre-adjusted diluted hydrochloric acid. Five different cobalt concentration profiles were recorded at 0, 23, 40, 60 and 80 degrees Celsius.

Functionalization – changing the metal core to solution distance. All comparative experiments were done at pH 2 and room temperature using the same parameters as outlined above.

Influence of electrochemical potential. Physical shell defect formation and resulting cobalt core metal oxidation was probed in the presence of noble metal ions (Au, Pd, 100 µg per mL). The rate of defect formation was again followed by a change in released cobalt ions (a) and, additionally, by measuring the remaining free noble metal ion concentrations (b). Solutions were prepared from standard solutions for atomic absorption spectroscopy (TraceCert®, Fluka) adjusted to a pH of 2.0 by addition of 1 M KOH solution. Experiments were done at different pH levels and with optionally functionalized materials. The influence of noble metal ions was made more visible in specific experiments where an additional 10 mL of Au solution was injected after 5 minutes.

2.3   Results and discussion

A carbon coated metal nanoparticle must form a physical shell defect before the metal core can start disintegrating as shown in Scheme 2.1. Depending on the individual step rates (k_1 and k_2), the metal dissolution rate (overall observable) either reflects effect of the physical defect formation in the shell (k_1 is slow, hence determines the overall rate of particle destruction) or the subsequent metal core oxidation and leaching through the defect out of the particle. Direct migration of cobalt metal atoms through the carbon shell is too improbable under the experimental conditions and will therefore not be considered further.[152, 153] Such metal migrating through intact shells was only observed under elevated temperature (> 600 °C) or under electron irradiation.[91, 154, 155]

In a first part, the physical results will be discussed as to determine which step is rate limiting (shell defect formation rate or the metal core dissolution and leaching rate). In a second part, the observable metal core dissolution rate is discussed in view of potential mechanism and the role of standard parameters (pH, electrochemical potential difference over the shell, temperature).
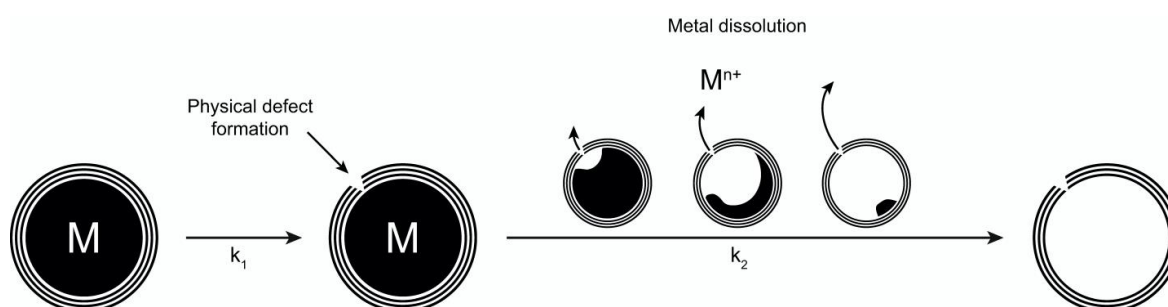
Scheme 2.1: *Subsequent steps during a particle disintegration, formation of a hole in the carbon layer (rate constant k_1) and cobalt core dissolution (rate constant k_2).*

2.3.1   Physical properties of C/Co nanoparticles

Electron micrographs confirm the C/Co material to consist of 5-50 nm sized core/shell particles with close to spherical geometry. The integrity, crystalline structure and purity of the core (absence of cobalt oxide) was confirmed by X-ray powder diffraction (XRD) revealing face centered cubic (fcc) metallic cobalt. The specific surface area (SSA) of the materials was measured by the BET-method using nitrogen adsorption at -196 °C[156] and yielded a mean, surface-equivalent nanoparticle diameter of d_{BET} = 17 nm which stays in agreement to the optically determined particle size (Figure 2.1).
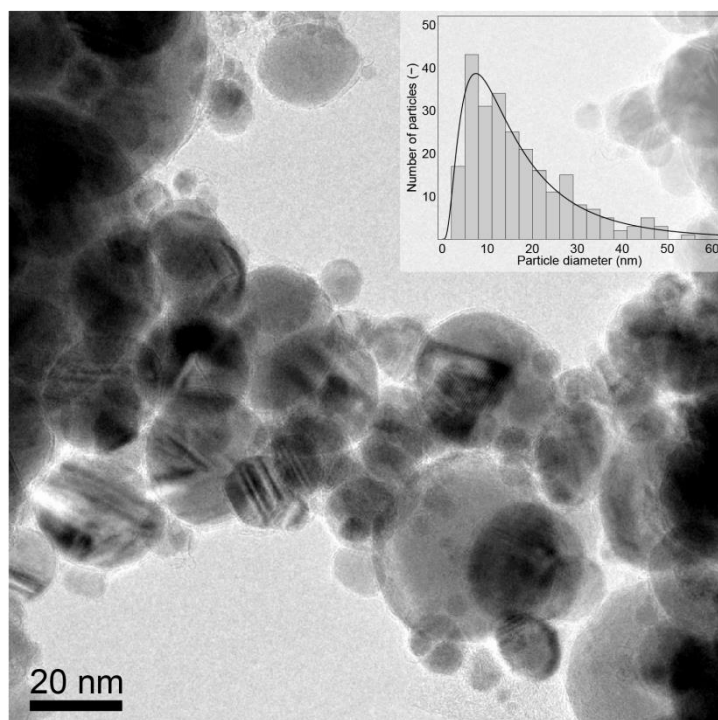
Figure 2.1: TEM micrograph of nearly spherical C/Co showing particles in the size range from 5-50 nm.

For all samples, the detailed surface structure (chemical functionalization) was measured by diffuse reflectance infrared Fourier-transform spectroscopy (DRIFTS). Spectra were compared to known reference compounds in Figure 2.2.[67] Element microanalysis was used to determine the number of covalently attached molecules per particle mass using a simple mass balance (C, H, N, F and I contents before and after derivatization). The physical properties of all materials are summarized in Table 2.1.
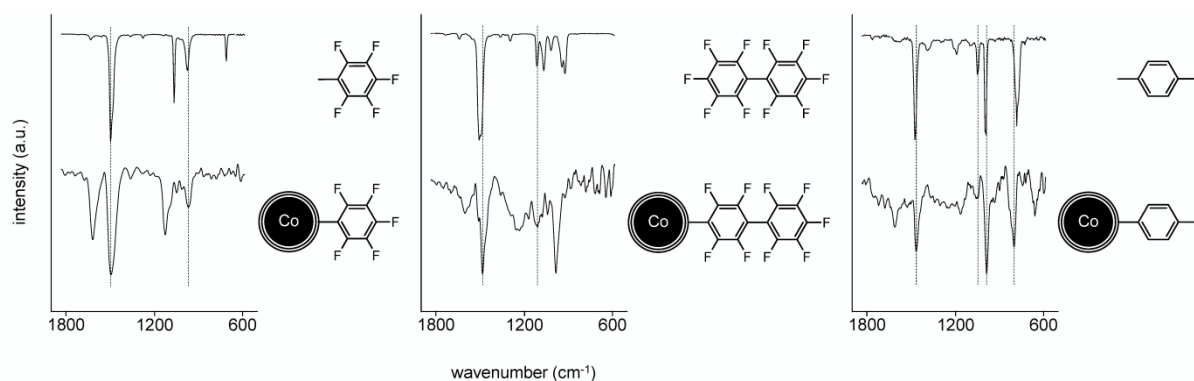
Figure 2.2: Diffuse reflectance infrared Fourier-transform spectra (DRIFTS) of the chemically functionalized C/Co and structure confirmation through comparison to known reference compounds. Minor peak shifts and intensity changes are a result of binding to the carbon surface layer and changes in molecular symmetry.

Table 2.1: *Physical properties of C/Co nanomaterials.*

treatment/ functionalization	Carbon (wt%)[a]	Halogen (wt%)[b]	Loading (mmol/g)[c]	specific surface area (m²/g)[d]
none	3.1	-	-	40
24 % HCl, 2 weeks	5.2	-	-	32
conc. HNO$_3$/HCl	15.8	-	-	26
-(C$_6$F$_5$)$_n$ high	5.7	0.96 (F)	0.10	27
-(C$_6$F$_5$)$_n$ low	5.7	0.72 (F)	0.08	32
-(C$_{10}$F$_9$)$_n$	6.0	0.75 (F)	0.04	36
-(C$_6$H$_4$I)$_n$	6.1	1.87 (I)	0.15	24

[a], [b] Carbon, fluorine and iodine content determined by element microanalysis. [c] Specific chemical functionalization loading calculated from fluorine content, respectively iodine content. [d] Specific surface area measured by nitrogen adsorption; errors ±10%.

2.3.2   Physical defect formation limits metal dissolution rate

Morphological evaluation of C/Co powders after a broad set of acidic treatment conditions (variations in time, temperature, acid strength and type) using TEM revealed only two types of particles: Intact C/Co nanoparticles with a high electron contrast core (metallic cobalt as confirmed by energy dispersive X-ray spectroscopy) and empty carbon shells (Figure 2.3). None of the treatment conditions resulted in the possibility to observe partially filled shells (Scheme 2.1) even after evaluating larger particle sets. If k_2 would be partially or fully determining the overall rate of metal core dissolution, the intermediate forms (partially filled shells) would be observable. In contrast, the absence of any partially filled shells and exclusive presence of either full (integer) or empty carbon shells proofs that the physical defect formation in the shell (k_1) is rate determining. After severe treatment with HNO$_3$/HCl, the average diameter of the intact particles turned out to be significantly higher according to the determined particle size distribution compared to the as-prepared material. A possible

explanation for this observation could be the magnitude of the shell curvature which influences the chemical durability. This means that the defect formation rate is increased on smaller particles, which makes them dissolve more readily.
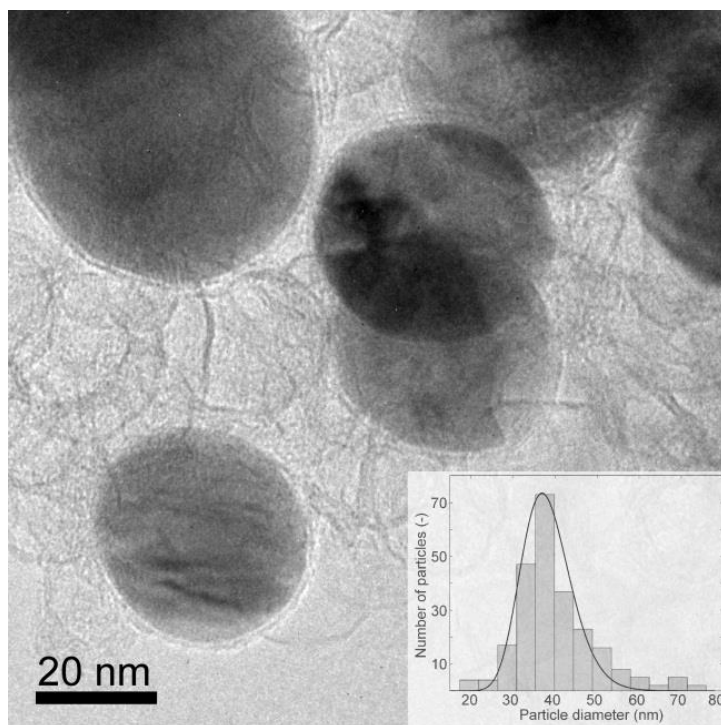
Figure 2.3: *TEM micrograph of HNO₃/HCl treated nearly spherical C/Co showing fully carbon-coated particles as well as a considerably large fraction of empty carbon shells resulting from the dissolution of the magnetic cores. The particle size distribution is shifted compared to the as-prepared C/Co due to the faster defect formation rate of smaller particles.*

In order to determine the degree of carbon loss during above shell defect formation, we quantitatively determined the amount of carbon in a specific sample of C/Co before and after a number of treatments (Table 2.2). No statistically relevant carbon loss was observable. The following discussion therefore assumes that the shell defect formation did not afford a carbon loss. During experimentation, the strong agglomeration tendency of these materials allowed quantitative material recovery (> 98 % by mass) at each step as confirmed gravimetrically.

Table 2.2: *Experimental and theoretical carbon content*

treatment	sample mass (g)[a]	carbon content (wt%)[b]	calculated carbon content (wt%)[c]
none	25.02	3.1	-
24 % HCl, 2 weeks	13.68	5.2	5.6
conc. HNO$_3$/HCl	4.45	15.8	16.0

[a] Determined ±0.01 g [b] Carbon content determined by microanalysis ±0.2 wt%. [c] Calculated from sample masses, assuming no carbon loss by acidic treatment.

2.3.3 Influence of pH and temperature

The rate of physical defect formation and subsequent fast metal release was followed over time by determination of the cobalt concentration in the used solutions (Figure 2.4). Increasing acidity and higher temperature both afforded faster metal release (Figure 2.4a, b). The metal release rate depends on the pre-treatment. If a sample had previously survived a harsh treatment (*e.g.* conc. HNO$_3$/HCl), it afforded an about 5 times reduced metal release (Figure 2.4c). Application of severe mechanical stress (grinding) to such comparably stable sample strongly increased its initial metal release rate (Figure 2.4c; sample C/Co-HNO$_3$/HCl, grinded) while the profile rapidly leveled off.
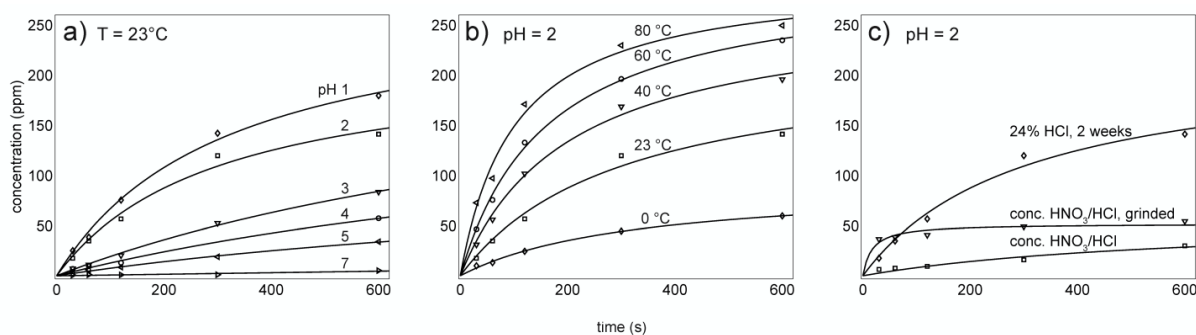
Figure 2.4: *Cobalt concentrations in leaching solutions show the C/Co particle dissolution rate as a function of pH (a) and temperature (b). Samples from previous treatments in strongly oxidizing conditions (conc. HNO$_3$/HCl) showed reduced metal dissolution (c) while mechanical treatment can increase the metal release rate.*

2.3.4   Electronic/redox effects on few layer graphene shell degradation

Physical defect formation as an oxidative destruction of the few layer graphene may depend on the subsequent metal core oxidation ($Co \rightarrow Co^{2+/3+}$). In this case, the use of coupled redox reactions to enhance or reduce the electrochemical potential between inside (metal cobalt core) and outside of the carbon shell would result in altered defect formation rates. Alternatively, the carbon shell degradation may be largely independent and thereby control the overall kinetics (see Scheme 1 with $k_1 << k_2$).

In order to probe electrochemical effects, carbon/cobalt nanoparticles were exposed to altered electrochemical gradients by introducing noble metal ions into the exposure solution. The overall gradient across the carbon shell can then be calculated using standard concepts from electrochemistry (Table 2.3). Time dependent cobalt release profiles (Figure 2.6b) afforded little change in the final metal release (Table 2.3). This result stays in line with the earlier absence of partially filled shells (Figure 2.3) and the possible cases for rate determining steps (k_1 vs. k_2; Scheme 2.1).

Table 2.3: *Shell thickness increase by chemical functionalization, final cobalt concentrations in acidic solutions and electrochemical potential gradients over particle shells*

treatment/ functionalization	loading (mmol/g)	shell thickness increase (nm)[a]	final cobalt concentration in solution after 10 minutes (ppm)
none	-	-	-
24 % HCl, 2 weeks	-	-	141 / 120[b]
24 % HCl, 2 weeks, Au reduction	-	-	- / 104[b]
conc. HNO$_3$/HCl	-	-	30
-(C$_6$F$_5$)$_n$ high	0.1	0.46	24
-(C$_6$F$_5$)$_n$ low	0.08	0.31	34
-(C$_{10}$F$_9$)$_n$	0.04	0.20	51
-(C$_6$H$_4$I)$_n$	0.15	0.80	13

reduced metal	electrochemical potential gradient (V)[c]
Au	1.30
Pd	0.86

[a] For calculation see supporting information [b] cobalt concentration after 5 minutes [c] For calculation see supplementary material.

In a second series of experiments, we further probed this reaction by systematically altering the shell through controlled chemical modification. This formally results in an altered shell thickness. If considering Marcus theory, such changed mean distance formally corresponds to an altered electron transport distance out/inside of a metal complex, if we consider a core metal atom as part of a complex with the carbon shell serving as a space-providing ligand. Corresponding chemical modifications are given in Figure 2.2 and increase shell thickness by 0.2 to 0.8 nm for nonafluorobiphenyl, pentafluorophenyl and iodophenyl groups using microanalysis data as earlier described.[86]
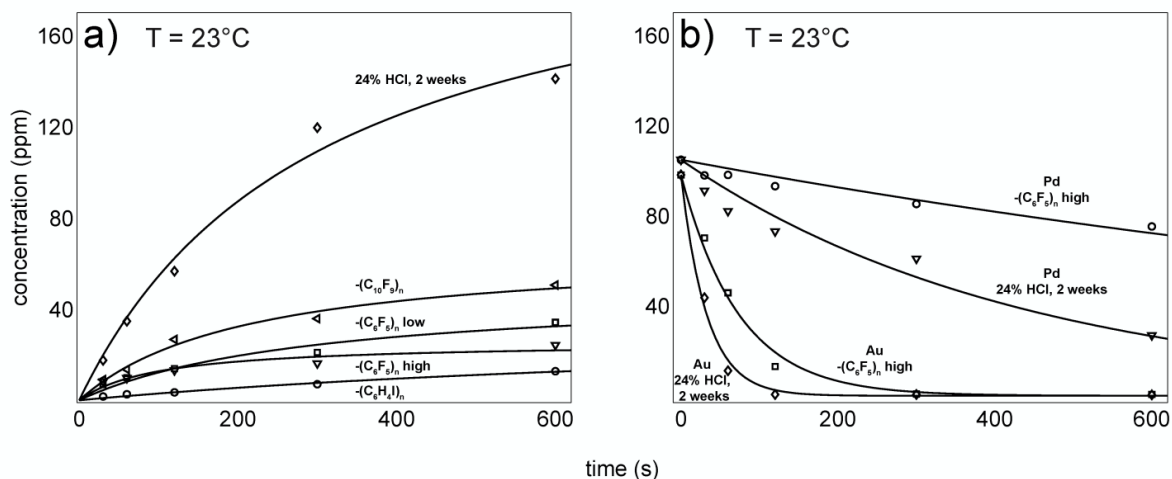
Figure 2.5: *(a) The influence of the chemical surface functionalization on the leaching rate of cobalt into the acidic solution at pH 2. The higher the functional loading the lower is the cobalt loss over time. The type of functional group is however not affecting the leaching rate. (b) Extraction performance at pH 2 of ionic gold and palladium on C/Co as well as C/Co-$(C_6F_5)_n$.*

Table 2.3 gives the altered shell thickness and the corresponding altered final metal release. The rates were found to strongly depend on the chemical functionalization, but the overall trends are complicated by the experimental limitations of different surface loadings (material specific differences).

Using both effects (electrochemical gradients and shell thickness), carbon shells with additional functionalization were found to afford reduced metal release rate, as expected from above experiments (Figure 2.5). As a further confirmation on the carbon shell's largely independent physical defect formation rate (*i.e.* the core metal is of minor influence), samples of C/Co were treated under altered electrochemical gradients ($PdCl_4^-$, $AuCl_4^-$, as an oxidant). The overall electrochemical potential over the few layer graphene shells was systematically altered through the presence of $AuCl_4^-$ in the solution and the pH since the potential can be described using the Nernst formalism (see supporting information for detailed calculations).

Figure 2.6c gives the corresponding rapidly falling ionic gold concentrations due to reduction to metallic gold (see scanning electron micrograph and energy-dispersive x-ray spectra in Figure 2.6d) as a result of the electron release to the solution around the carbon coated metal particles. Again, the here discussed mechanism of individual, rapid single particle decomposition ($k_2 \gg k_1$) is confirmed through these experiments as the reduced metallic gold is found as discrete, relatively large particles (Figure 2.6d, area 1). For a potential alternative

mechanism (slow, continued degradation and release of the core metal; $k_2 < k_1$) the deposited metallic gold after reduction would be expected to be scattered across all agglomerated particles. The accompanying cobalt ion release into the solution (Figure 2.6b) was in the range of the previous experiments without additional oxidant (see Figure 2.5a) and thereby again independently confirmed the rate determining role of shell defect formation. The experiments were done using two consecutive oxidant additions ($AuCl_4^-$ was added at time t = 0 and t = 300 s) and the change in cobalt release rate (Figure 2.6b) can largely be assigned to the associated dilution effect (see experimental description). The gold reduction (and accompanying cobalt core oxidation) showed a similar pH dependence as when particles were only treated in acid (see Figs. 2.6c and 2.4a).
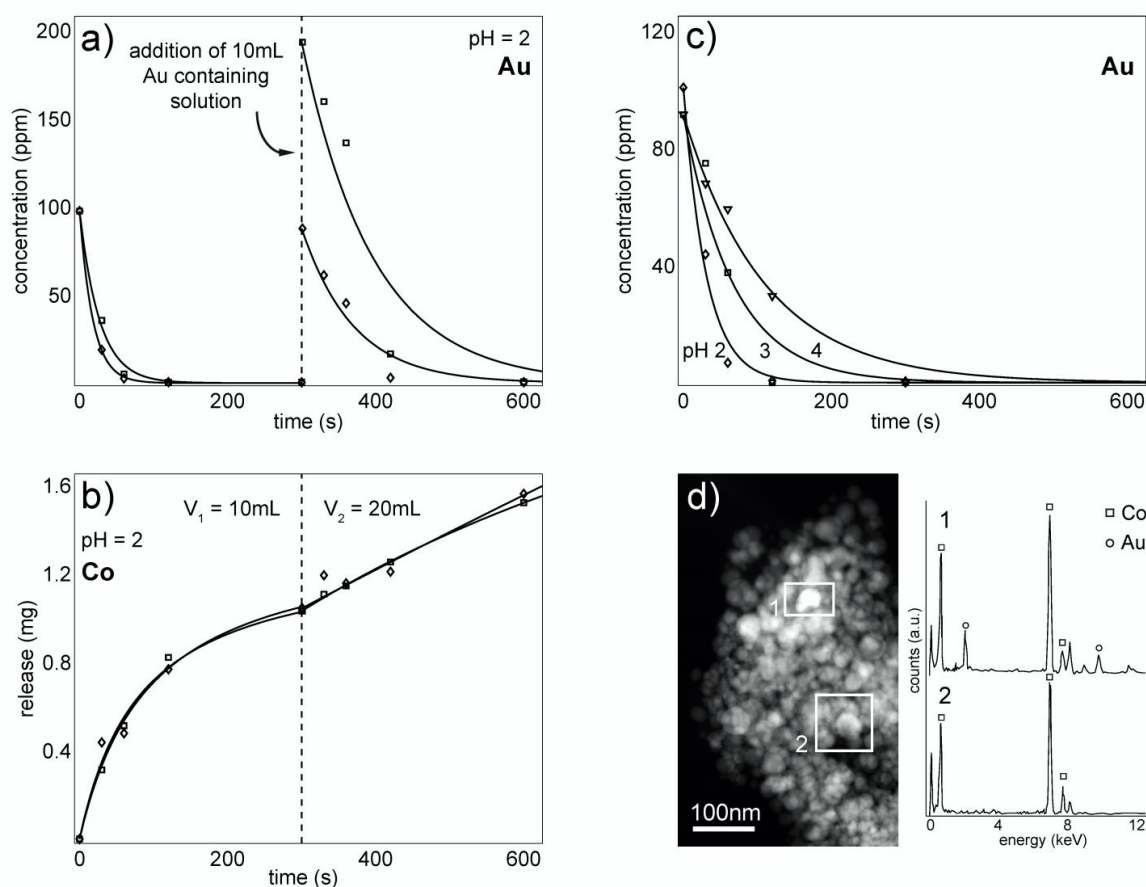
Figure 2.6: *(a, b) Two consecutive $AuCl_4^-$ additions at t = 0 and 300 s do not significantly alter the particle degradation (compare to figure 4). (c) Changes in acidity results in the alteration of the gold extraction rate as the particle degradation rate is lowered. (d) Addition of $AuCl_4^-$ solution increases the electrochemical potential across the few layer graphene and affords Au metal deposition as confirmed by high angle annular dark field scanning transmission electron microscopy (HAADF-STEM) and EDXS (Energy dispersive x-ray spectroscopy).*

2.3.5 Spectroscopic observations on the few layer graphene shell degradation

Carbon shell degradation as a partial, local oxidation was followed by diffuse reflectance IR spectroscopy (Figure 2.7) before and after acid treatment (24 wt% HCl) and after severe acidic/oxidizing conditions (conc. HNO_3/HCl). The treatments afford clear signals in the range of O-H stretch vibrations around 3400 cm^{-1} as well as C=O vibrations at 1650 cm^{-1}. The latter implies that holes in the graphene layers are generated as double bonds to oxygen require the breakage of C-C bonds within the carbon network. The treatment with strongly oxidizing concentrated HNO_3/HCl lead to even stronger IR-signals suggesting a higher degree of oxidation. These observations are in agreement with previous work[157, 158] displaying similar results for carbon nanotubes and core-shell materials manufactured by microwave irradiation.[159]
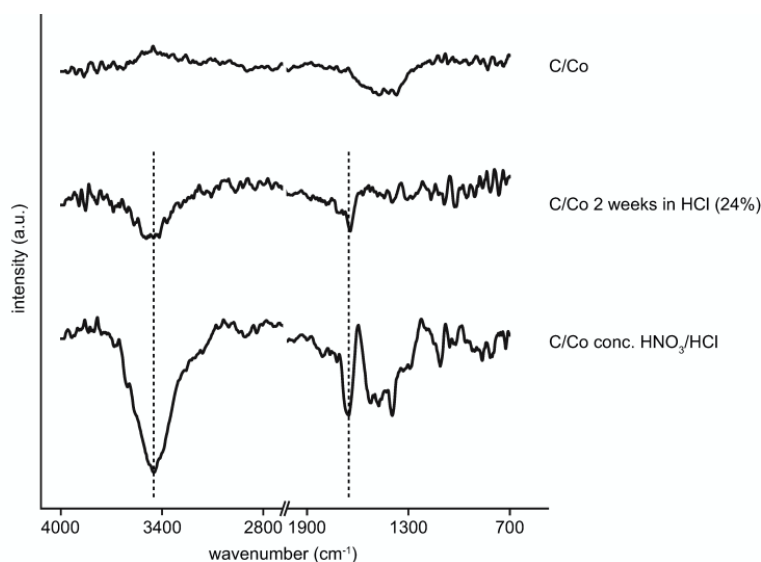
Figure 2.7: *Diffuse reflectance IR spectra of as prepared and acid-treated particles. The presence of C=O and O-H stretch vibrations implies the presence of a partial oxidation on the particle surfaces and stays in agreement with IR spectra of oxidized carbon nanotubes.[157]*

2.3.6 Physical defect density on shells

Above spectra confirm qualitatively the appearance of oxidized areas in the carbon shell (*i.e.* physical defects) but fail to provide any quantitative understanding on the degree of oxidation. Two experimental facts can be used in this regard: A) The gravimetrically measured carbon loss (Table 2.2) is smaller than 2 wt% (*i.e.* the accuracy of the measurement). B) Chemical functionalization using diazonium chemistry leads to the

presence of benzene-like structures on the outermost graphene plane.[160, 161] The molecule density (*i.e.* attached phenyl moieties per surface area) achievable on untreated or acid treated carbon coated particles is similar. A difference of more than 0.01 mmol per gram of nanomaterial would be detectable. Combined with the original hypothesis (Scheme 1; $k_1 \ll k_2$), these two facts refine our insight into the few layer graphene shell degradation and underline the mechanistic view that physical defects are few (on a single particle) and cover a negligible surface area.

2.4   Conclusion

The here provided systematic investigation on the degradation rate of carbon coated metal nanoparticles provides a quantitative insight into the formation of physical defects in few layer graphene when exposed to chemically demanding conditions. A series of independent arguments confirmed a shell degradation mechanism where a single defect results in a break-through and subsequent fast dissolution of the metal core. This affords emptied carbon shells with presumably a single physical defect (*i.e.* an opening). This understanding and the associated possibility to prepare well defined shells or containers may provide attractive tools to material sciences.

3. Nanoparticle-assisted, Catalytic Etching of Carbon Surfaces as a Method to Manufacture Nanogrooves
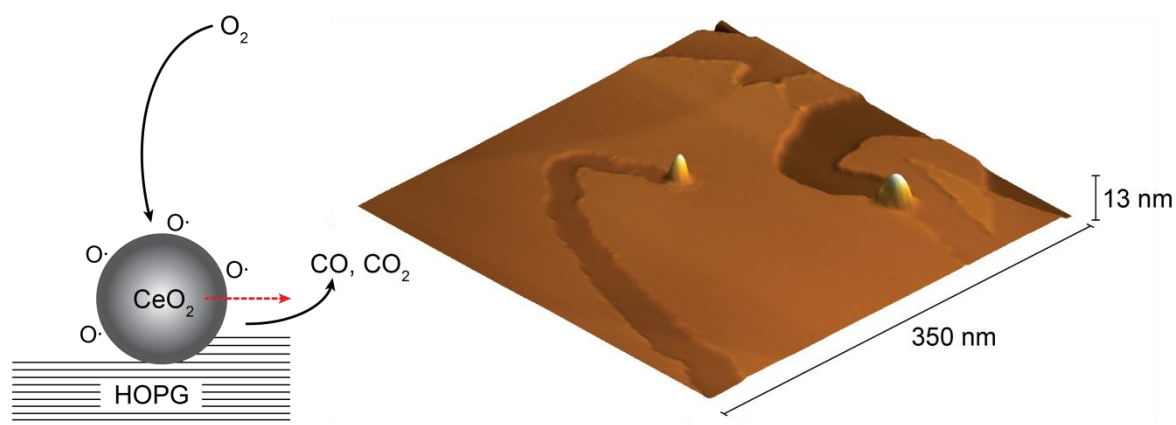
Published in parts as:

Christoph M. Schumacher, Fabian M. Koehler, Aline C. C. Rotzetter, Renzo A. Raso and Wendelin J. Stark

Abstract

A simple structuring method for graphitic structures based on the catalytic properties of cerium oxide nanoparticles under oxidizing conditions is presented. Highly oriented pyrolytic graphite chips were impregnated with well dispersed ceria nanoparticles and then treated at elevated temperatures for several hours. Oxidation activities on the particle surface appeared as crystallographically independent traces which were formed on the graphite and provide a simple method to manufacture nano-grooves at large scale. By altering treatment durations and temperatures, the optimal conditions and activity parameters of the particles were determined. A systematic AFM evaluation allowed formulating of a mechanism of the etching process. The findings provide a simple procedure for the patterning of graphitic structures, formation of nano-grooves and thereby a basic tool for material science with respect to the manufacturing of atmospheric nano-filters and ion-selective membranes.

3.1   Introduction

Highly oriented pyrolytic graphite is the base material from which graphene was derived at first[98] and today provides fascinating perspectives for semiconductor applications,[104, 162] ultracapacitors,[163] transparent electrodes[164, 165] or novel solar cell materials.[166, 167] The possibility to produce large-area graphene on copper foils and defect-free structures at the macro-scale[102, 111] has resulted in a shift of focus towards target-oriented structuring for tailoring physical properties.[168-170] Fundamental mechanical operations such as drilling, cutting, slicing and folding at the nanometer scale are at the core of manufacturing and largely unsolved at present. Moreover, controlled formation of small physical defects or cuts in carbon layers prospects for attractive use of graphene beyond electronics, namely in atmospheric nanofiltration[106, 108, 171, 172] and low-resistance ion-selective membranes.[109]

Next to electron / ion beam and plasma etching approaches,[112, 173-175] nanoparticle assisted lithography of highly oriented pyrolytic graphite and graphene structures represents the most significant contingent of the activities so far.[114, 176] Using reducing conditions and elevated temperatures, most of the present work relies on metal nanoparticles to etch crystallographically guided pathways through carbon layers.[115, 177-181] Noble metal particles under oxidizing conditions have been reported to show a similar, however not crystallographically directed etching behavior.[182, 183]

Catalytically active oxides (*e.g.* cerium oxide) are used for the removal (oxidation) of soot particles and carbon monoxide in the exhaust system of vehicles and as a material class, may provide interesting candidates for oxidative structuring of carbon layers. Here, we present and systematically investigate a simple nanolithography method on highly oriented pyrolytic graphite (HOPG) using cerium oxide nanoparticles under atmospheric conditions and elevated temperatures. We first scattered cerium oxide nanoparticles on HOPG chips by direct impregnation with diluted particle dispersions. Afterwards, the centimeter sized HOPG chips were heated to different temperatures for distinct times. The particle's etching activities resulted in nano-grooves and pathways which were largely independent of the crystallographic structure of the graphite layers. We investigated the influence of temperature, time and particle size on the etching depth and length using atomic force microscopy (AFM) and provide a simple tool to pattern HOPG layers with a few graphene layers deep trenches.

3.2 Experimental

3.2.1 Preparation of the cerium oxide dispersion

A sample of 80 mg of a 20 wt% cerium oxide particle dispersion (no surfactant, US Research Nanomaterials, Inc.) in 2-propanol / water (20 wt% / 80 wt%) was diluted with 80 mL of 2-propanol. The particles revealed a broad size distribution between 10 to 60 nm (determined from AFM images). Each time the dispersion was used in the experiments, it was extensively sonicated in an ultrasonic bath (Sonorex Digitec DT 103 H, 560 W, Bandelin) for 3 minutes to re-disperse precipitated particles and break larger agglomerates.

3.2.2 Preparation and impregnation of HOPG chips with cerium oxide nanoparticles

Before impregnation with particle-dispersion, fresh layers of HOPG chips (Plano GmbH, Germany) were exposed by withdrawing the top layers using the so called scotch-tape method. After this, the surface was fully covered with freshly sonicated cerium oxide dispersion. The chips were kept for a few minutes until all the solvent had evaporated.

3.2.3 Heating of the HOPG chips

The freshly impregnated HOPG chips were placed in a high precision oven (thermogravimetrical measuring device, Linseis TG / STAPT 1600 thermoanalyzer). The device was heated up at a fast rate of typically 30 °C / min until 100 °C below the desired final temperature to prevent a temperature overshooting and then at a lower rate of typically 10 °C / min to the desired temperature. This temperature was held for several hours (4 – 16 h) depending on the sample. During the treatment a constant air flow through the device of 6 L / h was maintained.

3.2.4 AFM imaging

Beside the possibility of non-destructive measurements, atomic force microscopy (AFM) provides high-resolution topological information about the examined sample. The vertical resolution allows determining the amount of single graphite layers steps and other kind of defects. All images were recorded on tapping mode (Cypher, atomic force microscope, Asylum research / silicon tips OMCL-AC160TS-R3, Olympus). Scanning electron microscopy (SEM) analysis was found to be inadequate for the characterization of the HOPG

chips as charging, limited vertical resolution, surface destruction and deposition of organic residues impeded the comparison of experimental data.

3.3 Results and discussion

3.3.1 Impregnation of HOPG surfaces

Freshly cleaved HOPG surfaces (by the scotch-tape method) usually reveal a lot of edges and therefore appear like a kind of multilevel terrain as shown in Figure 1a. Most of the steps are in the size-range of a few graphite layers. During the impregnation process particles are deposited randomly on the HOPG surface as schematically shown in Figure 3.1b. Figure 3.1c represents a typical AFM image with deposited larger and smaller particles (bright spots) after the impregnation process.
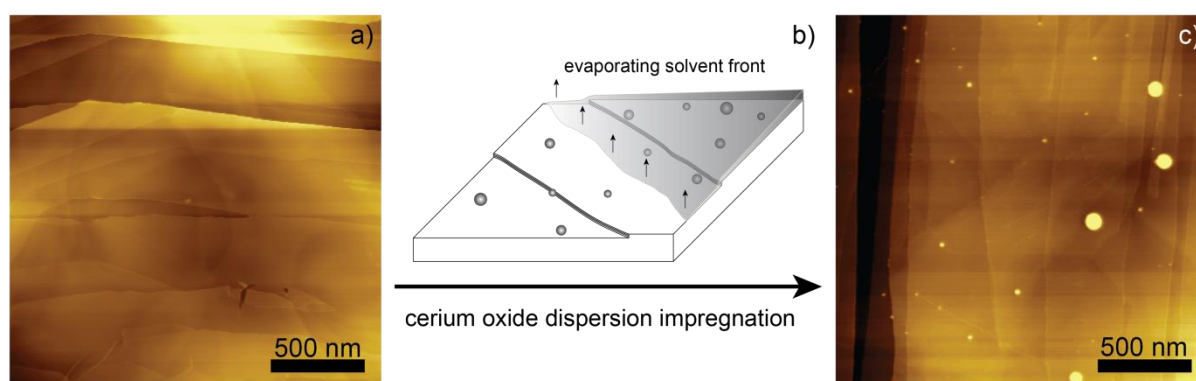
Figure 3.1: (a) AFM image of a freshly scotch-tape cleaved HOPG surface, revealing edges with heights of one to several graphite layers. (b) Schematic representation of an evaporating dispersion front entraining cerium oxide nanoparticles, which are retained on the surface. (c) AFM image of a cerium oxide impregnated HOPG surface revealing randomly scattered particles on the surface.

3.3.2 Heating and mobility

At temperatures of more than 300 °C, cerium oxide nanoparticles start to move on HOPG surfaces. After heating to 350 °C for 16 h, almost all particles are reclined to steps in the terraced environment as becomes apparent from Figure 3.2a. Obviously, the mobility towards the free planes is strongly limited after a particle eventually hits an edge.

3.3.3 Surface etching activities

At elevated temperatures and in the presence of oxygen cerium oxide is known to oxidize carbon catalytically to carbon dioxide and carbon monoxide. The crystalline structure of ceria provides oxygen vacancies which enable the formation of activated oxygen and its migration by diffusion within the lattice.[184] On HOPG surfaces this results in the formation of holes and traces in the close environment of the particles. Experiments resulted in 4 different observations of etching activities as depicted in a simplified form in Scheme 3.1. A first, and due to extensive sonication of the used dispersions, very rare case constitutes a larger agglomerate of particles that sinks into the surface due to its retarded planar mobility. Only a sparse fraction of particles starts a trace directly on an open graphite plane, which is depicted as the second etching type. The third type encloses a single particle that vertically forms a hole. This type of activity could again only be observed very scarcely. The fourth and by far most prominent activity comprises a particle that moves into one or several graphite layers starting at an edge. This process leaves back a trace with the depth of the edge-height where the particle was initially deposited. In most of the cases, the oxidation-traces appeared wedge-shaped. The path depths remain the same at all positions. Obviously the particles are changing their diameter while oxidizing the graphite layers, which will be discussed later on.
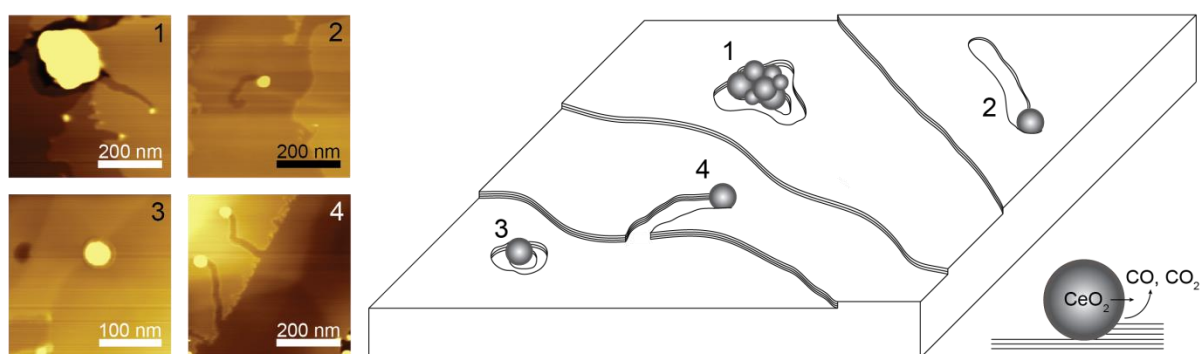
Scheme 3.1: *Schematic representation of the etching activities of cerium oxide nanoparticles on a HOPG surface. Graphite is catalytically oxidized to carbon-monoxide and carbon-dioxide when activated oxygen is migrating around the particle surface through oxygen vacancy sites in the crystalline structure of ceria. Four different types of oxidation activities can be observed, whereas the few graphene layer deep nano-groove oxidation type is by far most prominent. This process reliably etches at a constant depth of typically 1-5 graphene layers (see below).*

3.3.4 Temperature dependence of the oxidation activities

The activation of oxygen in ceria starts at elevated temperatures, around 350 °C. For a systematic investigation on the temperature dependence of the carbon etching activities, several HOPG chips were impregnated with cerium oxide dispersion as described above. The chips were maintained at 350 °C for 16 hours and at 375, 400, 425, 450 and 500 °C for a time period of 4 hours. As revealed in Figure 3.2a and 3.2b, there are no observable etching activities at 350 °C and 375 °C. At 400 °C and above, higher oxidation activity results in traces / nano-grooves in the graphitic structure which grow in intensity with increasing temperature (Figures 3.2c, d and e). Independent of particles, the structure of graphite edges begins to disorder at 500 °C, which is visible in AFM images such as in Figure 3.2f where the edges and parts of the planes have substantially changed their shape. This also emphasizes that structure defects such as edges are less stable than sheet core areas.
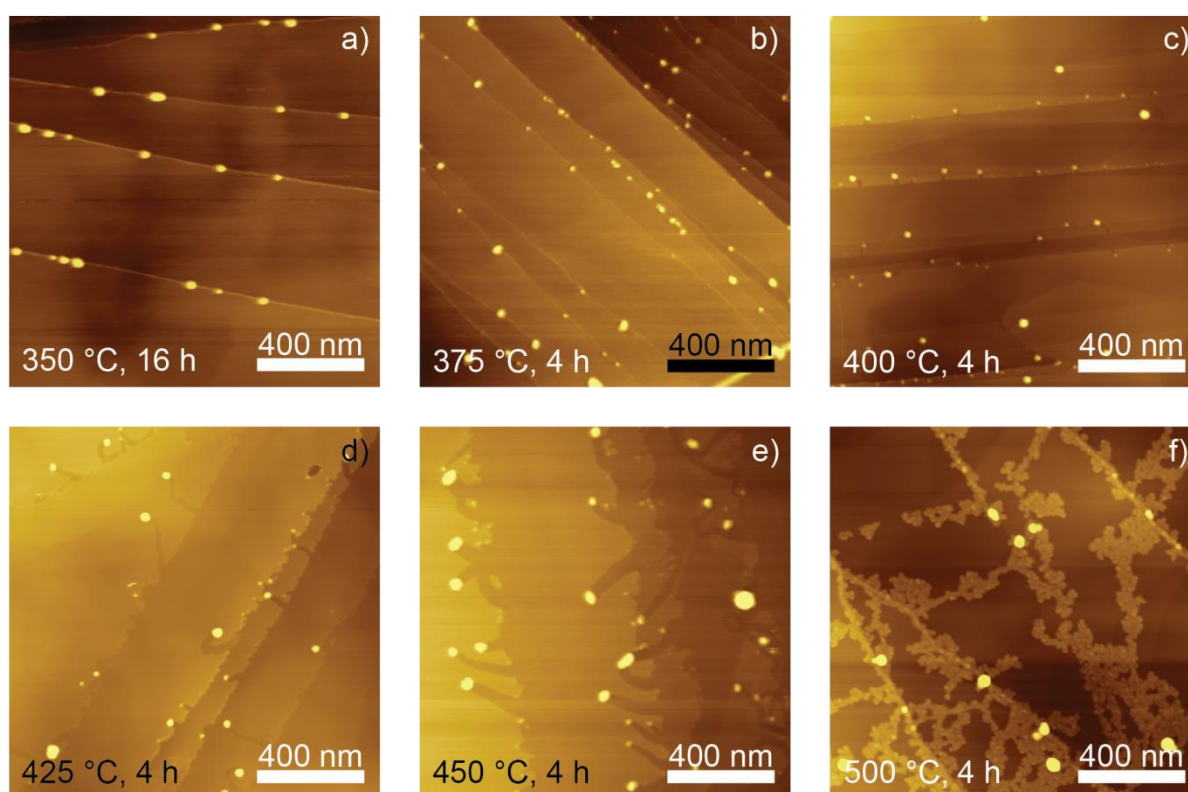
Figure 3.2: AFM images of catalytically active nanoparticles (cerium oxide) impregnated on HOPG surfaces and heated for distinct times and temperatures. At temperatures below 400 °C no catalytic oxidation of the graphite layers was visible. In the range between 400 °C and 450 °C, oxidation processes are increasing in intensity and yield few graphene layer deep nano-grooves. Above 450 °C the layer edges begin to oxidize spontaneously.

3.3.5 Statistical, quantitative evaluation of nano-groove / trace formation

AFM images provide spatially high-resolved information of the examined samples. The oxidation trace lengths (nano-grooves) and the final diameters of the particles were visually evaluated by retracing paths and particle shapes using commercially available imaging software. The geometry of the trenches reached from straight to highly tortuous. The changes in direction according to the images seem to appear by incident and no coherence with the treatment conditions could be established. A lot of the observed paths have a slightly wedge-shaped appearance. Detailed reasons for the path shapes will be discussed later on. The depth-distribution of the corresponding nano-grooves / paths was evaluated using the height information of the AFM images. The height resolution allows accurate determination of the number of single graphite layers at a step on the sample. Traces with a differing number of graphite layers at both borders of the trace (*i.e.* a particle moves along an edge) were statistically interpreted with their average number of layers, giving also half layer numbers in the evaluation. Following this approach, three different parameters, namely nano-groove / path length and depth and final particle diameter can be extracted for different temperatures and treatment durations.
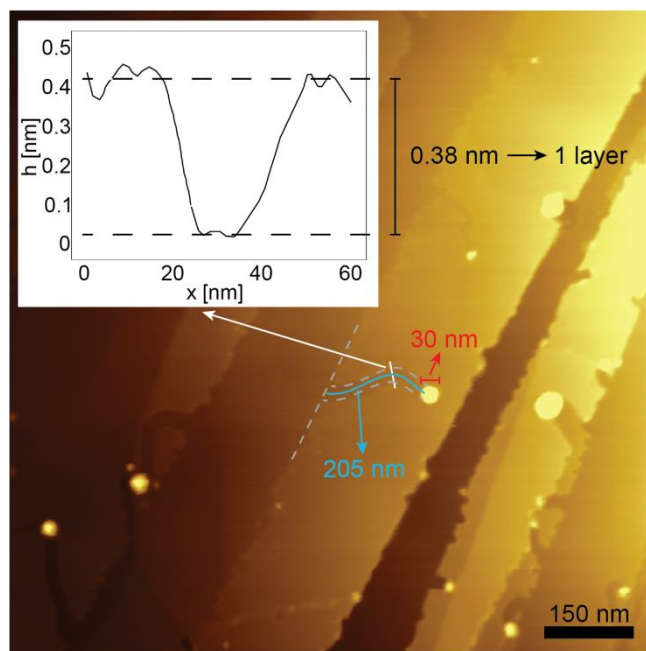
Figure 3.3: *AFM evaluation of an oxidation trace into a HOPG layer. The nano-groove or path as well as the particle diameter can be retraced and measured. A cross profile of the groove/path can be obtained from the height information of the image. In this example, the depth of the path suggests that one single graphite layer has been oxidized and a nano-groove of a single graphene layer depth was generated.*

Scatterplots of all experimental parameters against each other allow the identification of correlated quantities. Almost all particle etching activities leave traces with the depth of the edge-height where the oxidation started. Therefore, no correlation between the particle size and the trace depth becomes apparent. However, there are obvious dependencies between the trace lengths and the particle sizes as well as the trace lengths and the trace depths. Figure 3.4a depicts a scatterplot of the oxidation trace lengths versus the particle end diameter at different temperatures after 4 hours of treatment. It reveals that higher temperatures lead to a nonlinear acceleration of the oxidation activities. The formation of deeper oxidation traces (*i.e.* an etching path or nano-groove comprises several graphite layers) is occurring slower with increasing number of layers as clarified in Figure 3.4b. Analogously, a dependence on the treatment time can be observed as well (Figures 3.4c and 3.4d). From these correlations a closer insight into the oxidation mechanism can be obtained.
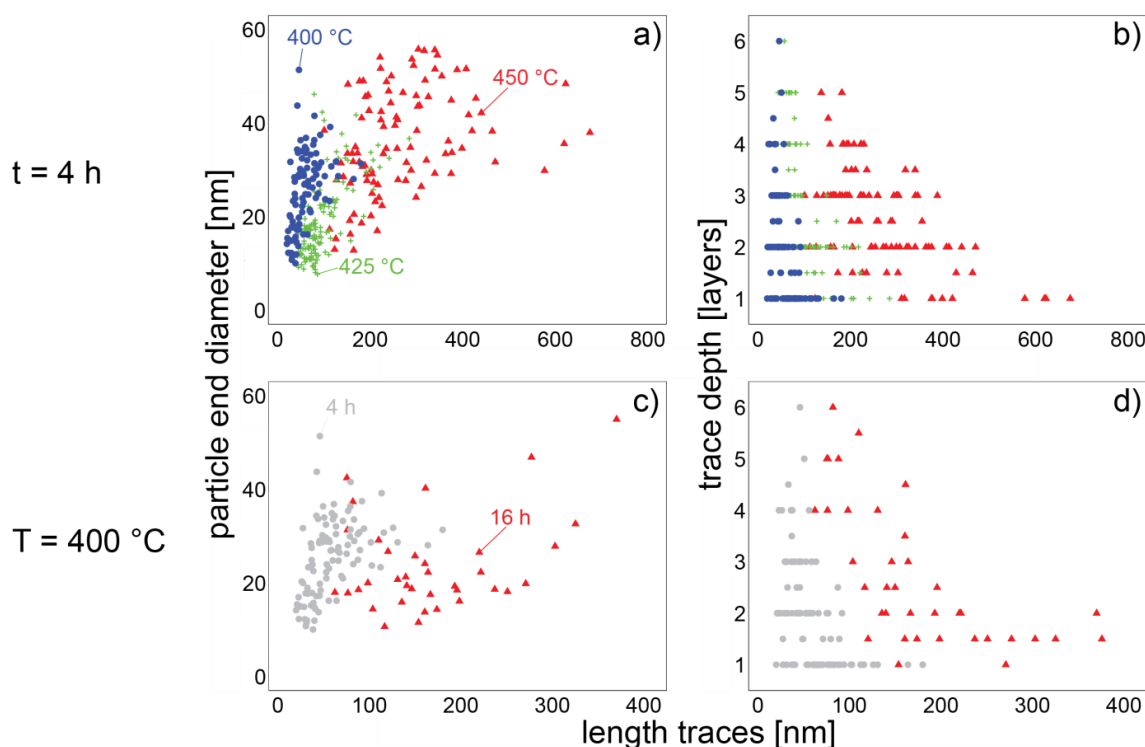
Figure 3.4: *(a) Oxidation trace length vs. end diameters of the particles and trace depths after 4 hours of treatment at 400 °C (circles), 425 °C (plus signs) and 450 °C (triangles). A clear activity ascent can be observed with raising temperatures. (b) The nano-groove or path length is also dependent on the depth, that is the number of single graphite layers being oxidized. (c) Oxidation trace length vs. end diameters of the particles after 4 hours (circles) and 16 hours (triangles) at 400 °C. A clear dependence of the treatment time and the trace length can be observed. (d) After 16 hours of treatment the dependence between trace length and depth appears analogously.*

3.3.6 Mechanistic interpretation of the oxidation

Active oxygen (oxygen radicals) reveals a high mobility within the crystal lattice of ceria and can easily diffuse to the particle surface. As the observed traces on the graphite planes all revealed a broadness of the related particle diameter or less, it can be concluded that the formed activated oxygen only reaches the carbon which is in close contact with the particle surface. This interpretation is in line with mechanistic studies on soot oxidation in diesel exhaust filters consisting of cerium ceramics.[185, 186] From Figure 3.4a it becomes obvious that larger particles in average generate longer trails. The generation of activated oxygen is related to the uptake of oxygen from the environment. The surface area of a single, specific particle therefore determines how much activated oxygen can be generated in a particle per time. The volume of the particle meanwhile acts as a reservoir for the formed reactive species. This interpretation is in line with a higher activity of larger particles. Secondly, in average, deeper traces are shorter. The more graphite layers are etched vertically, the more activated oxygen is needed per trace length. As there is a limited amount of activated oxygen available on a particle per time (our interpretation), this leads to a situation where traces shorten with increasing depth. Summarizing these observations it can be concluded that the formation of activated oxygen is rate limiting under all examined temperatures.

3.3.7 Particle depletion during oxidation

For most of the oxidation paths a slightly wedge-like shape can be identified. Especially in the case of smaller traces this becomes visually better apparent. A broadening of the traces over time after the contact with the particles can most probably be excluded since temperature based depletion only occurs at much higher temperatures together with significant, easy to distinguish structural changes as earlier shown in Figure 3.2f. The diameter of the particles is diminishing during the oxidation activities. In Figure 3.5, a wedge-like, representative trace is evaluated concerning its width at different distances away from its origin. AFM height information confirmed a trace depth of two graphite layers at all positions along the trace.
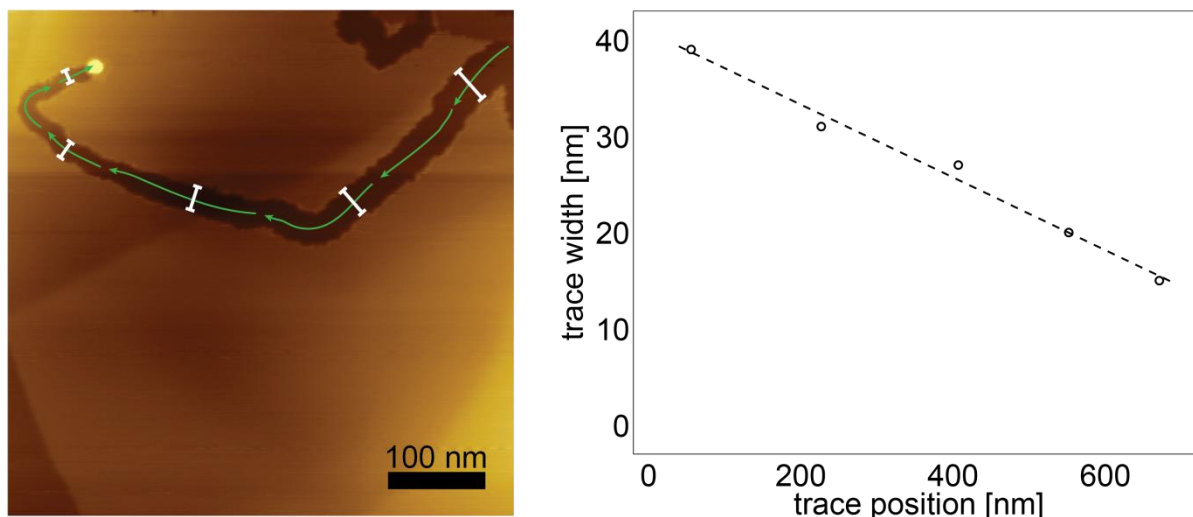
Figure 3.5: *An oxidation trace (nano-groove) with a depth of two graphite layers is evaluated regarding its width at various positions away from its origin (a step dislocation on top of the carbon). A clear and linear dependence between the width and the trace position can be observed.*

There is a linear dependence between the trace position and the trace width, which is associated with the particle diameter. Smaller particles generate shorter oxidation traces in average (*i.e.* move slower when etching). Volatility effects of nano-ceria are very unlike to occur at the here examined temperatures (the boiling point of cerium oxide is above 3000 °C). As the oxidation path width is narrowing linearly with the position, it is suggested that particle degradation is connected with the above explained surface reactions. This means that the particle is changing its diameter in conjunction with the rate it is depleting the graphite layers. If the depletion rate would be constant and independent from the surface reactions, the width - position dependence would not appear in a linear dependence, as the movement velocity of the particles is changing with their diameter. However, it remains unclear how exactly the cerium oxide is depleted on the carbon surface. There are no clearly visible residues of the particles in the traces. It can be speculated that carbides are formed in a side reaction beside the catalytic activity. An analytical proof concerning the presence of remaining cerium in the oxidation traces, at present, remains most challenging.

3.4   Conclusion

In this work we show a simple procedure to structure highly oriented pyrolytic graphite under easily achievable conditions using commercially available cerium oxide nanoparticles. By making use of their catalytic oxidation activity at comparably low temperatures above 375 °C

it was possible to cut crystallographically independent traces at a depth of one to several graphite layers into the examined samples. There is a strong temperature and treatment duration dependence of the length of the observed cuts. The ideal treatment temperature range was determined between 400 °C and 450 °C. At higher temperatures the here used few layer graphene models HOPG started to disorder from the edges of the structure. The particle induced oxidation activities are based on the formation of activated oxygen, which is formed on the particles at elevated temperatures. Most of the traces had a depth equal to the height of the original edge where the oxidation trace started. As deeper traces appear to be significantly shorter and larger particles with their higher surface areas produce longer traces, it can be concluded, that the formation of activated oxygen originating from air uptake is the rate limiting step of the trace formation process. Most of the observed paths revealed an unambiguous, linear change in width when following them from their origin to their end. As path broadening after particle contact could be excluded and the path depth remained always constant, it must be assumed that the ceria particles are depleted in a competing side reaction next to their catalytic activities. The linear position - broadness dependence in conjunction with the observation that smaller particles revealed lower oxidation rates further affirms that the particles are depleted in a second, however yet undetermined, surface reaction. By making use of the catalytic properties of cerium oxide at atmospheric conditions, our findings provide a simple method to structure graphite structures with prospect to future applications such as ion-selective membranes or atmospheric nano-filters. The geometric properties of the oxidation cuts or nano-grooves can easily be influenced by the chosen particle dimensions, applied conditions and treatment durations.

4. Quantitative Recovery of Magnetic Nanoparticles from Flowing Blood: Trace Analysis and the Role of Magnetization
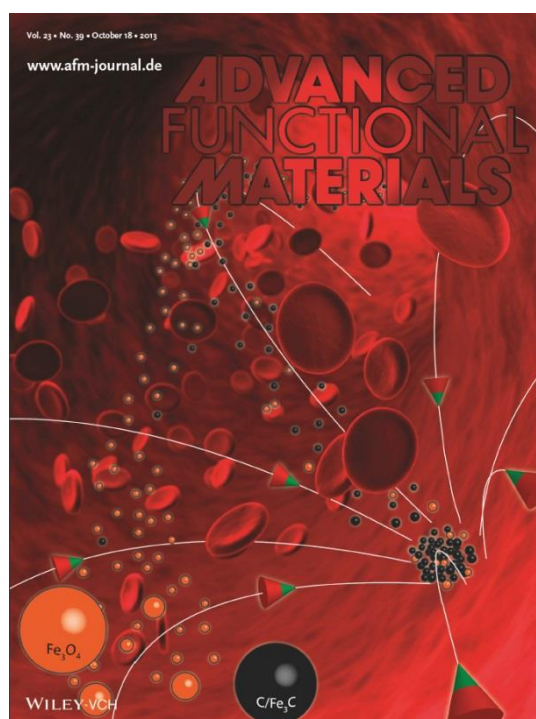
Published in part as:

Christoph M. Schumacher, Inge K. Herrmann, Stephanie B. Bubenhofer, Sabrina Gschwind, Ann-Marie Hirt, Beatrice Beck-Schimmer, Detlef Günther and Wendelin J. Stark

Abstract

Magnetic nanomaterials find increasing application as separation agents to rapidly isolate target compounds from complex biological media (*i.e.* blood purification). The responsiveness of the used materials to external magnetic fields (*i.e.* their saturation magnetization) is one of the most critical parameters for a fast and thorough separation. In the present study magnetite (Fe_3O_4) and non-oxidic cementite (Fe_3C) based carbon-coated nanomagnets are characterized in detail and compared regarding their separation behavior from human whole blood. A quantification approach for iron-based nanomaterials in biological samples with strong matrix effects (here, salts in blood) based on platinum spiking is shown. Both materials were functionalized with polyethyleneglycol (PEG) to improve cytocompatibility (confirmed by cell toxicity tests) and dispersability. The separation performance was tested in two setups, namely under stationary and different flow-conditions using fresh human blood. The results reveal a superior separation behavior of the cementite based nanomagnets and strongly suggest the use of nanomaterials with high saturation magnetizations for magnetic retention under common blood flow conditions such as in veins.

4.1   Introduction

Magnetic nanomaterials allow fascinating perspectives for biomedical applications.[42, 44, 94, 187] Particularly in targeted drug delivery,[123, 188-190] as contrast agents,[119-121, 191, 192] magnetic hyperthermia in cancer-treatment,[118, 193-196] magnetic labeling[197] and blood or tissue purification.[15, 125, 198-201] The ease to provoke a physical movement of a desired constituent through applications of an external magnetic field in a tissue pervading manner is most attractive. Movement is essentially controlled by the magnetic characteristics and volume of a particle next to the magnetic field's properties (strength and gradient). Decreasing the particle size in favor of a high-surface to volume ratio and mobility weakens the magnetic responsiveness.[202] Consequently, targeting of deep tissue sites and re-collection of magnetic particles under flow conditions (magnetic dialysis) requires particles with high magnetic moments. The size constraints imply that efficient magnetic targeting solely relies on the magnetic properties of the core material. Among the ferromagnetic elements iron, cobalt and nickel, the last two have been associated with adverse side effects at relatively low plasma concentrations (*e.g.* metal-on-metal hip implants).[127] Physiologically well-accepted iron in the form of polymer or silica coated magnetite exhibits a pronounced saturation magnetization (typically < 60 emu/g) and can easily be obtained as nano-sized and even superparamagnetic (*i.e.* no remaining magnetic moment without external field) particles by wet phase chemistry.[56, 203-206] Carbon-encapsulated non-oxidic cementite (Fe_3C) nanoparticles with a chemically stable C-coating have recently become available through reducing flame spray synthesis.[65] Cementite has an even higher saturation magnetization (up to 140 emu/g) than magnetite. The well-structured few-layer carbon surface coating furthermore offers a platform for stable covalent chemical functionalizations.[67]

Here, we report the synthesis and detailed physical and magnetic characterization of both magnetite and cementite particles with platinum doping (0.1 wt%) to establish an analytical tool for quantification of magnetic particles in biological samples with strong matrix effects (iron, salts in blood or tissue). A low detection limit for the nanoparticles was achieved through quantitative platinum analysis by inductively coupled plasma mass spectrometry. Platinum is chemically inert, not abundant in living organisms and therefore well-suited for analytical purposes. Both materials were functionalized with polyethylene glycol (PEG) surface groups to enhance dispersibility.[95, 207, 208] Recently, the detoxification of contaminated human whole blood using cementite nanoparticles was reported.[125] Due to its viscosity, the thorough separation of a magnetic nanomaterial from blood within a reasonable time-frame is challenging. We compared a stationary separation (no liquid movement) of the magnetic

particles from fresh human whole blood. Secondly, we analyzed the effectiveness of separation under continuous blood flow representing *in vivo* conditions in small (venules, tissue level) or even larger human veins (*e.g.* vena cubitalis, brachialis). Non-oxidic magnetic cementite nanoparticles could be quantitatively recollected even from flowing blood while less magnetic oxide-based nanoparticles stayed in the blood stream. The capability to reliably inject and remove a magnetic particle from flowing blood offers attractive perspectives for the development of novel treatment concepts such as *in vivo* extraction of toxins or infectious agents.

4.2   Experimental

4.2.1   Nanomaterial synthesis

Precursor synthesis

Platinum acetylacetonate (0.435 g, $\geq$ 98 %, ABCR-Chemicals) was dissolved in a mixture of 2-ethylhexanoic acid ($\geq$ 99%, Sigma-Aldrich) and THF ($\geq$ 99 %, Fisher Scientific) (60 mL, weight:weight ratio 1:1) to give a brownish precursor solution.

An aqueous 25 % NH_3 solution (688 g, Merck) was added stepwise to 2-ethylhexanoic acid (1442 g, technical grade, Soctech) using external cooling by an ice-water bath. Hereafter, $FeNO_3 \cdot 9H_2O$ (1820 g, $\geq$ 98 %, ABCR-Chemicals) was added successively under vigorous stirring. A brown, very viscous mixture resulted. Pentane ($\geq$ 98 %, Sigma-Aldrich) was added at discretion to obtain a reasonable viscosity to separate and reject the aqueous phase. Thereafter, the organic phase was dried using anhydrous $MgSO_4$ ($\geq$ 99.5 %, Sigma-Aldrich) and filtrated. The pentane was removed by distillation, resulting in a highly viscous brown liquid.

The metal content of the platinum precursor was calculated from the initial weights of all used substances (0.4 wt% Pt). The iron-content of the Fe-precursor was determined by adding small amounts of precursor into Erlenmeyer-flasks and burning of the organic contents by heating to 600 °C for 2 hours. Hereafter, the composition of the residues was determined using X-ray diffraction (XRD). By measuring the mass of the residues (pure Fe_2O_3) and knowing the initial amounts of precursor which was burnt, the metal content was calculated (11.4 wt% Fe).

Platinum spiked magnetite nanoparticles

The platinum and the iron precursor were mixed at a ratio to target 0.1 wt% platinum in magnetite (Fe_3O_4). This mixture was further diluted with THF (weight-ratio precursor:THF 2:1) and then used in a partially reducing flame-spray synthesis unit as previously described.[79] The oxygen content of the environment during the production was kept at a concentration of around 200-500 ppm (confirmed by online mass-spectroscopy). The resulting black powder was characterized by XRD, element microanalysis, magnetic hysteresis and first-order reversal curve (FORC) analysis.

Carbon-coated platinum spiked cementite nanoparticles

The platinum and the iron precursor were mixed to target 0.1 wt% platinum in cementite (Fe_3C) and then diluted with THF (Weight-ratio precursor:THF 2:1). Carbon-coated platinum-spiked cementite particles were produced in a reducing flame-spray synthesis unit with an entering acetylene stream above the flame.[65, 67] The oxygen content in the atmosphere was kept below 40 ppm during the synthesis. The resulting platinum-spiked carbon-coated cementite particles were thoroughly washed in HCl (24 %) for 1 week in total (acid exchange every day) to remove material which was improperly coated with carbon. By this procedure around 40 wt% of the material is lost, yielding a chemically very stable fraction of particles.[8] The resulting black powder was characterized by XRD, elemental microanalysis, hysteresis and FORC analysis.

4.2.2   Chemical functionalization

PEG-functionalization of platinum spiked magnetite nanoparticles

As-prepared platinum-spiked magnetite particles (100 mg), consecutively termed as Pt/Fe_3O_4, were added to DMF (50 mL, ≥ 99 %, Sigma-Aldrich) and dispersed by ultrasonication. Thereafter, methoxy-polyethyleneglycol-nitrodopamine (10 mg, molecular weight 5000 Da, SuSoS Surface Technology) was added. The dispersion was stirred for 24 h at 50 °C following previously established protocols.[95] After this, the particles were separated magnetically, washed with DMF (2x), H_2O (1x), iPrOH (2x) and then dried under vacuum. The surface functionality was confirmed by diffuse reflectance infrared Fourier transform spectroscopy (DRIFTS) and element microanalysis. The functionalized particles are subsequently termed as $PEG-Pt/Fe_3O_4$.

PEG-functionalization of carbon-coated platinum spiked cementite nanoparticles

Following pre-established protocols,[125] thiophenol groups were grafted covalently to the carbon-surface of as-prepared platinum-spiked carbon-coated cementite particles, consecutively termed as Pt/C/Fe$_3$C, using aqueous diazonium chemistry. The functional attachment was verified by DRIFTS and quantified by element microanalysis. Pt/C/Fe$_3$C (500 mg) was dispersed in PBS (50 mL, pH 7.2, 10 mM EDTA) by ultrasonication. Methoxy-polyethyleneglycol-maleimide (100 mg, molecular weight 5000 Da, NanoCS) was dissolved in dimethylacetamide (25 mL, $\geq$ 99.5 %, Acros).[209] Both solutions were mixed and then stirred for 6 hours at room temperature. After this, the particles were washed with H$_2$O (3x), ethanol (3x), dried under vacuum and again characterized by DRIFTS and elemental microanalysis. The particles are subsequently termed as PEG-Pt/C/Fe$_3$C.

4.2.3   Stationary magnetic separation from human whole blood

PEG-Pt/Fe$_3$O$_4$ (25 mg), respectively PEG-Pt/C/Fe$_3$C particles (25 mg) were dispersed in PBS (5 mL, pH 7.4) by ultrasonication. Portions (200 µL) of these dispersions were added to citrated human whole blood samples (800 µL) in glass vials (diameter 28 mm) to achieve initial particle concentrations of 1 mg particles per mL of fresh human blood. Every donor had signed a written consent approved by the ethical commission of Zurich (No. KEK-ZH 2012-0274) prior to the donation. In volunteers, after having obtained written informed consent, 5 tubes (4.5 mL, 0.129 M sodium citrate, Vacutainer) were withdrawn. After brief shaking an ultra-strong magnet (Nd$_2$Fe$_{14}$B 12x12x12 mm, ~0.5 Tesla) was placed near the samples for distinct times (10 s, 30 s, 1 min, 3 min, 30 min & 60 min) to separate the magnetic material as shown in Figure 4.1a. The particle content of the extracted blood samples was analyzed by the use of inductively coupled plasma mass spectrometry (ICP-MS).

4.2.4   In-flow magnetic separation from human whole blood

A setup, depicted in Figure 4.1b, was established to remove the different nanomaterials from flowing heparinized blood/particle-streams at a high and a low flow-rate (1 mL/min and 12.5 mL/min, respectively 2.4 mm/s and 30 mm/s average blood flow rate). Therefore, PEG-Pt/Fe$_3$O$_4$ (25 mg) or PEG-Pt/C/Fe$_3$C particles (25 mg) were dispersed in buffer (5 mL, PBS, pH 7.4) using 30 mL glass vials to give a particle concentration of 5 mg/mL. This dispersion was pumped into blood streams at rates of 0.2 mL/min, respectively 2.5 mL/min, using a

peristaltic pump. The blood was pumped at 1 or 12.5 mL/min using a second peristaltic pump approved for hemodialysis. After this pump the nanomaterial was re-collected using an ultra-strong permanent magnet ($Nd_2Fe_{14}B$ 12x12x12 mm, ~0.5 Tesla) which was placed at the side of the silicone-tube (3 mm inner diameter, 0.5 mm wall thickness).
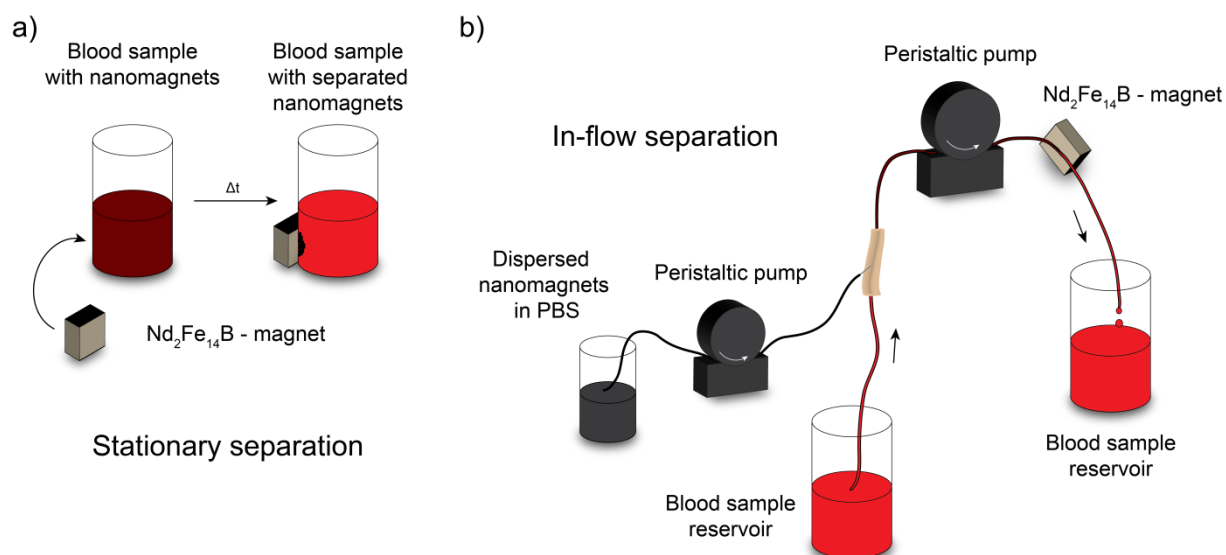
Figure 4.1: *a) A stationary magnetic separation setup was used to monitor the performance to remove magnetic materials from human whole blood using an ultra-strong permanent magnet which was placed at the side of a glass vial for different times. b) Well-dispersed nanomagnets in PBS were pumped into a flowing blood-stream and were later removed with a strong magnet which was placed at the side-wall of the silicone tubing. The flow-rate of both the nanomagnet-dispersion and the blood stream can be adjusted and results in different separation performances.*

4.2.5 Particle quantification in blood samples

Blood samples (typical amount of 1 g) spiked with known amounts of particles as well as the extracted blood samples were given into PTFE digestion tubes. Then HNO_3 (65 %), HCl (37 %) and H_2O_2 (35 %) at typical amounts of 1 g each were added. An additional rhodium spike of 0.25 mg/kg acted as a recovery-standard for the digestion. The samples were treated at 200 °C and 40 bar in a microwave based digestion system (ultraCLAVE II, Milestone Inc.). After this treatment the samples were diluted to 1:50 with respect to the initial blood sample amount using an acidic mixture containing HCl (1 %, v/v) and HNO_3 (1 %, v/v). Thereafter the samples were further diluted 1:20 and spiked with iridium as an internal standard (2.5 μg/kg). Suitable salt and acid concentrations for a measurement by ICP-MS were achieved

using this treatment. The corresponding calibration standards containing Rh (blank-7 µg/kg), Pt (blank-3.5 µg/kg) and Ir (2.5 µg/g) were prepared from blank blood samples to obtain the same blood matrix levels compared to the samples. Platinum concentrations and rhodium recoveries were quantified using a sector-field ICP-MS suitable for ultra-trace element analysis (Element 2, Thermo Fisher Scientific) by measuring the isotopes ^{103}Rh, ^{193}Ir, ^{194}Pt and ^{195}Pt.

4.2.6 Particle degradation and leaching

Due to their high specific surface area and depending on their chemical resistivity, material leaching into surrounding solutions is a frequently observed phenomenon for numerous nanomaterials. In order to test the leaching liability under physiological conditions small amounts of both PEG functionalized particles (1 mg) were given into PBS (3 mL) and then stirred vigorously for 1 hour. For a comparison under harsher, but not biologically relevant conditions the same experiment was carried out in HCl (3 mL, 0.1 M). After the nanomaterials were withdrawn magnetically from the supernatant and a drop of concentrated HCl was added to the PBS samples, a small amount of potassium thiocyanate was added to form the orange iron-thiocyanate complex. Solutions with known iron concentrations acted as calibration standards for an iron concentration determination by UV-VIS spectroscopy at 467 nm. The strong color of the iron-thiocyanate complex allows a simple quantification of iron (LOD ~ 0.2 mg/kg). This allowed calculation of the percentage of degraded particles.

4.2.7 Cell compatibility tests

Human microvascular endothelial cells (HMVEC, Lonza, Basel, Switzerland) were cultured as described elsewhere.[126] Cells were seeded in 96-well culture dishes (100'000 cells/mL, 0.1 mL per well). Both PEG-Pt/Fe_3O_4 and PEG-Pt/C/Fe_3C were pre-dispersed in PBS. The cells were then incubated with magnetic nanoparticles dispersed in cell culture medium (10 and 100 mg/kg). Lipopolysaccharide (LPS from Escherichia coli, serotype 055:B5 (2 µg/mL, Sigma-Aldrich, Buchs, Switzerland) was used as positive control. After incubation for 20 h, supernatants were collected and centrifuged. For cytotoxicity assays, some wells were incubated with lysing solution (from the assay kit, Promega, Madison, WI, USA) for 1 h (100% lysis, maximum lactate dehydrogenase (LDH) release). Cytotoxicity was measured following the manufacturer's protocol and values were calculated relative to the

positive control (100 % lysis). ELISAs for human interleukin-6 were performed following the manufacturer's protocol (R&D Systems Europe Ltd, Abingdon, UK).

4.3   Results and discussion

In a flame spray pyrolysis process under reducing atmosphere, iron-based magnetic nanoparticles with either magnetite (Fe_3O_4) or cementite (Fe_3C) cores were synthesized. As with growing applications of magnetic nanoparticles their detection in complex samples becomes increasingly important, the nanoparticles were spiked *in situ* with a tiny amount of platinum which serves as a tracer for particle detection in iron-rich biological sample matrices. The physicochemical characteristics of the nanoparticles including the shape, the size distribution, the magnetic properties and cytocompatibility were compared before the performance of the magnetic beads was assessed in a stationary and an in-flow magnetic separation process.

4.3.1   Material characterization – Physicochemical properties

The transmission electron micrograph (TEM) in Figure 4.2a shows spherical carbon-coated cementite nanoparticles with a size distribution between 10 and 50 nm. The carbon-coating appears as a few-layer graphene-like stacked structure, with thicknesses of 1 - 2 nm. This well-structured and very thin coating ensures high chemical resistivity[8] of the core material and furthermore allows a chemical functionalization by forming stable carbon-carbon bonds to the graphene-like surface.[67] The magnetite nanoparticles in Figure 4.2c appear as close to spherical crystallites with a size distribution between 5 and 25 nm. Corresponding X-ray diffractograms (Figures 4.2b, 4.2d) confirm a cementite, respectively magnetite phase. Due to the low platinum content of both particle types, indications for larger platinum crystals, if present, would be hardly observable in the diffraction patterns. Ideally, a platinum doping within the magnetite and the cementite crystal lattice occurs, which is not visible in XRD. As TEM micrographs did not show any separate crystallites (high contrast) which can be addressed to platinum and the harsh pretreatment of $Pt/C/Fe_3C$ with 24 % HCl did not result in any shift of the platinum concentration due to different dissolution characteristics (verified by ICP-MS measurements), it can be concluded that platinum is well-dispersed within both materials and not present as a separate phase.
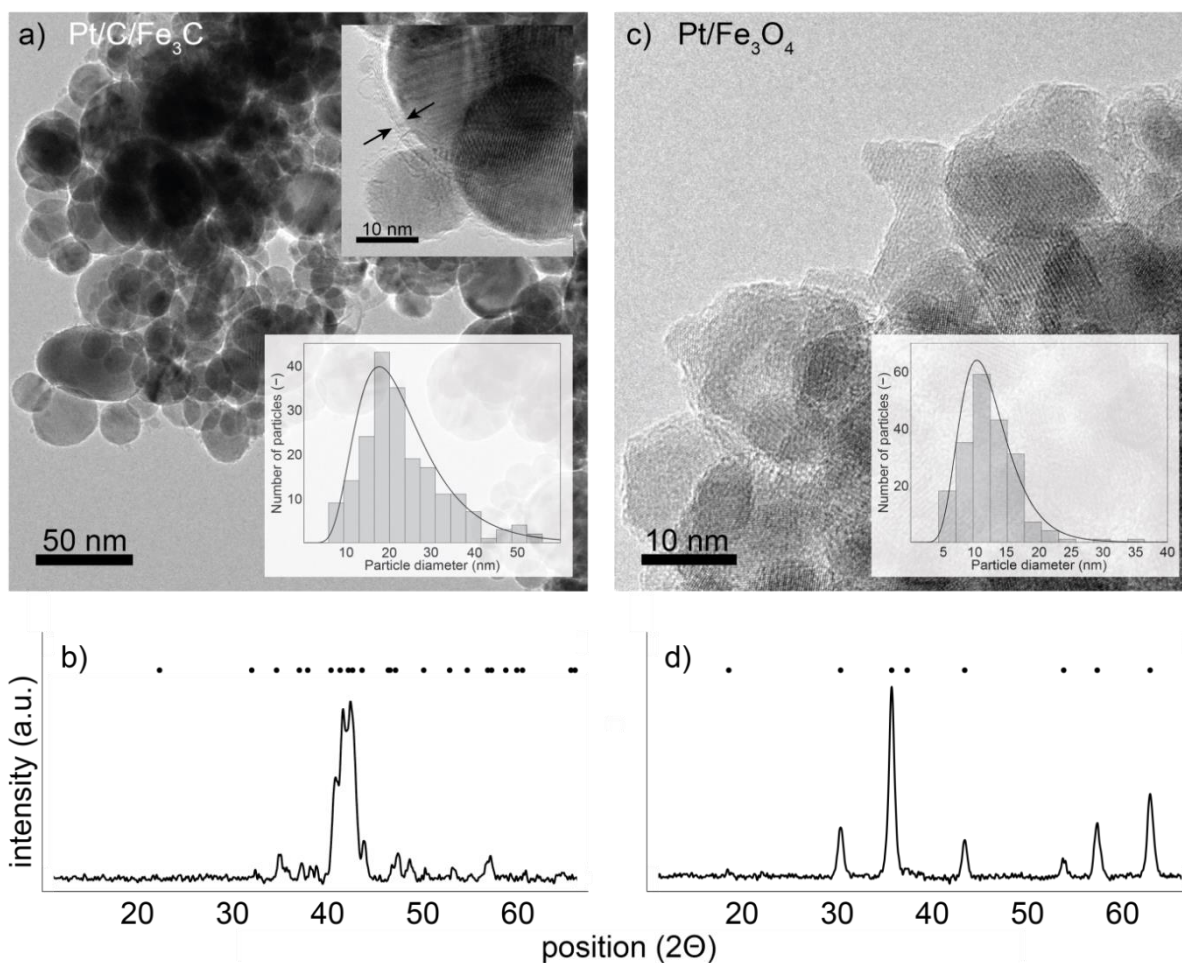
Figure 4.2: *a) Transmission electron micrographs showing spherical platinum-spiked cementite particles in the size-range of 10-50 nm. The insertion in the upper right depicts the multi-layer graphene-like stacked structure of the carbon-coating, which is responsible for an extraordinary chemical stability. c) Transmission electron micrograph of platinum-spiked magnetite particles in the size-range of 5-25 nm. b) The cementite and d) the magnetite structure were both confirmed by X-ray powder diffraction. No indications for a segregated platinum phase were found.*

Vibrating sample magnetometry was used to determine both the saturation magnetization and the magnetic remanence of the materials. The cementite particles reveal a significantly higher saturation magnetization (123.0 emu/g) compared to the magnetite particles (58.7 emu/g). The remanence of the cementite particles was found to be 27.6 emu/g, whereas the magnetite particles revealed an (almost) superparamagnetic behavior (remanence 2.4 emu/g) as shown in Figure 4.3. The magnetic characteristics changed only slightly after the chemical modification with PEG groups as the functional loading only accounts for around 3 wt% of the material according to elemental microanalysis in Table 4.1.
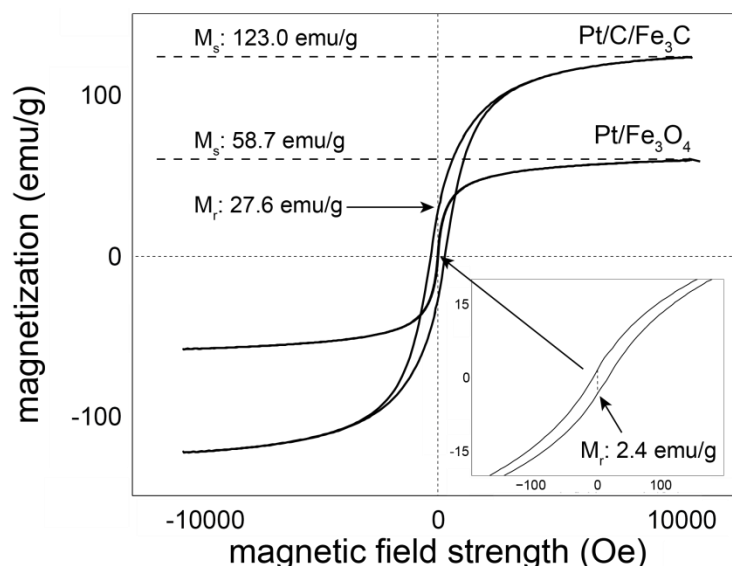
Figure 4.3: *Vibrating sample magnetometry hysteresis curves of platinum-spiked cementite (Pt/C/Fe₃C) and magnetite (Pt/Fe₃O₄) particles. The almost superparamagnetic magnetite particles show a substantially lower saturation magnetization than the cementite particles.*

Magnetic first order reversal curve (FORC) analysis is able to identify different magnetic phases which are present in a sample and therefore, in contrast to VSM, not only provides averaged information about the magnetic properties of a sample. Interactions between magnetic domains as well as size effects become apparent with this technique. The obtained FORC diagrams depicted in Figures 4.4a and 4.4b reveal a single phase for both materials (*i.e.* absence of multiple spots), which is in good agreement with the obtained XRD diffractograms. Furthermore, both profiles are narrow and almost symmetric in H_U direction (distribution of interaction fields), which suggests that the particles appear as magnetically independent domains. The centered coercivity plot of Pt/Fe_3O_4 in Figure 4.4c reveals that a large fraction of the magnetite nanomagnets shows a superparamagnetic behavior, whereas a smaller particle fraction (larger in size) is responsible for the residual magnetic remanence of the material which was quantified by VSM. The centered coercivity plot of $Pt/C/Fe_3C$ in Figure 4.4d shows a broad coercivity profile and superparamagnetic particles are absent.
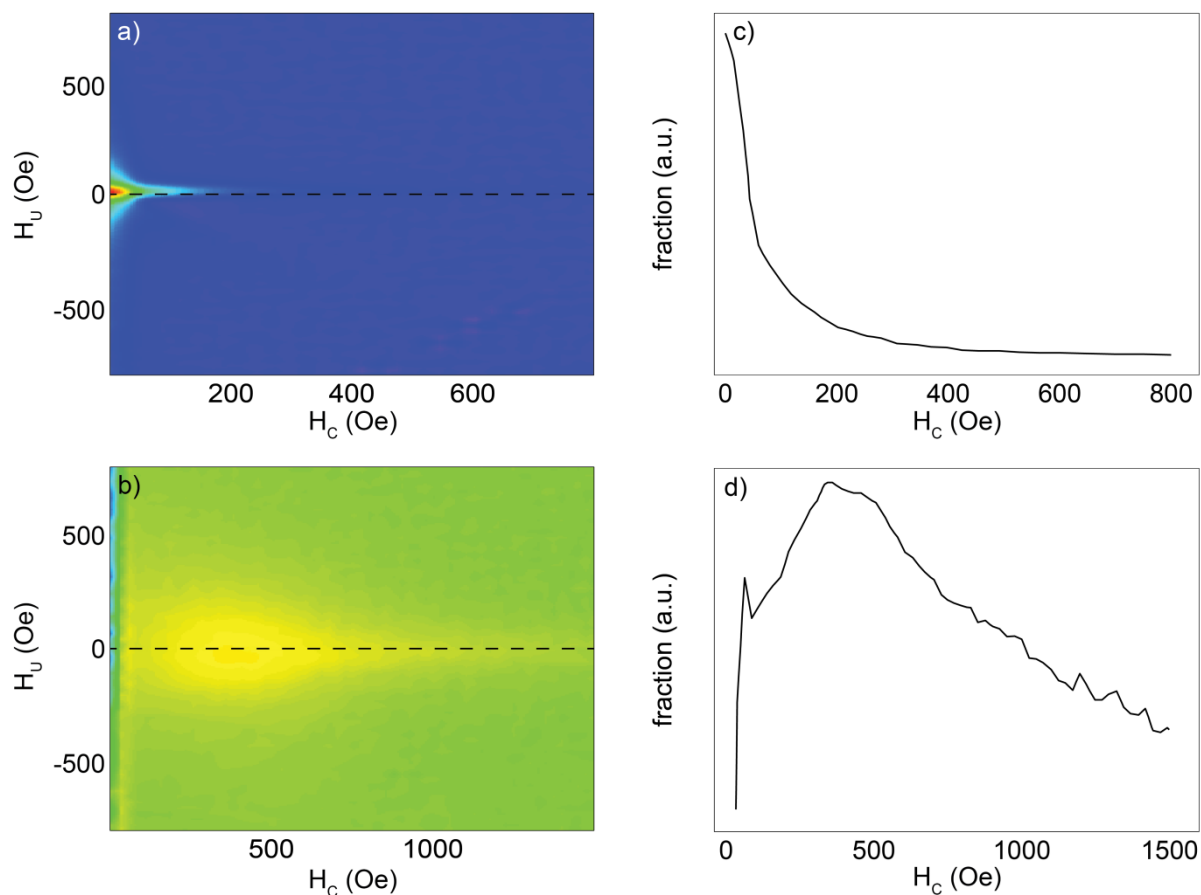
Figure 4.4: *a) FORC diagram of Pt/Fe₃O₄ revealing a single magnetic phase with magnetically independent domains (i.e. symmetrical in H_U direction). b) FORC diagram of Pt/C/Fe₃C showing magnetically independent domains. c) Centered coercivity distribution of Pt/Fe₃O₄ revealing a large fraction of superparamagnetic particles and a smaller fraction of particles (larger) with a magnetic coercivity. d) Centered coercivity distribution of Pt/C/Fe₃C. The material shows a broad coercivity distribution compared to the magnetite material, superparamagnetic particles are absent.*

4.3.2 Surface functionalization

PEG surface functionalizations are well-known to enhance the biocompatibility of nanomagnets in a major extent[210] and furthermore strongly enhance their aqueous dispersibility.[95] The PEG surface functionalization of both materials was confirmed by DRIFTS as shown in Figure 4.5. The obtained spectra were compared to the spectra of the corresponding pure surfactants and show a good agreement. Moreover, a strong stretching vibration absorption band at around 560 cm^{-1}, characteristic for magnetite,[211] can be observed.
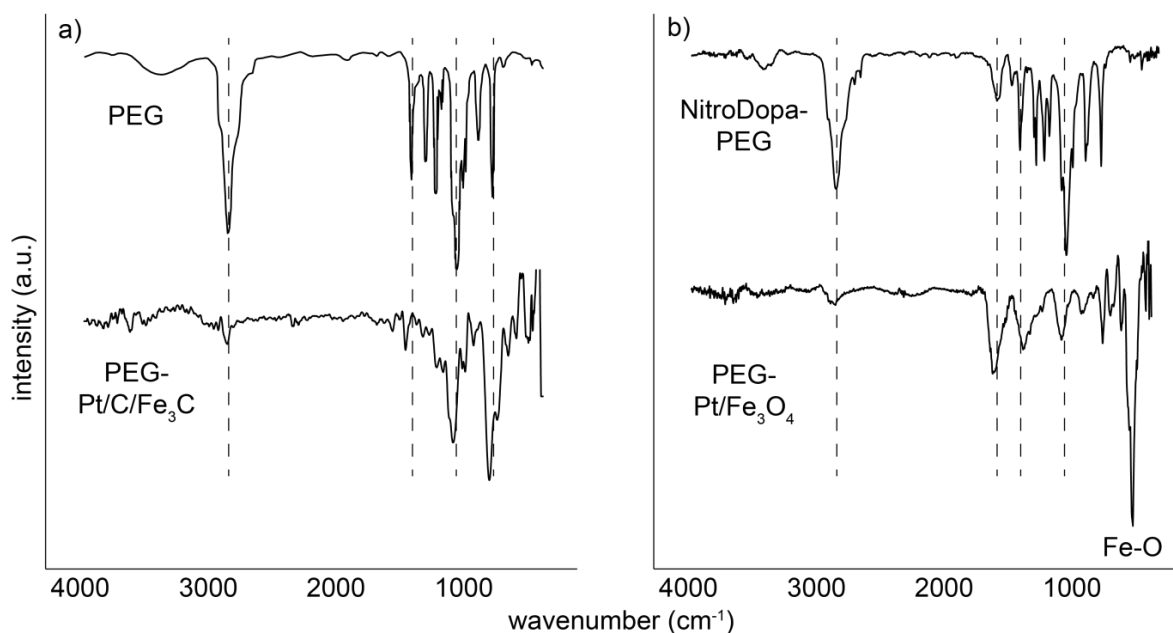
Figure 4.5: *Diffuse reflectance infrared Fourier-transform spectra (DRIFTS) of the chemically functionalized cementite a) and magnetite b) nanomagnets and structure confirmation by comparison to the pure surfactant compounds. Peak shifts and intensity changes are a result of binding to the surface and changes in molecular symmetry. The magnetite particles show a Fe-O stretching vibration at around 560 cm^{-1}.*

4.3.3 Particle degradation and leaching

Measuring the nanoparticle concentration in a biological media is not straight forward and is hindered by the complexity of the matrix. In addition, potential particle disintegration, generally labeled as leaching could lead to misinterpretations concerning the remaining particle amount in biological samples as dissolved material will not be magnetically removed, but would be considered as remaining particles in a sample from an analytical point of view. Therefore, knowledge about the particle stability is pivotal for a reliable quantification in biological samples. Iron-oxide based magnetic nanomaterials are considerably less stable against dissolution than carbon-coated metal nanomagnets.[212] Thus, it must be clarified whether leaching could occur under the examined conditions and time frames. Small amounts of material were stirred in PBS and in a second experimental run in 0.1 M HCl as explained in the experimental section (to simulate chemically harsh, but biologically irrelevant conditions). The iron-concentration in the PBS solutions remained below the limit of detection after 1 hour (approx. 0.2 mg/kg iron or 0.06 wt% particle loss), which is a typical duration for a proposed magnetic dialysis[96]. Under the relatively harsh acidic conditions (0.1 M HCl) 1.90 wt% of

PEG-Pt/Fe$_3$O$_4$ dissolved, whereas only 0.14 wt% of PEG-Pt/C/Fe$_3$C disintegrated. The significantly higher leaching of the magnetite based material is illustrated in Figure 4.6, where the iron release into the surrounding medium is visualized by the formation of the orange thiocyanate complex. These results clearly highlight the significantly higher chemical stability of the carbon-coated nanomagnets and the eligibility of the here applied protocols to quantify particles by platinum spiking under physiological conditions.
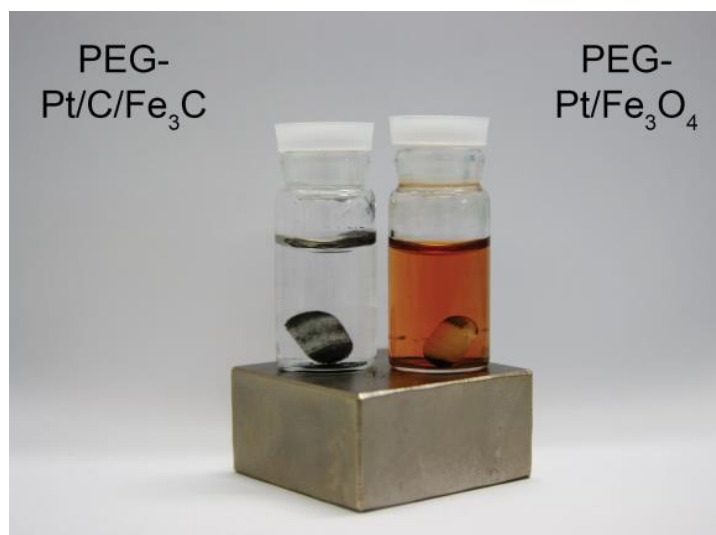
Figure 4.6: *Magnetically separated PEG-Pt/C/Fe$_3$C (left) and PEG-Pt/Fe$_3$O$_4$ (right) in 0.1 M HCl after 1 hour of vigorous stirring. The presence of potassium thiocyanate in the supernatant leads to the formation of an orange complex when ionic iron is present in the solution. The magnetite based material shows a strong leaching compared to the cementite based material.*

4.3.4 Platinum quantification in the nanomagnets (and in blood samples)

By quantification with ICP-MS, the platinum concentrations of the PEG-functionalized nanomagnets were determined. For this purpose several blank blood samples were spiked with small amounts of particles. The results listed in Table 4.1 confirm a good agreement between the added amount of platinum in the precursor solution and the concentration found in the particles.

Table 4.1*: C, H, N contents of the different materials determined by elemental microanalysis as well as platinum contents determined using inductively coupled plasma mass spectrometry (ICP-MS).*

Material	C [wt%]	H [wt%]	N [wt%]	Pt [wt%]
Pt/Fe$_3$O$_4$	2.01	0.53	0.07	0.090 ± 0.001
Pt/C/Fe$_3$C	9.87	0.04	0.01	0.105 ± 0.001
PEG-Pt/Fe$_3$O$_4$	3.46	0.75	0.18	0.088 ± 0.001
PEG-Pt/C/Fe$_3$C	13.04	0.24	0.14	0.101 ± 0.001

4.3.5 Cytocompatibility of platinum-doped nanomagnets

The surface functionalization of particles is the key parameter for biocompatibility. Polyethyleneglycol coatings are known as good dispersion agents and are frequently used to enhance the biological compatibility.[95] Cytocompatibility of the synthesized nanoparticles was measured by exposing human microvascular endothelial cells, which line the blood vessels, to nanoparticles for a time period of 20 hours. The release of lactate dehydrogenase (LDH, a protein which is released upon break down of the cellular membrane) was then quantified as a measure for cytotoxicity. Human interleukin 6 (hIL-6) was quantified as a measure for potential inflammatory reactions in response to particles exposure. There were no significant differences in the h-IL6 concentration as well as LDH release for the different particle types and concentrations compared to the controls after 20 hours of incubation (Figure 4.7). Therefore it can be concluded that the nanomagnets do not reveal any obvious adverse effects on the used tissue cultures under the examined conditions.
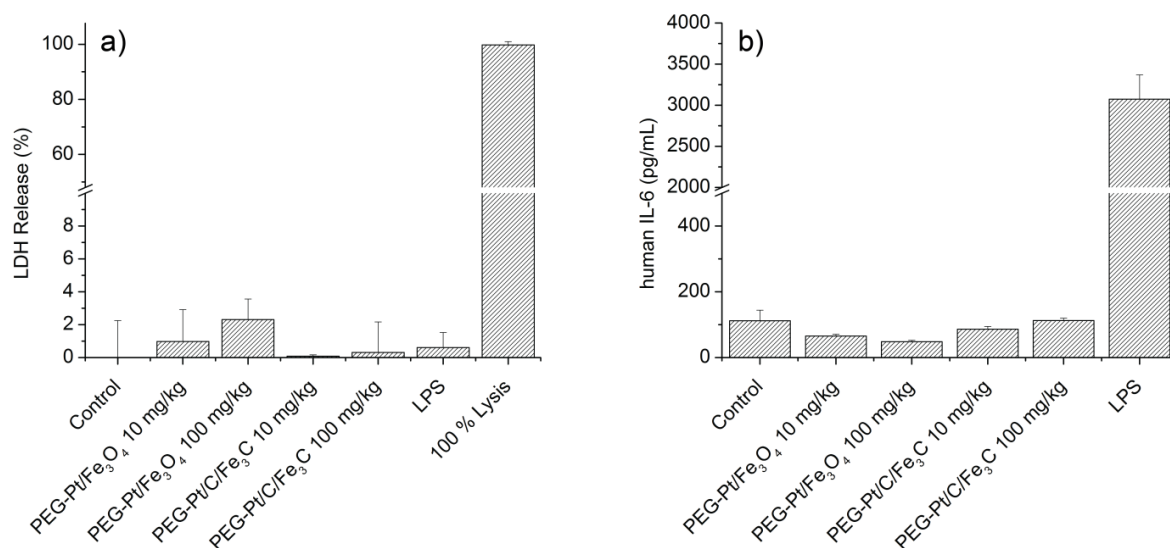
Figure 4.7: *a) LDH release of human microvascular endothelial cells which were exposed to polyethylene coated magnetite and cementite particles. There are no significant differences in protein release compared to the control. b) h-IL6 concentrations in the cell media after 20 hours of incubation showing no increased inflammatory responses compared to the control.*

4.3.6 Nanoparticle detection in biosamples by means of platinum content measurements

Blood, on average, contains around close to 0.9 wt% (*i.e.* 9000 mg/kg) dissolved salts.[213] ICP-MS used for trace element analysis is sensitive to high salt loadings. After the digestion procedure the samples were diluted in two subsequent steps to obtain an acceptable salt load of around 100 mg/kg (1:1000). Therefore, an initial concentration of 1 mg particles with 0.1 wt% platinum per mL of blood results in a platinum content of around 1 μg/kg after dilution. The limit of detection in the here used protocols was in the range of 5 ng/kg platinum, or 5 mg/kg particles in blood respectively. The quantification of even lower platinum concentrations with mass spectrometry is cumbersome and therefore discloses the limits of the here used quantification technique. Higher platinum doping of the particles to enhance (lower) the detection capabilities could alter the material properties in a considerable extent and moreover leads to platinum phase segregation (i.e. no doping any more). This could lead to misinterpretations of the particle concentration after a magnetic separation as platinum crystals could not be properly conjoined to the nanomagnets.

4.3.7 Magnetic separation from human whole blood

Stationary extraction experiments

Unlike to dispersions in pure water, the magnetic separation occurs comparatively rapid in ion-rich buffers or blood. The effectiveness of stabilizing agents such as polyethylene glycols is limited in media with high salt concentrations. Thus, particles can aggregate easier, which strongly influences the magnetic separation velocity enhancement factor.[15] These effects manifest in the results of the stationary separation experiments depicted in Figure 4.8 where a particle contaminated blood volume of 1 mL was cleaned. In a rapid initial extraction phase within the first seconds the concentrations of both particle types were strongly depressed, whereas the separation of the cementite particles occurred slightly more rapidly. Thereafter, the cementite concentration further decreased, whereas the magnetite concentration got only slightly lower and finally stagnated. The used vials for the separation had a diameter of 28 mm. A close proximity to the strong magnet becomes critical for a complete and rapid separation. A higher saturation magnetization of the extracted particles not only enhances their separation rate, but also the separation reach within a stagnant medium.
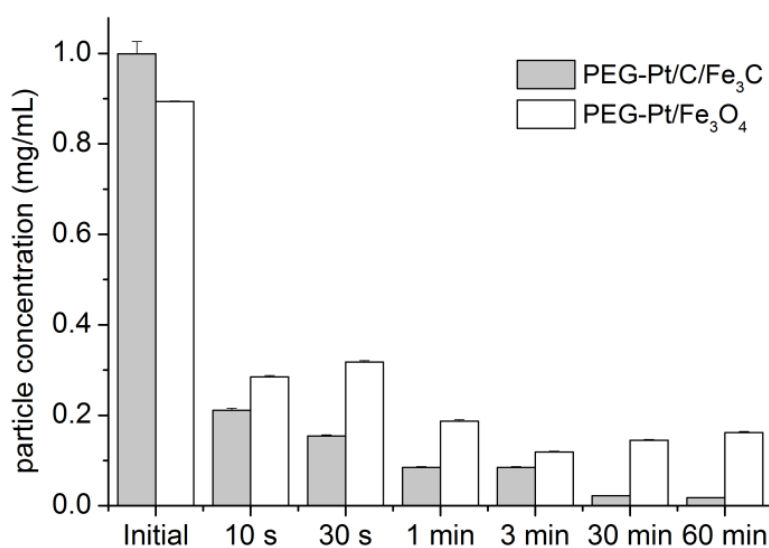
Figure 4.8: *Remaining magnetic particle concentrations in blood samples after stationary magnetic extraction. After a rapid initial separation period, the progress is slowed down as the proximity to the magnet is not sufficient at all sections of the vial. In contrast to the cementite particles, the magnetite particles which were too distant from the magnet could not be collected even after prolonged exposition to the magnetic field.*

In-flow extraction experiments

Different flow velocities within various blood vessels are going along with different shear stress levels. A higher blood flow velocity therefore increasingly complicates a reliable and efficient nanomagnet separation by an external magnetic field. In a first in-flow separation experiment, a moderate blood flow velocity (2.4 mm/s) was chosen. This flow is comparable to the flow conditions that can be found in small venules (< 20 μm inner diameter), whereas a higher flow (30 mm/s) was chosen to simulate the flow in a larger, therapeutically relevant vein (< 5 mm inner diameter).[214] Table 4.2 shows the relative particle concentration levels of both PEGylated magnetic nanomaterials in contaminated human blood before and after a simple magnetic separator under low- and high-flow conditions. In the low-flow scenario both materials were separated to such an extent, that the platinum content of the blood samples was below the limit of detection. Under high-flow conditions however, only 56 % of the magnetite material was removed, whereas the cementite level in the samples still remained below the limit of detection. In this context, it must be highlighted that the here used magnetite particles still reveal a high saturation magnetization after their chemical functionalization with PEG surface groups (around 3 wt% carbon increase for both materials following elemental microanalysis results in Table 4.1). In most reported works[207, 215, 216] PEGylated magnetite particles, mostly due to high functional loadings, reveal significantly lower saturation magnetizations (a few emu/g). The separation performance of these materials suffers strongly when being extracted from biological samples, resulting in prolonged separation durations and incomplete separation. Under flow-conditions, where the residence time at the separation point is usually system-inherently limited, this can result in serious disadvantages of such kinds of materials.

Table 4.2: Nanomagnet separation efficiency under different flow conditions

Material	Low flow (2.4 mm/s)	High flow (30 mm/s)
PEG-Pt/Fe$_3$O$_4$	> 99.5 %	56.0 %
PEG-Pt/C/Fe$_3$C	> 99.5 %	> 99.5 %

4.4   Conclusion

The viscosity of biological fluids makes rapid movement of magnetic particles challenging. A high magnetization is required to provide sufficient force for targeted particle movement, particularly in a flow situation. Disadvantageous agglomeration effects can be suppressed by

chemical modification (*e.g.* PEG[96]). This study shows that the commonly cited necessity for superparamagnetic behavior in magnetic particles is of limited validity.[87] While the chemical stability of carbon-encapsulated metal nanoparticles offers significant technological advantages, it may have its downside in terms of safety when applied *in vivo*, and biomedical treatments will have to account for the fate of traces of particles that remain in a patient for a prolonged time. The here proposed platinum doping allows quantitative analysis of tissue sections or blood when using iron-based nanoparticles, even though biological background iron as well as salt concentrations are high (matrix effects). The capability to reliably remove magnetic nanoparticles from flowing blood now permits development of magnetic blood extraction, where a noxious compound is mechanically removed out of a living organism.

5. Conclusion and outlook

This work is focused on graphite-based nanomaterials. A main focus rests upon a more fundamental understanding of the chemical stability of few layered graphite, particularly on magnetic metal nanoparticles. These only 1-2 nm thick highly-ordered surface coatings entirely change the material characteristics from highly unstable to the most stable known magnetic nanomaterial. Despite the chemical stability of graphite was intensively studied before, namely as few-layer graphene or two-dimensionally bent carbon nanotubes, only little works focused on three-dimensionally bent graphite as here. This work thus reveals important influences on the resistivity of metal-carbon core-shell nanocomposites. Following the findings, stability can be substantially enhanced by simple surface modifications using diazonium chemistry. Despite improving a material's properties in favor of a higher firmness often appears tantalizing, future work should at least in some cases also target the exact opposite. Persistence of synthetic materials could, or in many cases already has, developed into one of the biggest problems of mankind. Accumulation in environmental compartments can occur when the decay rate of a good is surmounted by its rate of creation (respectively uncontrolled spillage). Well-known examples are the great plastic patch in the Pacific Ocean or anthropogenic gaseous waste-products. Predicting the consequences of a particular accumulation-circle is often complex. What stays for sure, is that accumulation problems can have various negative impacts for our wealth and progress. Fallibility is an inevitable human stain which, in favor of accumulation prevention, forwards reasonably predetermined breaking points in commodities to one of the future industrial challenges. This story is valid as well for nanomaterials. In order to refocus on carbon-coated nanomagnets, which are suggested for nanomedical applications, this means that serious adverse effects for an organism could result from long-term deposition in *i.e.* inner organs, despite of the fact that the acute toxicity is negligible. In order to minimize these risks, it would be desirable to develop a material that will safely decay after the time scope of its therapeutic usage. Within the current work however, no opportunities have been found to deliberately lower the chemical resistivity of the used metal-carbon composites.

Graphite and graphene nanostructuring remains a major challenge for future applications including semiconductors or highly efficient nanofilters. Despite the versatility of the here presented new approach for slicing and cutting, the generated trenches in the graphite layers cannot be controlled in such a manner as in present semiconductor manufacturing. This puts a questionsmark behind the future applicability in this direction. Better chances however arise for nanofiltration applications. Perforated graphene (single layer graphite) in principle represents an ultimately thin separation layer with extremely favorable resistance attributes. If

the presented etching technique could be successfully transferred to large-sized single layer graphite, a convenient pore generation tool would be established that could render atmospheric nanofiltration feasible.

Trace analytical methods to quantitatively detect nanomaterials in body compartments after prolonged exposition are still rare. Biological abundance of iron in organisms as well as degradation of surface-bond markers frequently hamper detection of low concentrated iron-based nanomagnets in blood or tissue samples. Despite the here acquired method circumvents these issues by introduction of inert noble metal doping, some limitations are still present. An inconvenience from an analytical point of view is the required considerable dilution of digested biosamples before introduction into an inductively coupled plasma mass spectrometer (ICP-MS). The high salt contents of the samples would otherwise overload sensitive components of the equipment. Furthermore, the doping amount of platinum into the presented materials is limited. Higher amounts lead to phase segregation of platinum (*i.e.* forming of separate platinum crystallites). Like this, the quantified platinum amounts could not be addressed to the actual particle contents of the samples any more. In summary, both issues lead to particle detection limits in the range of parts per million (regarding sample mass) despite actually parts per trillion of platinum are quantified within a sample. In order to enhance this analytical approach, the maximally possible platinum doping amount without particle phase segregation should be determined. This amount is however expected to be below 1 weight percent particle mass since unpublished trials have shown extensive segregation issues at 5 weight percent platinum per particle mass. Hence, a most efficient, but very costly approach would be the use of isotope enriched nanomagnets on the base of *i.e.* ^{54}Fe or ^{57}Fe. Since mass spectrometry allows the determination of isotope distribution patterns, a differentiation between body's own and nanomagnet-native iron would be possible. This would lower the limits of nanomagnet detection drastically and permits plenty of freedom for future investigations.

Appendix: Supplementary material

A.1 Supporting information to chapter 2

TEM imaging of HNO$_3$/HCl treated C/Co
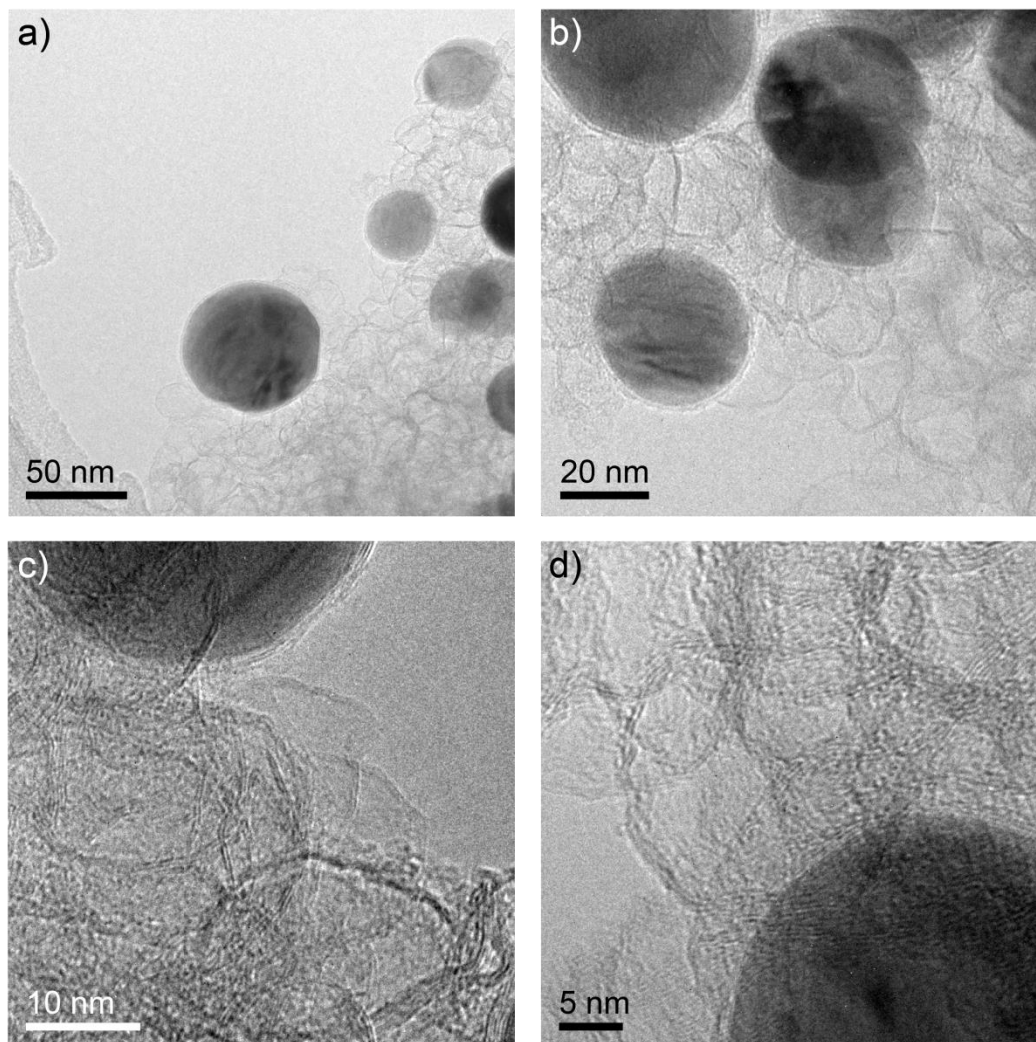
Figure S2.1: *(a-d) Transmission electron micrographs (TEM) of HNO$_3$/HCl treated C/Co reveal empty carbon shells as well as intact particles. No partially filled materials was detected during TEM evaluation.*

Functional loading and shell thickness increase

The chemical functionalization density on a particle surface can be calculated from the elemental microanalysis data.

For example:

$C/Co\text{-}(C_6F_5)_n$ 0.96 wt% Fluorine   5 Fluorine Atoms per functional unit

$$\text{Functional loading} = \frac{\text{wt\% F}\cdot 10^{-2}}{\text{Molecular weight F}}\cdot 10^3 \cdot \frac{1}{\text{Number of F}} = \frac{0.96\cdot 10^{-2}}{18.998\ \text{g/mol}}\cdot 10^3 \cdot \frac{1}{5} = 0.101\ \frac{\text{mmol}}{\text{g}}$$

The related increase of the particle shell thickness is calculated as follows.

For example:

$C/Co\text{-}(C_6F_5)_n$ 0.101 mmol/g functional loading
Density 2,3,4,5,6-Pentafluorotoluene   1440 kg/m^3
Specific surface area   27000 m^2/kg
Molecular weight $\text{-}(C_6F_5)_n$ 179 g/mol

$$\text{Thickness increase} = \frac{\text{wt\% Functionalization}\cdot 10^{-2}}{\frac{\text{Density functionalization}}{\text{Specific surface area}}} = \frac{0.101\cdot 10^{-3}\ \text{mol/g}\cdot 179\ \text{g/mol}}{\frac{1440\ \text{kg/m}^3}{27000\ \text{m}^2\text{/kg}}} = 0.46\ \text{nm}$$

Calculation of electrochemical potential differences using the Nernst formalism

$$\Delta E = \Delta E^0 - \frac{RT}{zF} \log\left(\frac{c_{Red}}{c_{Ox}}\right)$$

R = 8.314 J/(mol·K)

F = 96485 C/mol

T = 296 K

$Co^{2+} + 2e^- \rightleftharpoons Co$ $\Delta E^0_{red} = -0.28V$

$PdCl_4^{2-} + 2e^- \rightleftharpoons Pd + 4Cl^-$ $\Delta E^0_{red} = 0.591V$

$AuCl_4^- + 3e^- \rightleftharpoons Au + 4Cl^-$ $\Delta E^0_{red} = 1.002V$

$2AuCl_4^- + 3Co \rightarrow 2Au + 3Co^{2+} + 4Cl^-$
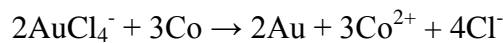
$c_{Red} = [Co^{2+}]^3$ $c_{Ox} = [AuCl_4^-]^2$ $\Delta E^0 = 1.282V$

$PdCl_4^{2-} + Co \rightarrow Pd + Co^{2+} + 4Cl^-$
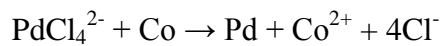
$c_{Red} = [Co^{2+}]$ $c_{Ox} = [PdCl_4^{2-}]$ $\Delta E^0 = 0.871V$

Electrochemical potential differences are calculated for concentrations of 100 ppm metals in solution.

100 ppm Co $c = 1.70 \cdot 10^{-3}$ mol/L

100 ppm Pd $c = 9.40 \cdot 10^{-4}$ mol/L

100 ppm Au $c = 5.08 \cdot 10^{-4}$ mol/L

Au : z = 6 **ΔE = 1.30 V**

Pd : z = 2 **ΔE = 0.86 V**

References

(1)   Binnig, G.; Rohrer, H.; Gerber, C.; Weibel, E., Tunneling through a controllable vacuum gap. *Applied Physics Letters* **1982,** 40, (2), 178-180.

(2)   Binnig, G.; Rohrer, H.; Gerber, C.; Weibel, E., Surface Studies by Scanning Tunneling Microscopy. *Physical Review Letters* **1982,** 49, (1), 57-61.

(3)   Rose, H. H., Optics of high-performance electron microscopes. *Science and Technology of Advanced Materials* **2008,** 9, (1), 014107.

(4)   Rose, H., Outline of a Spherically Corrected Semiaplanatic Medium-Voltage Transmission Electron-Microscope. *Optik* **1990,** 85, (1), 19-24.

(5)   Haider, M.; Uhlemann, S.; Schwan, E.; Rose, H.; Kabius, B.; Urban, K., Electron microscopy image enhanced. *Nature* **1998,** 392, (6678), 768-769.

(6)   Ramsden, J., *Nanotechnology: An Introduction*. William Andrew: 2011.

(7)   Roduner, E., Size matters: why nanomaterials are different. *Chemical Society Reviews* **2006,** 35, (7), 583-592.

(8)   Schumacher, C. M.; Grass, R. N.; Rossier, M.; Athanassiou, E. K.; Stark, W. J., Physical Defect Formation in Few Layer Graphene-like Carbon on Metals: Influence of Temperature, Acidity, and Chemical Functionalization. *Langmuir* **2012,** 28, (9), 4565-4572.

(9)   Schumacher, C. M.; Koehler, F. M.; Rotzetter, A. C. C.; Raso, R. A.; Stark, W. J., Nanoparticle-Assisted, Catalytic Etching of Carbon Surfaces as a Method to Manufacture Nanogrooves. *The Journal of Physical Chemistry C* **2012,** 116, (25), 13693-13698.

(10)   Alexiou, C.; Schmid, R. J.; Jurgons, R.; Kremer, M.; Wanner, G.; Bergemann, C.; Huenges, E.; Nawroth, T.; Arnold, W.; Parak, F. G., Targeting cancer cells: magnetic nanoparticles as drug carriers. *European Biophysics Journal with Biophysics Letters* **2006,** 35, (5), 446-450.

(11)   Dobson, J., Magnetic nanoparticles for drug delivery. *Drug Development Research* **2006,** 67, (1), 55-60.

(12)   Arruebo, M.; Fernandez-Pacheco, R.; Ibarra, M. R.; Santamaria, J., Magnetic nanoparticles for drug delivery. *Nano Today* **2007,** 2, (3), 22-32.

(13)   McBain, S. C.; Yiu, H. H. P.; Dobson, J., Magnetic nanoparticles for gene and drug delivery. *International Journal of Nanomedicine* **2008,** 3, (2), 169-180.

(14)   Ito, A.; Shinkai, M.; Honda, H.; Kobayashi, T., Medical application of functionalized magnetic nanoparticles. *Journal of Bioscience and Bioengineering* **2005,** 100, (1), 1-11.

(15)   Herrmann, I. K.; Grass, R. N.; Stark, W. J., High-strength metal nanomagnets for diagnostics and medicine: carbon shells allow long-term stability and reliable linker chemistry. *Nanomedicine* **2009,** 4, (7), 787-798.

(16)   Banerjee, S. S.; Chen, D. H., Magnetic nanoparticles grafted with cyclodextrin for hydrophobic drug delivery. *Chemistry of Materials* **2007,** 19, (25), 6345-6349.

(17)   Jain, T. K.; Morales, M. A.; Sahoo, S. K.; Leslie-Pelecky, D. L.; Labhasetwar, V., Iron oxide nanoparticles for sustained delivery of anticancer agents. *Molecular Pharmaceutics* **2005,** 2, (3), 194-205.

(18)   Yu, M. K.; Jeong, Y. Y.; Park, J.; Park, S.; Kim, J. W.; Min, J. J.; Kim, K.; Jon, S., Drug-loaded superparamagnetic iron oxide nanoparticles for combined cancer imaging and therapy in vivo. *Angewandte Chemie-International Edition* **2008,** 47, (29), 5362-5365.

(19)   Yallapu, M. M.; Othman, S. F.; Curtis, E. T.; Gupta, B. K.; Jaggi, M.; Chauhan, S. C., Multi-functional magnetic nanoparticles for magnetic resonance imaging and cancer therapy. *Biomaterials* **2011,** 32, (7), 1890-1905.

(20)   Sengupta, J.; Ghosh, S.; Datta, P.; Gomes, A., Physiologically Important Metal Nanoparticles and Their Toxicity. *Journal of Nanoscience and Nanotechnology* **2014,** 14, (1), 990-1006.

(21)   Kim, J. S.; Yoon, T. J.; Kim, B. G.; Park, S. J.; Kim, H. W.; Lee, K. H.; Park, S. B.; Lee, J. K.; Cho, M. H., Toxicity and tissue distribution of magnetic nanoparticles in mice. *Toxicological Sciences* **2006,** 89, (1), 338-347.

(22)   Reddy, L. H.; Arias, J. L.; Nicolas, J.; Couvreur, P., Magnetic Nanoparticles: Design and Characterization, Toxicity and Biocompatibility, Pharmaceutical and Biomedical Applications. *Chemical Reviews* **2012,** 112, (11), 5818-5878.

(23)   Liu, G.; Gao, J. H.; Ai, H.; Chen, X. Y., Applications and Potential Toxicity of Magnetic Iron Oxide Nanoparticles. *Small* **2013,** 9, (9-10), 1533-1545.

(24)   Oh, J.; Feldman, M. D.; Kim, J.; Condit, C.; Emelianov, S.; Milner, T. E., Detection of magnetic nanoparticles in tissue using magneto-motive ultrasound. *Nanotechnology* **2006,** 17, (16), 4183-4190.

(25)   Bouchard, L. S.; Anwar, M. S.; Liu, G. L.; Hann, B.; Xie, Z. H.; Gray, J. W.; Wang, X. D.; Pines, A.; Chen, F. F., Picomolar sensitivity MRI and photoacoustic imaging of cobalt nanoparticles. *Proceedings of the National Academy of Sciences of the United States of America* **2009,** 106, (11), 4085-4089.

(26)   Schumacher, C. M.; Herrmann, I. K.; Bubenhofer, S. B.; Gschwind, S.; Hirt, A.-M.; Beck-Schimmer, B.; Günther, D.; Stark, W. J., Quantitative Recovery of Magnetic Nanoparticles from Flowing Blood: Trace Analysis and the Role of Magnetization. *Advanced Functional Materials* **2013,** 23, (39), 4888-4896.

(27)   Brey, W. S.; Krieger, K. A., The surface area and catalytic activity of aluminum oxide. *Journal of the American Chemical Society* **1949,** 71, (11), 3637-3641.

(28)   Rioux, R. M.; Song, H.; Hoefelmeyer, J. D.; Yang, P.; Somorjai, G. A., High-Surface-Area Catalyst Design: Synthesis, Characterization, and Reaction Studies of Platinum Nanoparticles in Mesoporous SBA-15 Silica. *The Journal of Physical Chemistry B* **2004,** 109, (6), 2192-2202.

(29)   Schüth, F., Endo- and Exotemplating to Create High-Surface-Area Inorganic Materials. *Angewandte Chemie International Edition* **2003,** 42, (31), 3604-3622.

(30)   Bell, A. T., The Impact of Nanoscience on Heterogeneous Catalysis. *Science* **2003,** 299, (5613), 1688-1691.

(31)   Sharma, V.; Park, K.; Srinivasarao, M., Colloidal dispersion of gold nanorods: Historical background, optical properties, seed-mediated synthesis, shape separation and self-assembly. *Materials Science and Engineering: R: Reports* **2009,** 65, (1–3), 1-38.

(32)   Balazs, A. C.; Emrick, T.; Russell, T. P., Nanoparticle Polymer Composites: Where Two Small Worlds Meet. *Science* **2006,** 314, (5802), 1107-1110.

(33)   Grass, R. N.; Albrecht, T. F.; Krumeich, F.; Stark, W. J., Large-scale preparation of ceria/bismuth metal-matrix nano-composites with a hardness comparable to steel. *Journal of Materials Chemistry* **2007,** 17, (15), 1485-1490.

(34)   Lu, A. H.; Salabas, E. L.; Schuth, F., Magnetic nanoparticles: Synthesis, protection, functionalization, and application. *Angewandte Chemie-International Edition* **2007,** 46, (8), 1222-1244.

(35)   Slowing, II; Vivero-Escoto, J. L.; Wu, C. W.; Lin, V. S. Y., Mesoporous silica nanoparticles as controlled release drug delivery and gene transfection carriers. *Advanced Drug Delivery Reviews* **2008,** 60, (11), 1278-1288.

(36)   Mout, R.; Moyano, D. F.; Rana, S.; Rotello, V. M., Surface functionalization of nanoparticles for nanomedicine. *Chemical Society Reviews* **2012,** 41, (7), 2539-2544.

(37)   Kainz, Q. M.; Linhardt, R.; Grass, R. N.; Vilé, G.; Pérez-Ramírez, J.; Stark, W. J.; Reiser, O., Palladium Nanoparticles Supported on Magnetic Carbon-Coated Cobalt Nanobeads: Highly Active and Recyclable Catalysts for Alkene Hydrogenation. *Advanced Functional Materials* **2014,** 24, (14), 2020-2027.

(38)   Schatz, A.; Long, T. R.; Grass, R. N.; Stark, W. J.; Hanson, P. R.; Reiser, O., Immobilization on a Nanomagnetic Co/C Surface Using ROM Polymerization: Generation of a Hybrid Material as Support for a Recyclable Palladium Catalyst. *Advanced Functional Materials* **2010,** 20, (24), 4323-4328.

(39)   Yoon, T.-J.; Lee, W.; Oh, Y.-S.; Lee, J.-K., Magnetic nanoparticles as a catalyst vehicle for simple and easy recycling. *New J. Chem.* **2003,** 27, (2), 227-229.

(40)   Stevens, P. D.; Li, G.; Fan, J.; Yen, M.; Gao, Y., Recycling of homogeneous Pd catalysts using superparamagnetic nanoparticles as novel soluble supports for Suzuki, Heck, and Sonogashira cross-coupling reactions. *Chemical Communications* **2005**, (35), 4435-4437.

(41)   Che, C.; Li, W.; Lin, S.; Chen, J.; Zheng, J.; Wu, J.-c.; Zheng, Q.; Zhang, G.; Yang, Z.; Jiang, B., Magnetic nanoparticle-supported Hoveyda–Grubbs catalysts for ring-closing metathesis reactions. *Chemical Communications* **2009**, (40), 5990-5992.

(42)   Pankhurst, Q. A.; Thanh, N. T. K.; Jones, S. K.; Dobson, J., Progress in applications of magnetic nanoparticles in biomedicine. *Journal of Physics D-Applied Physics* **2009,** 42, (22).

(43)   Mornet, S.; Vasseur, S.; Grasset, F.; Duguet, E., Magnetic nanoparticle design for medical diagnosis and therapy. *Journal of Materials Chemistry* **2004,** 14, (14), 2161-2175.

(44)   Pankhurst, Q. A.; Connolly, J.; Jones, S. K.; Dobson, J., Applications of magnetic nanoparticles in biomedicine. *Journal of Physics D-Applied Physics* **2003,** 36, (13), R167-R181.

(45)   Nitin, N.; LaConte, L.; Zurkiya, O.; Hu, X.; Bao, G., Functionalization and peptide-based delivery of magnetic nanoparticles as an intracellular MRI contrast agent. *JBIC Journal of Biological Inorganic Chemistry* **2004,** 9, (6), 706-712.

(46)   Fang, C.; Zhang, M., Multifunctional magnetic nanoparticles for medical imaging applications. *Journal of Materials Chemistry* **2009,** 19, (35), 6258-6266.

(47)   Suleiman, J. S.; Hu, B.; Peng, H.; Huang, C., Separation/preconcentration of trace amounts of Cr, Cu and Pb in environmental samples by magnetic solid-phase extraction with Bismuthiol-II-immobilized magnetic nanoparticles and their determination by ICP-OES. *Talanta* **2009,** 77, (5), 1579-1583.

(48)   Herr, J. K.; Smith, J. E.; Medley, C. D.; Shangguan, D.; Tan, W., Aptamer-Conjugated Nanoparticles for Selective Collection and Detection of Cancer Cells. *Analytical Chemistry* **2006,** 78, (9), 2918-2924.

(49)   Hua, M.; Zhang, S.; Pan, B.; Zhang, W.; Lv, L.; Zhang, Q., Heavy metal removal from water/wastewater by nanosized metal oxides: A review. *Journal of Hazardous Materials* **2012,** 211–212, (0), 317-331.

(50)   Laurent, S.; Forge, D.; Port, M.; Roch, A.; Robic, C.; Vander Elst, L.; Muller, R. N., Magnetic iron oxide nanoparticles: synthesis, stabilization, vectorization, physicochemical characterizations, and biological applications. *Chemical Reviews* **2008,** 108, (6), 2064-2110.

(51)   Willard, M. A.; Kurihara, L. K.; Carpenter, E. E.; Calvin, S.; Harris, V. G., Chemically prepared magnetic nanoparticles. *International Materials Reviews* **2004,** 49, (3-4), 125-170.

(52)   Rossier, M.; Schaetz, A.; Athanassiou, E. K.; Grass, R. N.; Stark, W. J., Reversible As (V) adsorption on magnetic nanoparticles and pH dependent desorption concentrates dilute solutions and realizes true moving bed reactor systems. *Chemical Engineering Journal* **2011,** 175, 244-250.

(53)   Weissleder, R.; Kelly, K.; Sun, E. Y.; Shtatland, T.; Josephson, L., Cell-specific targeting of nanoparticles by multivalent attachment of small molecules. *Nat Biotech* **2005,** 23, (11), 1418-1423.

(54)   Lewin, M.; Carlesso, N.; Tung, C.-H.; Tang, X.-W.; Cory, D.; Scadden, D. T.; Weissleder, R., Tat peptide-derivatized magnetic nanoparticles allow in vivo tracking and recovery of progenitor cells. *Nat Biotech* **2000,** 18, (4), 410-414.

(55)   Huber, D. L., Synthesis, Properties, and Applications of Iron Nanoparticles. *Small* **2005,** 1, (5), 482-501.

(56)   Dresco, P. A.; Zaitsev, V. S.; Gambino, R. J.; Chu, B., Preparation and properties of magnetite and polymer magnetite nanoparticles. *Langmuir* **1999,** 15, (6), 1945-1951.

(57)   Qu, S. C.; Yang, H. B.; Ren, D. W.; Kan, S. H.; Zou, G. T.; Li, D. M.; Li, M. H., Magnetite nanoparticles prepared by precipitation from partially reduced ferric chloride aqueous solutions. *Journal of Colloid and Interface Science* **1999,** 215, (1), 190-192.

(58)   Zhu, Y. H.; Wu, Q. F., Synthesis of magnetite nanoparticles by precipitation with forced mixing. *Journal of Nanoparticle Research* **1999,** 1, (3), 393-396.

(59)   Bodker, F.; Hansen, M. F.; Koch, C. B.; Lefmann, K.; Morup, S., Magnetic properties of hematite nanoparticles. *Physical Review B* **2000,** 61, (10), 6826-6838.

(60)   Teleki, A.; Suter, M.; Kidambi, P. R.; Ergeneman, O.; Krumeich, F.; Nelson, B. J.; Pratsinis, S. E., Hermetically Coated Superparamagnetic Fe2O3 Particles with SiO2 Nanofilms. *Chemistry of Materials* **2009,** 21, (10), 2094-2100.

(61)   Rondinone, A. J.; Liu, C.; Zhang, Z. J., Determination of magnetic anisotropy distribution and anisotropy constant of manganese spinel ferrite nanoparticles. *Journal of Physical Chemistry B* **2001,** 105, (33), 7967-7971.

(62)   Zeng, H.; Rice, P. M.; Wang, S. X.; Sun, S., Shape-Controlled Synthesis and Shape-Induced Texture of MnFe2O4 Nanoparticles. *Journal of the American Chemical Society* **2004,** 126, (37), 11458-11459.

(63)   Rondinone, A. J.; Samia, A. C. S.; Zhang, Z. J., Characterizing the magnetic anisotropy constant of spinel cobalt ferrite nanoparticles. *Applied Physics Letters* **2000,** 76, (24), 3624-3626.

(64)   Klabunde, K. J.; Zhang, D.; Glavee, G. N.; Sorensen, C. M.; Hadjipanayis, G. C., Encapsulated Nanoparticles of Iron Metal. *Chemistry of Materials* **1994,** 6, (6), 784-787.

(65)   Herrmann, I. K.; Grass, R. N.; Mazunin, D.; Stark, W. J., Synthesis and Covalent Surface Functionalization of Nonoxidic Iron Core-Shell Nanomagnets. *Chemistry of Materials* **2009,** 21, (14), 3275-3281.

(66)   Seshadri, R.; Sen, R.; Subbanna, G. N.; Kannan, K. R.; Rao, C. N. R., Iron, Cobalt and Nickel Nanoparticles Encapsulated in Carbon Obtained by the Arc Evaporation of Graphite with the Metals. *Chemical Physics Letters* **1994,** 231, (2-3), 308-313.

(67)   Grass, R. N.; Athanassiou, E. K.; Stark, W. J., Covalently functionalized cobalt nanoparticles as a platform for magnetic separations in organic synthesis. *Angewandte Chemie-International Edition* **2007,** 46, (26), 4909-4912.

(68)   Grass, R. N.; Stark, W. J., Gas phase synthesis of fcc-cobalt nanoparticles. *Journal of Materials Chemistry* **2006,** 16, (19), 1825-1830.

(69)   Maaz, K.; Mumtaz, A.; Hasanain, S. K.; Ceylan, A., Synthesis and magnetic properties of cobalt ferrite ($CoFe_2O_4$) nanoparticles prepared by wet chemical route. *Journal of Magnetism and Magnetic Materials* **2007,** 308, (2), 289-295.

(70)   Sun, S.; Zeng, H., Size-Controlled Synthesis of Magnetite Nanoparticles. *Journal of the American Chemical Society* **2002,** 124, (28), 8204-8205.

(71)   Lattuada, M.; Hatton, T. A., Functionalization of Monodisperse Magnetic Nanoparticles. *Langmuir* **2006,** 23, (4), 2158-2168.

(72)   Yang, H.; Ogawa, T.; Hasegawa, D.; Takahashi, M., Synthesis and magnetic properties of monodisperse magnetite nanocubes. *Journal of Applied Physics* **2008,** 103, (7), 07D526.

(73)   Yang, H. T.; Shen, C. M.; Wang, Y. G.; Su, Y. K.; Yang, T. Z.; Gao, H. J., Stable cobalt nanoparticles passivated with oleic acid and triphenylphosphine. *Nanotechnology* **2004,** 15, (1), 70.

(74)   Roig, A.; Molins, E.; González-Carreño, T.; Serna, C., Magnetic characterization of γ-Fe_2O_3 nanoparticles fabricated by aerosol pyrolysis. *Journal of Applied Physics* **1998,** 83, (6), 3256-3262.

(75)   Geng, J.; Jefferson, D. A.; Johnson, B. F., Direct conversion of iron stearate into magnetic Fe and Fe_3C nanocrystals encapsulated in polyhedral graphite cages. *Chemical Communications* **2004**, (21), 2442-2443.

(76)   Stark, W. J.; Pratsinis, S. E., Aerosol flame reactors for manufacture of nanoparticles. *Powder Technology* **2002,** 126, (2), 103-108.

(77)   Ulrich, G. D., Theory of particle formation and growth in oxide synthesis flames. *Combustion Science and Technology* **1971,** 4, (1), 47-57.

(78)   Mädler, L.; Stark, W.; Pratsinis, S., Flame-made ceria nanoparticles. *Journal of Materials Research* **2002,** 17, (06), 1356-1362.

(79)   Bubenhofer, S. B.; Schumacher, C. M.; Koehler, F. M.; Luechinger, N. A.; Grass, R. N.; Stark, W. J., Large-Scale Synthesis of PbS–TiO_2 Heterojunction Nanoparticles in a Single Step for Solar Cell Application. *The Journal of Physical Chemistry C* **2012,** 116, (30), 16264-16270.

(80)   Strobel, R.; Pratsinis, S. E., Flame aerosol synthesis of smart nanostructured materials. *Journal of Materials Chemistry* **2007,** 17, (45), 4743-4756.

(81)   Grass, R. N.; Stark, W. J., Flame synthesis of calcium-, strontium-, barium fluoride nanoparticles and sodium chloride. *Chemical Communications* **2005**, (13), 1767-1769.

(82)   Qin, X.; Ju, Y.; Bernhard, S.; Yao, N., Europium-doped yttrium silicate nanophosphors prepared by flame synthesis. *Materials Research Bulletin* **2007,** 42, (8), 1440-1449.

(83)   Teleki, A.; Bjelobrk, N.; Pratsinis, S. E., Flame-made Nb- and Cu-doped TiO_2 sensors for CO and ethanol. *Sensors and Actuators B: Chemical* **2008,** 130, (1), 449-457.

(84)   Schulz, H.; Stark, W. J.; Maciejewski, M.; Pratsinis, S. E.; Baiker, A., Flame-made nanocrystalline ceria/zirconia doped with alumina or silica: structural properties and enhanced oxygen exchange capacity. *Journal of Materials Chemistry* **2003,** 13, (12), 2979-2984.

(85)   Bubenhofer, S. B.; Krumeich, F.; Fuhrer, R.; Athanassiou, E. K.; Stark, W. J.; Grass, R. N., From Embedded to Supported Metal/Oxide Nanomaterials: Thermal Behavior and Structural Evolution at Elevated Temperatures. *The Journal of Physical Chemistry C* **2010,** 115, (4), 1269-1276.

(86)   Athanassiou, E. K.; Grass, R. N.; Stark, W. J., Large-scale production of carbon-coated copper nanoparticles for sensor applications. *Nanotechnology* **2006,** 17, (6), 1668-1673.

(87)   Zeltner, M.; Grass, R. N.; Schaetz, A.; Bubenhofer, S. B.; Luechinger, N. A.; Stark, W. J., Stable dispersions of ferromagnetic carbon-coated metal nanoparticles: preparation via surface initiated atom transfer radical polymerization. *Journal of Materials Chemistry* **2012,** 22, (24), 12064-12071.

(88)   Schätz, A.; Hager, M.; Reiser, O., Cu(II)-Azabis(oxazoline)-Complexes Immobilized on Superparamagnetic Magnetite@Silica-Nanoparticles: A Highly Selective and Recyclable Catalyst for the Kinetic Resolution of 1,2-Diols. *Advanced Functional Materials* **2009,** 19, (13), 2109-2115.

(89)   Schaetz, A.; Zeltner, M.; Michl, T. D.; Rossier, M.; Fuhrer, R.; Stark, W. J., Magnetic Silyl Scaffold Enables Efficient Recycling of Protecting Groups. *Chemistry – A European Journal* **2011,** 17, (38), 10566-10573.

(90)   Tomita, S.; Hikita, M.; Fujii, M.; Hayashi, S.; Yamamoto, K., A new and simple method for thin graphitic coating of magnetic-metal nanoparticles. *Chemical Physics Letters* **2000,** 316, (5), 361-364.

(91)   Banhart, F.; Redlich, P.; Ajayan, P. M., The migration of metal atoms through carbon onions. *Chemical Physics Letters* **1998,** 292, (4-6), 554-560.

(92)   Banhart, F.; Grobert, N.; Terrones, M.; Charlier, J.-C.; Ajayan, P., Metal atoms in carbon nanotubes and related nanoparticles. *International Journal of Modern Physics B* **2001,** 15, (31), 4037-4069.

(93)   Ruoff, R. S.; Lorents, D. C.; Chan, B.; Malhotra, R.; Subramoney, S., Single crystal metals encapsulated in carbon nanoparticles. *Science* **1993,** 259, 346-346.

(94)   Gupta, A. K.; Gupta, M., Synthesis and surface engineering of iron oxide nanoparticles for biomedical applications. *Biomaterials* **2005,** 26, (18), 3995-4021.

(95)   Amstad, E.; Gillich, T.; Bilecka, I.; Textor, M.; Reimhult, E., Ultrastable Iron Oxide Nanoparticle Colloidal Suspensions Using Dispersants with Catechol-Derived Anchor Groups. *Nano Letters* **2009,** 9, (12), 4042-4048.

(96) Herrmann, I. K.; Bernabei, R. E.; Urner, M.; Grass, R. N.; Beck-Schimmer, B.; Stark, W. J., Device for continuous extracorporeal blood purification using target-specific metal nanomagnets. *Nephrology Dialysis Transplantation* **2011,** 26, (9), 2948-U1516.

(97) Amici, R. M.; Belmont, J. A.; Galloway, C. P. Reaction of carbon black with diazonium salts, resultant carbon black products and their uses. Patent US5851280 A **1998**.

(98) Novoselov, K. S.; Geim, A. K.; Morozov, S. V.; Jiang, D.; Zhang, Y.; Dubonos, S. V.; Grigorieva, I. V.; Firsov, A. A., Electric field effect in atomically thin carbon films. *Science* **2004,** 306, (5696), 666-669.

(99) Li, D.; Muller, M. B.; Gilje, S.; Kaner, R. B.; Wallace, G. G., Processable aqueous dispersions of graphene nanosheets. *Nat Nano* **2008,** 3, (2), 101-105.

(100) Geim, A. K., Graphene: Status and Prospects. *Science* **2009,** 324, (5934), 1530-1534.

(101) Geim, A. K.; Novoselov, K. S., The rise of graphene. *Nat Mater* **2007,** 6, (3), 183-191.

(102) Li, X. S.; Cai, W. W.; An, J. H.; Kim, S.; Nah, J.; Yang, D. X.; Piner, R.; Velamakanni, A.; Jung, I.; Tutuc, E.; Banerjee, S. K.; Colombo, L.; Ruoff, R. S., Large-Area Synthesis of High-Quality and Uniform Graphene Films on Copper Foils. *Science* **2009,** 324, (5932), 1312-1314.

(103) Li, X.; Zhu, Y.; Cai, W.; Borysiak, M.; Han, B.; Chen, D.; Piner, R. D.; Colombo, L.; Ruoff, R. S., Transfer of Large-Area Graphene Films for High-Performance Transparent Conductive Electrodes. *Nano Letters* **2009,** 9, (12), 4359-4363.

(104) Li, X. L.; Wang, X. R.; Zhang, L.; Lee, S. W.; Dai, H. J., Chemically derived, ultrasmooth graphene nanoribbon semiconductors. *Science* **2008,** 319, (5867), 1229-1232.

(105) Chen, Z.; Lin, Y.-M.; Rooks, M. J.; Avouris, P., Graphene nano-ribbon electronics. *Physica E: Low-dimensional Systems and Nanostructures* **2007,** 40, (2), 228-232.

(106) Jiang, D. E.; Cooper, V. R.; Dai, S., Porous Graphene as the Ultimate Membrane for Gas Separation. *Nano Letters* **2009,** 9, (12), 4019-4024.

(107) Schrier, J., Helium Separation Using Porous Graphene Membranes. *The Journal of Physical Chemistry Letters* **2010,** 1, (15), 2284-2287.

(108) Du, H. L.; Li, J. Y.; Zhang, J.; Su, G.; Li, X. Y.; Zhao, Y. L., Separation of Hydrogen and Nitrogen Gases with Porous Graphene Membrane. *Journal of Physical Chemistry C* **2011,** 115, (47), 23261-23266.

(109) Sint, K.; Wang, B.; Kral, P., Selective Ion Passage through Functionalized Graphene Nanopores. *Journal of the American Chemical Society* **2008,** 130, (49), 16448-16449.

(110) Lemme, M. C.; Echtermeyer, T. J.; Baus, M.; Kurz, H., A graphene field-effect device. *Electron Device Letters, IEEE* **2007,** 28, (4), 282-284.

(111) Bae, S.; Kim, H.; Lee, Y.; Xu, X. F.; Park, J. S.; Zheng, Y.; Balakrishnan, J.; Lei, T.; Kim, H. R.; Song, Y. I.; Kim, Y. J.; Kim, K. S.; Ozyilmaz, B.; Ahn, J. H.; Hong, B. H.; Iijima, S., Roll-to-roll production of 30-inch graphene films for transparent electrodes. *Nature Nanotechnology* **2010,** 5, (8), 574-578.

(112) Bell, D. C.; Lemme, M. C.; Stern, L. A.; Marcus, C. M., Precision material modification and patterning with He ions. *Journal of Vacuum Science & Technology B* **2009,** 27, (6), 2755-2758.

(113) Shivaraman, S.; Barton, R. A.; Yu, X.; Alden, J.; Herman, L.; Chandrashekhar, M. V. S.; Park, J.; McEuen, P. L.; Parpia, J. M.; Craighead, H. G.; Spencer, M. G., Free-Standing Epitaxial Graphene. *Nano Letters* **2009,** 9, (9), 3100-3105.

(114) Biro, L. P.; Lambin, P., Nanopatterning of graphene with crystallographic orientation control. *Carbon* **2010,** 48, (10), 2677-2689.

(115) Ci, L.; Xu, Z. P.; Wang, L. L.; Gao, W.; Ding, F.; Kelly, K. F.; Yakobson, B. I.; Ajayan, P. M., Controlled Nanocutting of Graphene. *Nano Research* **2008,** 1, (2), 116-122.

(116) Johannsen, M.; Thiesen, B.; Wust, P.; Jordan, A., Magnetic nanoparticle hyperthermia for prostate cancer. *International Journal of Hyperthermia* **2010,** 26, (8), 790-795.

(117) Xu, Y.; Mahmood, M.; Li, Z. R.; Dervishi, E.; Trigwell, S.; Zharov, V. P.; Ali, N.; Saini, V.; Biris, A. R.; Lupu, D.; Boldor, D.; Biris, A. S., Cobalt nanoparticles coated with graphitic shells as localized radio frequency absorbers for cancer therapy. *Nanotechnology* **2008,** 19, (43).

(118) Mohapatra, S.; Mallick, S. K.; Maiti, T. K.; Ghosh, S. K.; Pramanik, P., Synthesis of highly stable folic acid conjugated magnetite nanoparticles for targeting cancer cells. *Nanotechnology* **2007,** 18, (38).

(119) Basly, B.; Felder-Flesch, D.; Perriat, P.; Billotey, C.; Taleb, J.; Pourroy, G.; Begin-Colin, S., Dendronized iron oxide nanoparticles as contrast agents for MRI. *Chemical Communications* **2010,** 46, (6), 985-987.

(120) Na, H. B.; Song, I. C.; Hyeon, T., Inorganic Nanoparticles for MRI Contrast Agents. *Advanced Materials* **2009,** 21, (21), 2133-2148.

(121) Zhao, M.; Beauregard, D. A.; Loizou, L.; Davletov, B.; Brindle, K. M., Non-invasive detection of apoptosis using magnetic resonance imaging and a targeted contrast agent. *Nature Medicine* **2001,** 7, (11), 1241-1244.

(122) Neuberger, T.; Schopf, B.; Hofmann, H.; Hofmann, M.; von Rechenberg, B., Superparamagnetic nanoparticles for biomedical applications: Possibilities and limitations of a new drug delivery system. *Journal of Magnetism and Magnetic Materials* **2005,** 293, (1), 483-496.

(123) LaVan, D. A.; McGuire, T.; Langer, R., Small-scale systems for in vivo drug delivery. *Nature Biotechnology* **2003,** 21, (10), 1184-1191.

(124) Herrmann, I. K.; Schlegel, A.; Graf, R.; Schumacher, C. M.; Senn, N.; Hasler, M.; Gschwind, S.; Hirt, A.-M.; Günther, D.; Clavien, P.-A., Nanomagnet-based removal of lead and digoxin from living rats. *Nanoscale* **2013,** 5, (18), 8718-8723.

(125) Herrmann, I. K.; Urner, M.; Koehler, F. M.; Hasler, M.; Roth-Z'Graggen, B.; Grass, R. N.; Ziegler, U.; Beck-Schimmer, B.; Stark, W. J., Blood Purification Using Functionalized Core/Shell Nanomagnets. *Small* **2010,** 6, (13), 1388-1392.

(126) Herrmann, I. K.; Urner, M.; Hasler, M.; Roth-Z'Graggen, B.; Aemisegger, C.; Baulig, W.; Athanassiou, E. K.; Regenass, S.; Stark, W. J.; Beck-Schimmer, B., Iron core/shell nanoparticles as magnetic drug carriers: possible interactions with the vascular compartment. *Nanomedicine* **2011,** 6, (7), 1199-1213.

(127) Heneghan, C.; Langton, D.; Thompson, M., Ongoing problems with metal-on-metal hip implants. *British Medical Journal* **2012,** 344.

(128) Shubayev, V. I.; Pisanic Ii, T. R.; Jin, S., Magnetic nanoparticles for theragnostics. *Advanced Drug Delivery Reviews* **2009,** 61, (6), 467-477.

(129) Bertorelle, F.; Wilhelm, C.; Roger, J.; Gazeau, F.; Ménager, C.; Cabuil, V., Fluorescence-Modified Superparamagnetic Nanoparticles: Intracellular Uptake and Use in Cellular Imaging. *Langmuir* **2006,** 22, (12), 5385-5391.

(130) Sun, C.; Lee, J. S. H.; Zhang, M., Magnetic nanoparticles in MR imaging and drug delivery. *Advanced Drug Delivery Reviews* **2008,** 60, (11), 1252-1265.

(131) Gallo, J.; Long, N. J.; Aboagye, E. O., Magnetic nanoparticles as contrast agents in the diagnosis and treatment of cancer. *Chemical Society Reviews* **2013,** 42, (19), 7816-7833.

(132) Luo, N.; Li, X. J.; Wang, X. H.; Mo, F.; Wang, H. T., Synthesis of Carbon-Encapsulated Metal Nanoparticles by a Detonation Method. *Combustion Explosion and Shock Waves* **2010,** 46, (5), 609-613.

(133) Lu, A. H.; Li, W. C.; Matoussevitch, N.; Spliethoff, B.; Bonnemann, H.; Schuth, F., Highly stable carbon-protected cobalt nanoparticles and graphite shells. *Chemical Communications* **2005**, (1), 98-100.

(134) Zeltner, M.; Schatz, A.; Hefti, M. L.; Stark, W. J., Magnetothermally responsive C/Co@PNIPAM-nanoparticles enable preparation of self-separating phase-switching palladium catalysts. *Journal of Materials Chemistry* **2011,** 21, (9), 2991-2996.

(135) Tan, C. G.; Grass, R. N., Suzuki cross-coupling reactions on the surface of carbon-coated cobalt: expanding the applicability of core–shell nano-magnets. *Chemical Communications* **2008**, (36), 4297-4299.

(136) Lin, J. H.; Wu, Z. H.; Tseng, W. L., Extraction of environmental pollutants using magnetic nanomaterials. *Analytical Methods* **2010,** 2, (12), 1874-1879.

(137) Liu, J. F.; Zhao, Z. S.; Jiang, G. B., Coating Fe_3O_4 magnetic nanoparticles with humic acid for high efficient removal of heavy metals in water. *Environmental Science & Technology* **2008,** 42, (18), 6949-6954.

(138) Rossier, M.; Schaetz, A.; Athanassiou, E. K.; Grass, R. N.; Stark, W. J., Reversible As (V) adsorption on magnetic nanoparticles and pH dependent desorption concentrates dilute solutions and realizes true moving bed reactor systems. *Chemical Engineering Journal* **2011**.

(139) Schaetz, A.; Zeltner, M.; Michl, T. D.; Rossier, M.; Fuhrer, R.; Stark, W. J., Magnetic Silyl Scaffold Enables Efficient Recycling of Protecting Groups. *Chemistry - A European Journal* **2011,** 17, (38), 10566-10573.

(140) Wittmann, S.; Schätz, A.; Grass, R. N.; Stark, W. J.; Reiser, O., A Recyclable Nanoparticle-Supported Palladium Catalyst for the Hydroxycarbonylation of Aryl Halides in Water. *Angewandte Chemie International Edition* **2010,** 49, (10), 1867-1870.

(141) Stark, W. J., Nanoparticles in Biological Systems. *Angewandte Chemie-International Edition* **2011,** 50, (6), 1242-1258.

(142) Veiseh, O.; Gunn, J. W.; Zhang, M. Q., Design and fabrication of magnetic nanoparticles for targeted drug delivery and imaging. *Advanced Drug Delivery Reviews* **2010,** 62, (3), 284-304.

(143) Chorny, M.; Polyak, B.; Alferiev, I. S.; Walsh, K.; Friedman, G.; Levy, R. J., Magnetically driven plasmid DNA delivery with biodegradable polymeric nanoparticles. *Faseb Journal* **2007,** 21, (10), 2510-2519.

(144) Sherlock, S. P.; Tabakman, S. M.; Xie, L. M.; Dai, H. J., Photothermally Enhanced Drug Delivery by Ultrasmall Multifunctional FeCo/Graphitic Shell Nanocrystals. *Acs Nano* **2011,** 5, (2), 1505-1512.

(145) Foy, S. P.; Manthe, R. L.; Foy, S. T.; Dimitrijevic, S.; Krishnamurthy, N.; Labhasetwar, V., Optical Imaging and Magnetic Field Targeting of Magnetic Nanoparticles in Tumors. *ACS Nano* **2010,** 4, (9), 5217-5224.

(146) Maier-Hauff, K.; Ulrich, F.; Nestler, D.; Niehoff, H.; Wust, P.; Thiesen, B.; Orawa, H.; Budach, V.; Jordan, A., Efficacy and safety of intratumoral thermotherapy using magnetic iron-oxide nanoparticles combined with external beam radiotherapy on patients with recurrent glioblastoma multiforme. *Journal of Neuro-Oncology* **2011,** 103, (2), 317-324.

(147) Wust, P.; Gneveckow, U.; Johannsen, M.; Bohmer, D.; Henkel, T.; Kahmann, F.; Sehouli, J.; Felix, R.; Ricke, J.; Jordan, A., Magnetic nanoparticles for interstitial thermotherapy - feasibility, tolerance and achieved temperatures. *International Journal of Hyperthermia* **2006,** 22, (8), 673-685.

(148) Sun, C.; Fang, C.; Stephen, Z.; Veiseh, O.; Hansen, S.; Lee, D.; Ellenbogen, R. G.; Olson, J.; Zhang, M. Q., Tumor-targeted drug delivery and MRI contrast enhancement by chlorotoxin-conjugated iron oxide nanoparticles. *Nanomedicine* **2008,** 3, (4), 495-505.

(149) Seo, W. S.; Lee, J. H.; Sun, X. M.; Suzuki, Y.; Mann, D.; Liu, Z.; Terashima, M.; Yang, P. C.; McConnell, M. V.; Nishimura, D. G.; Dai, H. J., FeCo/graphitic-shell nanocrystals as advanced magnetic-resonance-imaging and near-infrared agents. *Nature Materials* **2006,** 5, (12), 971-976.

(150) Rossier, M.; Koehler, F. M.; Athanassiou, E. K.; Grass, R. N.; Aeschlimann, B.; Gunther, D.; Stark, W. J., Gold adsorption on the carbon surface of C/Co nanoparticles allows magnetic extraction from extremely diluted aqueous solutions. *Journal of Materials Chemistry* **2009,** 19, (43), 8239-8243.

(151) Fuhrer, R.; Athanassiou, E. K.; Luechinger, N. A.; Stark, W. J., Crosslinking Metal Nanoparticles into the Polymer Backbone of Hydrogels Enables Preparation of Soft, Magnetic Field-Driven Actuators with Muscle-Like Flexibility. *Small* **2009,** 5, (3), 383-388.

(152) Zhang, W.; Sun, L.; Xu, Z.; Krasheninnikov, A. V.; Huai, P.; Zhu, Z.; Banhart, F., Migration of gold atoms in graphene ribbons: Role of the edges. *Physical Review B* **2010,** 81, (12).

(153) Cretu, O.; Krasheninnikov, A. V.; Rodriguez-Manzo, J. A.; Sun, L. T.; Nieminen, R. M.; Banhart, F., Migration and Localization of Metal Atoms on Strained Graphene. *Physical Review Letters* **2010,** 105, (19).

(154) Gan, Y. J.; Sun, L. T.; Banhart, F., One- and two-dimensional diffusion of metal atoms in graphene. *Small* **2008,** 4, (5), 587-591.

(155) Gan, Y. J.; Banhart, F., The Mobility of Carbon Atoms in Graphitic Nanoparticles Studied by the Relaxation of Strain in Carbon Onions. *Advanced Materials* **2008,** 20, (24), 4751-4754.

(156) Bubenhofer, S. B.; Krumeich, F.; Fuhrer, R.; Athanassiou, E. K.; Stark, W. J.; Grass, R. N., From Embedded to Supported Metal/Oxide Nanomaterials: Thermal Behavior and Structural Evolution at Elevated Temperatures. *The Journal of Physical Chemistry C* **2011**.

(157) Kitamura, H.; Sekido, M.; Takeuchi, H.; Ohno, M., The method for surface functionalization of single-walled carbon nanotubes with fuming nitric acid. *Carbon* **2011,** 49, (12), 3851-3856.

(158) Datsyuk, V.; Kalyva, M.; Papagelis, K.; Parthenios, J.; Tasis, D.; Siokou, A.; Kallitsis, I.; Galiotis, C., Chemical oxidation of multiwalled carbon nanotubes. *Carbon* **2008,** 46, (6), 833-840.

(159) Chen, K.; Wang, C.; Ma, D.; Huang, W.; Bao, X., Graphitic carbon nanostructures via a facile microwave-induced solid-state process. *Chemical Communications* **2008**, (24), 2765-2767.

(160) Koehler, F. M.; Luechinger, N. A.; Ziegler, D.; Athanassiou, E. K.; Grass, R. N.; Rossi, A.; Hierold, C.; Stemmer, A.; Stark, W. J., Permanent Pattern-Resolved Adjustment of the Surface Potential of Graphene-Like Carbon through Chemical Functionalization. *Angewandte Chemie-International Edition* **2009,** 48, (1), 224-227.

(161) Bekyarova, E.; Itkis, M. E.; Ramesh, P.; Berger, C.; Sprinkle, M.; de Heer, W. A.; Haddon, R. C., Chemical Modification of Epitaxial Graphene: Spontaneous Grafting of Aryl Groups. *Journal of the American Chemical Society* **2009,** 131, (4), 1336-1337.

(162) Gilje, S.; Han, S.; Wang, M.; Wang, K. L.; Kaner, R. B., A chemical route to graphene for device applications. *Nano Letters* **2007,** 7, (11), 3394-3398.

(163) Yu, D. S.; Dai, L. M., Self-Assembled Graphene/Carbon Nanotube Hybrid Films for Supercapacitors. *Journal of Physical Chemistry Letters* **2010,** 1, (2), 467-470.

(164) Wassei, J. K.; Kaner, R. B., Graphene, a promising transparent conductor. *Materials Today* **2010,** 13, (3), 52-59.

(165) Wang, X.; Zhi, L. J.; Mullen, K., Transparent, conductive graphene electrodes for dye-sensitized solar cells. *Nano Letters* **2008,** 8, (1), 323-327.

(166) Bi, H.; Sun, S. R.; Huang, F. Q.; Xie, X. M.; Jiang, M. H., Direct growth of few-layer graphene films on SiO_2 substrates and their photovoltaic applications. *Journal of Materials Chemistry* **2012,** 22, (2), 411-416.

(167) Kalita, G.; Matsushima, M.; Uchida, H.; Wakita, K.; Umeno, M., Graphene constructed carbon thin films as transparent electrodes for solar cell applications. *Journal of Materials Chemistry* **2010,** 20, (43), 9713-9717.

(168) Zhang, L. M.; Diao, S. O.; Nie, Y. F.; Yan, K.; Liu, N.; Dai, B. Y.; Xie, Q.; Reina, A.; Kong, J.; Liu, Z. F., Photocatalytic Patterning and Modification of Graphene. *Journal of the American Chemical Society* **2011,** 133, (8), 2706-2713.

(169) Preacutevel, B.; Benoit, J. M.; Bardotti, L.; Meacutelinon, P.; Ouerghi, A.; Lucot, D.; Bourhis, E.; Gierak, J., Nanostructuring graphene on SiC by focused ion beam: Effect of the ion fluence. *Applied Physics Letters* **2011,** 99, (8), 083116 (3 pp.).

(170) Nemes-Incze, P.; Magda, G.; Kamaras, K.; Biro, L. P., Crystallographically selective nanopatterning of graphene on SiO_2. *Nano Research* **2010,** 3, (2), 110-116.

(171) Hauser, A. W.; Schwerdtfeger, P., Nanoporous Graphene Membranes for Efficient $^3He/^4He$ Separation. *Journal of Physical Chemistry Letters* **2012,** 3, (2), 209-213.

(172) Blankenburg, S.; Bieri, M.; Fasel, R.; Mullen, K.; Pignedoli, C. A.; Passerone, D., Porous Graphene as an Atmospheric Nanofilter. *Small* **2010,** 6, (20), 2266-2271.

(173) Fox, D.; O'Neill, A.; Zhou, D.; Boese, M.; Coleman, J. N.; Zhang, H. Z., Nitrogen assisted etching of graphene layers in a scanning electron microscope. *Applied Physics Letters* **2011,** 98, (24), 243117.

(174) Fredriksson, H.; Chakarov, D.; Kasemo, B., Patterning of highly oriented pyrolytic graphite and glassy carbon surfaces by nanolithography and oxygen plasma etching. *Carbon* **2009,** 47, (5), 1335-1342.

(175) Bottcher, A.; Heil, M.; Sturzl, N.; Jester, S. S.; Malik, S.; Perez-Willard, F.; Brenner, P.; Gerthsen, D.; Kappes, M. M., Nanostructuring the graphite basal plane by focused ion beam patterning and oxygen etching. *Nanotechnology* **2006,** 17, (23), 5889-5894.

(176) Yasuda, K.; Siroma, Z.; Ishii, K.; Miyazaki, Y.; Inaba, M.; Tasaka, A., Imaging of highly oriented pyrolytic graphite corrosion accelerated by Pt particles. *Electrochemistry Communications* **2005,** 7, (11), 1153-1156.

(177) Schaffel, F.; Warner, J. H.; Bachmatiuk, A.; Rellinghaus, B.; Buchner, B.; Schultz, L.; Rummeli, M. H., Shedding Light on the Crystallographic Etching of Multi-Layer Graphene at the Atomic Scale. *Nano Research* **2009,** 2, (9), 695-705.

(178) Campos, L. C.; Manfrinato, V. R.; Sanchez-Yamagishi, J. D.; Kong, J.; Jarillo-Herrero, P., Anisotropic Etching and Nanoribbon Formation in Single-Layer Graphene. *Nano Letters* **2009,** 9, (7), 2600-2604.

(179) Datta, S. S.; Strachan, D. R.; Khamis, S. M.; Johnson, A. T. C., Crystallographic etching of few-layer graphene. *Nano Letters* **2008,** 8, (7), 1912-1915.

(180) Konishi, S.; Sugimoto, W.; Murakami, Y.; Takasu, Y., Catalytic creation of channels in the surface layers of highly oriented pyrolytic graphite by cobalt nanoparticles. *Carbon* **2006,** 44, (11), 2338-2340.

(181) Tsukamoto, T.; Ogino, T., Graphene etching controlled by atomic structures on the substrate surface. *Carbon* **2012,** 50, (2), 674-679.

(182) Murphy, S.; Nielsen, R. M.; Strebel, C.; Johansson, M.; Nielsen, J. H., Catalytic oxidation of graphite by mass-selected ruthenium nanoparticles. *Carbon* **2011,** 49, (2), 376-385.

(183) Severin, N.; Kirstein, S.; Sokolov, I. M.; Rabe, J. P., Rapid Trench Channeling of Graphenes with Catalytic Silver Nanoparticles. *Nano Letters* **2009,** 9, (1), 457-461.

(184) Issa, M.; Mahzoul, H.; Brillard, A.; Brilhac, J. F., Catalytic Carbon Oxidation in The Presence of Cerium Oxide: Experimental Study and Modeling of The Effect of Oxygen Concentration. *Chemical Engineering & Technology* **2009,** 32, (12), 1859-1865.

(185) Setiabudi, A.; Chen, J. L.; Mul, G.; Makkee, M.; Moulijn, J. A., CeO_2 catalysed soot oxidation - The role of active oxygen to accelerate the oxidation conversion. *Applied Catalysis B-Environmental* **2004,** 51, (1), 9-19.

(186) Tikhomirov, K.; Krocher, O.; Elsener, M.; Wokaun, A., MnO_x-CeO_2 mixed oxides for the low-temperature oxidation of diesel soot. *Applied Catalysis B-Environmental* **2006,** 64, (1-2), 72-78.

(187) Wagner, V.; Dullaart, A.; Bock, A. K.; Zweck, A., The emerging nanomedicine landscape. *Nature Biotechnology* **2006,** 24, (10), 1211-1217.

(188) Kayal, S.; Ramanujan, R. V., Doxorubicin loaded PVA coated iron oxide nanoparticles for targeted drug delivery. *Materials Science & Engineering C* **2010,** 30, (3), 484-490.

(189) Guo, S. J.; Li, D.; Zhang, L. M.; Li, J.; Wang, E. K., Monodisperse mesoporous superparamagnetic single-crystal magnetite nanoparticles for drug delivery. *Biomaterials* **2009,** 30, (10), 1881-1889.

(190) Amirfazli, A., Magnetic nanoparticles hit the target. *Nature Nanotechnology* **2007,** 2, (8), 467-468.

(191) Uchida, M.; Terashima, M.; Cunningham, C. H.; Suzuki, Y.; Willits, D. A.; Willis, A. F.; Yang, P. C.; Tsao, P. S.; McConnell, M. V.; Young, M. J.; Douglas, T., A Human Ferritin Iron Oxide Nano-composite Magnetic Resonance Contrast Agent. *Magnetic Resonance in Medicine* **2008,** 60, (5), 1073-1081.

(192)   Hong, R. Y.; Feng, B.; Chen, L. L.; Liu, G. H.; Li, H. Z.; Zheng, Y.; Wei, D. G., Synthesis, characterization and MRI application of dextran-coated Fe_3O_4 magnetic nanoparticles. *Biochemical Engineering Journal* **2008,** 42, (3), 290-300.

(193)   Mahmoudi, M.; Sant, S.; Wang, B.; Laurent, S.; Sen, T., Superparamagnetic iron oxide nanoparticles (SPIONs): Development, surface modification and applications in chemotherapy. *Advanced Drug Delivery Reviews* **2011,** 63, (1-2), 24-46.

(194)   Li, Z. X.; Kawashita, M.; Araki, N.; Mitsumori, M.; Hiraoka, M.; Doi, M., Magnetite nanoparticles with high heating efficiencies for application in the hyperthermia of cancer. *Materials Science & Engineering C* **2010,** 30, (7), 990-996.

(195)   Andronescu, E.; Ficai, M.; Voicu, G.; Ficai, D.; Maganu, M.; Ficai, A., Synthesis and characterization of collagen/hydroxyapatite: magnetite composite material for bone cancer treatment. *Journal of Materials Science-Materials in Medicine* **2010,** 21, (7), 2237-2242.

(196)   Cheng, Z. L.; Al Zaki, A.; Hui, J. Z.; Muzykantov, V. R.; Tsourkas, A., Multifunctional Nanoparticles: Cost Versus Benefit of Adding Targeting and Imaging Capabilities. *Science* **2012,** 338, (6109), 903-910.

(197)   Fan, C. X.; Gao, W. H.; Chen, Z. X.; Fan, H. Y.; Lie, M. Y.; Deng, F. J.; Chen, Z. L., Tumor selectivity of stealth multi-functionalized superparamagnetic iron oxide nanoparticles. *International Journal of Pharmaceutics* **2011,** 404, (1-2), 180-190.

(198)   Zhang, M.; Cheng, D.; He, X. W.; Chen, L. X.; Zhang, Y. K., Magnetic Silica-Coated Sub-Microspheres with Immobilized Metal Ions for the Selective Removal of Bovine Hemoglobin from Bovine Blood. *Chemistry - An Asian Journal* **2010,** 5, (6), 1332-1340.

(199)   Takahashi, M.; Yoshino, T.; Takeyama, H.; Matsunaga, T., Direct Magnetic Separation of Immune Cells from Whole Blood Using Bacterial Magnetic Particles Displaying Protein G. *Biotechnology Progress* **2009,** 25, (1), 219-226.

(200)   Mandal, S.; Ghosh, A.; Mandal, M., Iron Oxide Nanoparticle Assisted Purification and Mass Spectrometry Based Proteolytic Mapping of Intact CD4(+)T Cells from Human Blood. *Preparative Biochemistry & Biotechnology* **2009,** 39, (1), 20-31.

(201)   Jin, J.; Yang, F.; Zhang, F. W.; Hu, W. Q.; Sun, S. B.; Ma, J. T., 2,2'-(phenylazanediyl) diacetic acid modified Fe_3O_4@PEI for selective removal of cadmium ions from blood. *Nanoscale* **2012,** 4, (3), 733-736.

(202)   Schaller, V.; Kraling, U.; Rusu, C.; Petersson, K.; Wipenmyr, J.; Krozer, A.; Wahnstrom, G.; Sanz-Velasco, A.; Enoksson, P.; Johansson, C., Motion of nanometer sized magnetic particles in a magnetic field gradient. *Journal of Applied Physics* **2008,** 104, (9).

(203)   Sun, S. H.; Zeng, H., Size-controlled synthesis of magnetite nanoparticles. *Journal of the American Chemical Society* **2002,** 124, (28), 8204-8205.

(204)   Yu, W. W.; Falkner, J. C.; Yavuz, C. T.; Colvin, V. L., Synthesis of monodisperse iron oxide nanocrystals by thermal decomposition of iron carboxylate salts. *Chemical Communications* **2004**, (20), 2306-2307.

(205) Zhou, Z. H.; Wang, J.; Liu, X.; Chan, H. S. O., Synthesis of Fe_3O_4 nanoparticles from emulsions. *Journal of Materials Chemistry* **2001,** 11, (6), 1704-1709.

(206) Hou, Y. L.; Yu, J. F.; Gao, S., Solvothermal reduction synthesis and characterization of superparamagnetic magnetite nanoparticles. *Journal of Materials Chemistry* **2003,** 13, (8), 1983-1987.

(207) Amstad, E.; Textor, M.; Reimhult, E., Stabilization and functionalization of iron oxide nanoparticles for biomedical applications. *Nanoscale* **2011,** 3, (7), 2819-2843.

(208) Xie, J.; Xu, C.; Kohler, N.; Hou, Y.; Sun, S., Controlled PEGylation of monodisperse Fe_3O_4 nanoparticles for reduced non-specific uptake by macrophage cells. *Advanced Materials* **2007,** 19, (20), 3163-3166.

(209) Hermanson, G. T., *Bioconjugate Techniques*. Academic Press: 2008.

(210) Sun, J.; Zhou, S. B.; Hou, P.; Yang, Y.; Weng, J.; Li, X. H.; Li, M. Y., Synthesis and characterization of biocompatible Fe3O4 nanoparticles. *Journal of Biomedical Materials Research Part A* **2007,** 80A, (2), 333-341.

(211) Marquez, F.; Herrera, G. M.; Campo, T.; Cotto, M.; Duconge, J.; Sanz, J. M.; Elizalde, E.; Perales, O.; Morant, C., Preparation of hollow magnetite microspheres and their applications as drugs carriers. *Nanoscale Research Letters* **2012,** 7.

(212) Schaetz, A.; Zeltner, M.; Michl, T. D.; Rossier, M.; Fuhrer, R.; Stark, W. J., Magnetic Silyl Scaffold Enables Efficient Recycling of Protecting Groups. *Chemistry - A European Journal* **2011,** 17, (38), 10565-10572.

(213) Butler, A. M.; MacKay, E. M., The influence of the sodium and potassium content of the diet upon the sodium concentration of human centrifuged red blood cells. *Journal of Biological Chemistry* **1934,** 106, (1), 107-112.

(214) Klinke, R.; Bauer, C., *Physiologie*. 5 ed.; Thieme: 2005.

(215) Park, J. Y.; Daksha, P.; Lee, G. H.; Woo, S.; Chang, Y. M., Highly water-dispersible PEG surface modified ultra small superparamagnetic iron oxide nanoparticles useful for target-specific biomedical applications. *Nanotechnology* **2008,** 19, (36).

(216) Shkilnyy, A.; Munnier, E.; Herve, K.; Souce, M.; Benoit, R.; Cohen-Jonathan, S.; Limelette, P.; Saboungi, M. L.; Dubois, P.; Chourpa, I., Synthesis and Evaluation of Novel Biocompatible Super-paramagnetic Iron Oxide Nanoparticles as Magnetic Anticancer Drug Carrier and Fluorescence Active Label. *Journal of Physical Chemistry C* **2010,** 114, (13), 5850-5858.

CURRICULUM VITAE

Christoph Martin Schumacher

Functional Materials Laboratory

Institute for Chemical and Bioengineering

Department of Chemistry and Applied Biosciences

ETH Zurich, Vladimir-Prelog-Weg 1, HCI E113

8093 Zurich

Switzerland

Phone: +41 44 632 45 45

Fax: +41 44 633 15 71

Email: ch.schumacher@chem.ethz.ch

Homepage: www.fml.ethz.ch

Private Address:

Christoph Schumacher

Grosswiesenstrasse 71

8051 Zurich

Switzerland

Born December 27th, 1985 in Wattwil (SG)

Citizen of Switzerland

Education

3/2013 – 6/2013	International Program Associate at the Bioengineering Laboratory of Prof. Mizuo Maeda, RIKEN Institute Tokyo, Saitama, Japan
12/2010 – present	PhD-student at the Institute of Chemical- and Bioengineering, Functional Materials Laboratory of Prof. Wendelin J. Stark, ETH Zurich
10/2010 – 12/2010	Research-assistant at the Institute of Chemical and Bioengineering, Functional Materials Laboratory of Prof. Wendelin J. Stark, ETH Zurich
9/2010 – 10/2010	Semester-Thesis at the Institute of Chemical and Bioengineering, Functional Materials Laboratory of Prof. Wendelin J. Stark, ETH Zurich
2/2010 – 6/2010	Master-Thesis at the Institute of Process Engineering, Separation Processes Laboratory of Prof. Marco Mazzotti, ETH Zurich
10/2009 – 10/2010	Master studies in Chemical and Bioengineering, ETH Zurich
10/2005 – 9/2009	Bachelor studies in Chemical Engineering, ETH Zurich
11/2004 – 9/2005	Military service, Swiss Armed Forces
8/2000 – 9/2004	Commercial High School, Wattwil, SG
8/1998 – 7/2000	Secondary School, Wattwil, SG
8/1992 – 7/1998	Primary School, Wattwil, SG

Work experience

3/2013 – present	CTO and co-founder of the ETH spinoff company Novamem LLC, Zurich
12/2010 – present	PhD-student at the Institute of Chemical and Bioengineering, Functional Materials Laboratory of Prof. Wendelin J. Stark, ETH Zurich

10/2010 – 11/2010   Research-assistant at the Institute of Chemical and Bioengineering, Functional Materials Laboratory of Prof. Wendelin J. Stark, ETH Zurich

Refereed Journal Articles

18. M. Loepfe, <u>C.M. Schumacher</u>, W.J. Stark, Design, performance and reinforcement of bearing-free soft silicone combustion-driven pumps, **Ind. Eng. Chem. Res.**, 53 (31), 12519–12526 (2014).

17. L. Bircher, O.M. Theusinger, S. Locher, P. Eugster, B. Roth-Z'graggen, <u>C.M. Schumacher</u>, J.D. Studt, M. Manz, W.J. Stark, B. Beck-Schimmer, I.K. Herrmann, Characterization of Carbon-Coated Magnetic Nanoparticles using Clinical Blood Coagulation Assays: Effect of PEG-Functionalization and Comparison to Silica Nanoparticles, **J. Mater. Chem. B**, 2, 3753-3758 (2014).

16. <u>C.M. Schumacher</u>, M. Loepfe, R. Fuhrer, R.N. Grass, W.J. Stark, 3D printed lost-wax casted soft silicone monoblocks enable heart-inspired pumping by internal combustion, **RSC Advances**, 4, 16039-16042 (2014).

Scientific coverage:

Featured in RSC Chemistry World, April 2014: "Pumping gone soft"

15. A. Stepuk, G. Casola, <u>C.M. Schumacher</u>, K. Krämer, W.J. Stark, Purification of $NaYF_4$ based upconversion phosphors, **Chem. of Mat.**, 26, 2015-2020 (2014).

14. A.C.C. Rotzetter, R. Fuhrer, R.N. Grass, <u>C.M. Schumacher</u>, P.R. Stoessel, W.J. Stark, Micro Mirror Polymer Composite Offers Mechanically Switchable Light Transmittance, **Adv. Eng. Mater.**, available online (2014).

13. C.R. Kellenberger, S.C. Hess, <u>C.M. Schumacher</u>, M. Loepfe, J.E. Nussbaumer, R.N. Grass, W.J. Stark, Roll-to-Roll Preparation of Mesoporous Membranes by Nanoparticle Template Removal, **Ind. Eng. Chem. Res.**, available online (2013).

12. A.C.C. Rotzetter, <u>C.M. Schumacher</u>, T. Zako, W.J. Stark, M. Maeda, Rapid Surface-Biostructure Interaction Analysis using strong Metal-based Nanomagnets, **Langmuir**, 29, 14117-14123 (2013).

   Shared first author contribution

11. I.K. Herrmann, A. Schlegel, R. Graf, <u>C.M. Schumacher</u>, N. Senn, M. Hasler, S. Gschwind, A.M. Hirt, D. Günther, P.A. Clavien, W.J. Stark and B. Beck-Schimmer, Nanomagnet-based removal of lead and digoxin from living rats, **Nanoscale**, 5, 8718-8723 (2013).

10. A.C.C. Rotzetter, C.R. Kellenberger, <u>C.M. Schumacher</u>, C. Mora, R.N. Grass, M. Loepfe, N.A. Luechinger, W.J. Stark, Combining Phosphate and Bacteria Removal on Chemically Active Filter Membranes Allows Prolonged Storage of Drinking Water, **Adv. Mater.**, 42, 6057-6063 (2013).

   Featured on the **Adv. Mater. cover**, 25(42), (2013).

9. <u>C.M. Schumacher</u>, I.K. Herrmann, S.B. Bubenhofer, S. Gschwind, A.M. Hirt, B. Beck-Schimmer, D. Günther and W.J. Stark, Quantitative Recovery of Magnetic Nanoparticles from Flowing Blood: Trace Analysis and the Role of Magnetization, **Adv. Funct. Mater.**, 23(39), 4888-4896 (2013).

   Featured on the **Adv. Funct. Mater. cover**, 23, 39 (2013).

8. R. Fuhrer, <u>C.M. Schumacher</u>, M. Zeltner and W.J. Stark, Soft iron/silicon composite tubes for magnetic, peristaltic pumping: Frequency dependent pressure and volume flow, **Adv. Funct. Mater.**, 23 (31), 3845-3849 (2013).

7. D.O. Raemy, R.N. Grass, W.J. Stark, <u>C.M. Schumacher</u>, M.J.D. Clift, P. Gehr and B. Rothen – Rutishauser, Effects of flame made zinc oxide particles in human lung cells - a comparison of aerosol and suspension exposures, **Particle and Fibre Toxicology**, 9:33, (2012).

6. A.C.C. Rotzetter, <u>C.M. Schumacher</u>, S.B. Bubenhofer, R.N. Grass, L.C. Gerber, M. Zeltner, W.J. Stark, Thermoresponsive polymer induced sweating surfaces as an efficient way to passively cool buildings, **Adv. Mater.**, 24 (39), 5352-5356 (2012).

   Featured on the **Adv. Mater. cover**, 24, 49 (2012).

Scientific coverage:

Highlighted in **Nature**, 480, 180 (2012): "Hydrogel makes buildings sweat"

Featured in RSC Chemistry World, September 2012: "Sweaty buildings cool themselves"

Media coverage:

Discovery News – USA – Oct. 2, 2012

20 Minuten – Switzerland – Oct. 2, 2012

Schweizer Fernsehen, Tagesschau – Switzerland – Oct. 2, 2012

ETH Life – Switzerland – Oct 2, 2012

5. I.K. Herrmann, M. Urner, S. Graf, <u>C.M. Schumacher</u>, B. Roth-Z'graggen, M. Hasler, W.J. Stark and B. Beck-Schimmer, Endotoxin removal by magnetic separation-based blood purification, **Adv. Healthc. Mater.**, 2 (6), 829-835 (2012).

4. <u>C.M. Schumacher</u>, F.M. Koehler, A.C.C. Rotzetter, R.A. Raso, W.J. Stark, Nanoparticle-assisted, Catalytic etching of carbon surfaces as a method to manufacture nanogrooves, **J. Phys. Chem. C**, 116 (25), 13693–13698 (2012).

3. S.B. Bubenhofer, <u>C.M. Schumacher</u>, F.M. Koehler, N.A. Luechinger, R.N. Grass, W. J. Stark, Large scale synthesis of PbS-TiO2 heterojunction nanoparticles in a single step for solar cell application, **J. Phys. Chem. C**, 116, 16246-16270 (2012).

2. S.B. Bubenhofer, <u>C.M. Schumacher</u>, F.M. Koehler, N.A. Luechinger, G.A. Sotiriou, R.N. Grass, W.J. Stark, Electrical resistivity of assembled transparent inorganic oxide nanoparticle thin layers: Influence of silica, insulating impurities and surfactant layer thickness, **ACS Appl. Mater. Interfaces**, 4 (5), 2664–267 (2012).

1. <u>C.M. Schumacher</u>, R.N. Grass, M. Rossier, E.K. Athanassiou, W.J. Stark, Physical Defect Formation in Few Layer Graphene-like Carbon on Metals: Influence of Temperature, Acidity, and Chemical Functionalization, **Langmuir**, 28, 4565-4572 (2012).

Presentations and Proceedings

6. C.M. Schumacher, C.R. Kellenberger, S. Hess, J.N. Nussbaumer, W.J. Stark, A novel approach for highly temperature stable battery separator membrane production, ICOM 2014, Suzhou, Jiangsu, China, July 20-25, 2014.

5. C.R. Kellenberger, <u>C.M. Schumacher</u>, A.C.C. Rotzetter, C. Mora, M. Loepfe, N.A. Luechinger, M. Rossier, R.N. Grass, W.J. Stark, Manufacturing of nano- to microporous membranes from high-performance polymers, poster presentation, MRS Fall Meeting, Boston, Massachusetts, USA, December 1-6, 2013.

4. <u>C.M. Schumacher</u>, Engineered nanomaterials and methods to trace them at low concentrations, invited talk, FHNW, Muttenz, Switzerland, October 14, 2013.

3. <u>C.M. Schumacher</u>, R.N. Grass, M. Rossier, E.K. Athanassiou, W.J. Stark, Physical defect formation in few layer graphene-like carbon on metal nanoparticles, MRS Fall Meeting, Boston, Massachusetts, USA, November 25-30, 2012.

2. <u>C.M. Schumacher</u>, R.N. Grass, M. Rossier, E.K. Athanassiou, W.J. Stark, Physical defect formation in few layer graphene-like carbon on aerosol-made metal nanoparticles, European Aerosol Conference 2012, Granada, Andalucía, Spain, September 2-5, 2012.

1. <u>C.M. Schumacher</u>, R.N. Grass, A. Schätz, W.J. Stark, Core-shell nanomagnets for magnetic chemistry and precious metal recovery: Long-term stability in acids and organic solvents, AIChE Annual Meeting, Minneapolis, Minnesota, USA, October 17-21, 2011.

Student supervision

4. Urs Lustenberger (Semester-Thesis, 3/2014 – present) – Development of a mobile gas powering unit for soft silicone combustion-driven motors

3. Cornelia Burri (Research assistant, 9/2013 – 12/2014) - Computer-aided design of novel soft actuators

2. Michael Loepfe (Master-Thesis, 3/2013 - 7/2013) - Therapeutic bubble design: a balloon approach for sonography

1. Luc Weydert (Research assistant, 9/2012 - 12/2012) - Development of a magnetic particle separation device

Teaching experience

3/2011 – 6/2011   Laboratory course - chemistry for sport sciences, ETH Zurich

Languages

German   native

English   fluent

French   business fluent

Spanish   basic skills

Varia

Member of the Materials Research Society (MRS)